DESIGN IMPROVEMENTS ON MIXED FLOW PUMPS BY MEANS OF COMPUTATIONAL FLUID DYNAMICS

A THESIS SUBMITTED TO
THE GRADUATE SCHOOL OF NATURAL AND APPLIED SCIENCES
OF
MIDDLE EAST TECHNICAL UNIVERSITY

BY

ONUR ÖZGEN

IN PARTIAL FULFILLMENT OF THE REQUIREMENTS
FOR
THE DEGREE OF MASTER OF SCIENCE
IN
MECHANICAL ENGINEERING

DECEMBER 2006

Approval of the Graduate School of Natural and Applied Sciences

Prof. Dr. Canan ÖZGEN
Director

I certify that this thesis satisfies all the requirements as a thesis for the degree of Master of Science.

Prof. Dr. S. Kemal İDER
Head of Department

This is to certify that we have read this thesis and that in our opinion it is fully adequate, in scope and quality, as a thesis for the degree of Master of Science.

Prof. Dr. Kahraman ALBAYRAK
Supervisor

Examining Committee Members

Prof. Dr. O. Cahit ERALP	(METU, ME)	
Prof. Dr. Kahraman ALBAYRAK	(METU, ME)	
Prof. Dr. Haluk AKSEL	(METU, ME)	
Dr. Tahsin A. ÇETİNKAYA	(METU, ME)	
M. Sc. Onur KONURALP	(Layne Bowler)	

I hereby declare that all information in this document has been obtained and presented in accordance with academic rules and ethical conduct. I also declare that, as required by these rules and conduct, I have fully cited and referenced all material and results that are not original to this work.

Name, Last name : Onur Özgen

Signature :

ABSTRACT

DESIGN IMPROVEMENTS ON MIXED FLOW PUMPS
BY MEANS OF COMPUTATIONAL FLUID DYNAMICS

Özgen, Onur
M. S., Department of Mechanical Engineering
Supervisor : Prof. Dr. Kahraman Albayrak

December 2006, 105 pages

The demand on high efficiency pumps leads the manufacturers to develop new design and manufacturing techniques for rotodynamic pumps. Computational Fluid Dynamics (CFD) software are started to be used during the design periods for this reason in order to validate the designs before the pumps are produced. However the integration process of CFD software into the design procedure should be made carefully in order to improve the designs.

In this thesis, the CFD software is aimed to be integrated into the pump design procedure. In this frame, a vertical turbine type mixed flow pump is aimed to be designed and design improvements are intended to be made by applying numerical experimentations on the pump. The pump that is designed in this study can deliver 115 l/s flow rate against the head of 16 mWC in 2900 rpm. The effects of various parameters in the design are investigated by the help of CFD software during the design and best performance characteristics of the pump are aimed to be reached.

The pump that is designed in this study is manufactured and tested in Layne Bowler Pumps Company Inc. The design point of the pump is reached within the tolerance limits given in the related standard.

In addition, the results of actual test and numerical experimentation are compared and found to be in agreement with each other. The integration of CFD code to the design procedure is found quite useful by means of shortening design periods, lowering manufacturing and testing costs. In deed the effects of the design parameters are understood better by applying numerical experimentations to the designed pump.

Keywords: Rotodynamic pump, Vertical turbine mixed flow pump, CFD analysis, Impeller layout profile, Pump performance test

ÖZ

KARIŞIK AKIŞLI POMPALARDA HESAPLAMALI AKIŞKANLAR DİNAMİĞİ İLE TASARIM İYİLEŞTİRMELERİ

Özgen, Onur
Yüksek Lisans, Makina Mühendisliği Bölümü
Tez Yöneticisi : Prof. Dr. Kahraman Albayrak

Aralık 2006, 105 sayfa

Yüksek verimli pompalara duyulan talep, üreticileri yeni tasarım ve imalat teknikleri geliştirmeye yönlendirmektedir. Bu nedenden dolayı, pompaların imalatlarından önce tasarımların doğrulanması için tasarım süreçlerinde Hesaplamalı Akışkanlar Dinamiği (HAD) yazılımları kullanılmaya başlanmaktadır. Fakat tasarımların geliştirilmesi için HAD yazılımlarının tasarım süreçlerine entegrasyonu dikkatli bir biçimde yapılmalıdır.

Bu tezde, HAD yazılımının pompa tasarım sürecine entegrasyonu hedeflenmiştir. Bu kapsamda karışık akışlı dik türbin pompa tasarımı hedeflenmiş ve tasarım geliştirmeleri, tasarlanan pompa üstünde sayısal deneyler uygulanarak sağlanmaya çalışılmıştır. Tasarımı yapılan pompa 115 l/s debiyi 16 mSS basma yüksekliğine 2900 d/d'da sağlamaktadır. Tasarımdaki farklı parametrelerin etkileri HAD yazılımı ile incelenmiş olup pompanın en iyi performans değerlerine ulaşılması hedeflenmiştir.

Bu çalışmada tasarlanan pompa, Layne Bowler Pompa Sanayi A.Ş.' de üretilmiş ve test edilmiştir. Tasarım noktasına standartlarda verilen tolerans limitleri içinde ulaşılmıştır.

Ayrıca, gerçek test sonuçları ve HAD sonuçları karşılaştırılmış, bulunan pompa karakteristiklerinin birbirleri ile tutarlı olduğu görülmüştür. HAD yazılımının pompa tasarım sürecine entegrasyonu tasarım sürecinin kısaltılması, pompa üretim ve test maliyetlerinin düşürülmesi açısından faydalı bulunmuştur. Bununla beraber, tasarım parametrelerinin etkileri tasarlanan pompa üstünde sayısal deneyler yapılarak daha iyi anlaşılmıştır.

Anahtar Kelimeler: Rotodinamik pompa, Dik türbin karışık akışlı pompa, HAD analizi, Çark profili, Pompa performans testleri

To My Parents

ACKNOWLEDGEMENTS

The author would like to express his sincere thanks to his supervisor Prof. Dr. Kahraman Albayrak for his guidance, support and encouragement throughout this study.

This work is based on the project supported by TÜBİTAK – TEYDEP which is proposed by Layne Bowler Pumps Company Inc. The author wishes to thank Mr. Onur Konuralp, manager of Layne Bowler Project and Quality Control Department, for his invaluable support and encouragement throughout the thesis. The author would like to thank Dr. Ertuğrul Başeşme for his cooperation, support and guidance during the work. The patient help of Mr. Kayhan Cengiz, Mr. Ramazan Özcan, and Mr. Ali Cirit is gratefully acknowledged. The author also would like to thank his colleague Mr. Vacit Hamamcıoğlu for his support during the manufacturing steps of the work.

The sincere and restless efforts of Mr. Ertan Engin throughout the thesis are also acknowledged. This work would not be completed without his encouragement and supports.

Finally, the author would like to express his deepest thanks to his parents İclal Gülçin Özgen and Ömer Özgen, and also his sister Gülnur Özgen for their never ending supports, encouragements and love.

TABLE OF CONTENTS

LIST OF TABLES

TABLES

LIST OF FIGURES

FIGURES

LIST OF SYMBOLS

SYMBOLS

b	breadth
d	diameter
e	length of midstreamline
g	gravitational acceleration
m	mass
n	rotational speed
r	radius
s	blade thickness, standard deviation, vane thickness
t	arc length
w	rotational speed
x	value of measured quantity
$\bar{x}$	average of measured quantity
z	number of blades, number of vanes
A	area
C	correction factor (see equation 2.33)
H	pump head
K	empirical coefficient (see equation 2.7)
M	static moment
N	specific speed
P	power
Q	flow rate
T	torque
U	uncertainty, tangential component of velocity
V	volume

α	fluid angle
β	blade angle
Δ	specific diameter
δ	angle of incidence
λ	angle between breadth and streamline
η	efficiency
φ	constriction coefficient
θ	tangential component of the velocity
π	pi number
ρ	density of pumping fluid
τ	torsional stress

INDICES

0	inlet eye of the impeller
1	inlet of the blade
2	exit of the blade
3	exit of blade
4	inlet of bowl
5	exit of bowl
dyn	dynamic
f	fluid
h	hydraulic
i	inlet
m	median, manometer, mass, mean, meridional, mechanical
n	number of measurements
o	exit
p	Pfleiderer, pump, pipe
s	shaft
t	total
th	theoretical

u	tangential direction
v	volumetric
Hdyn	dynamic water level
Hm	head measured by manometer
Ht	total head
P	power
Q	flow rate
R	random
S	systematic
T	total
V	volume
ηs	system efficiency of pump
θ	tangential direction
ρ	density of fluid
∞	infinity

CHAPTER 1

INTRODUCTION

1.1 General Layout of the Thesis

In this thesis, a vertical turbine type mixed flow pump is aimed to be designed and manufactured. The commercial Computational Fluid Dynamics (CFD) software is also aimed to be integrated into design. Making the comparison between the actual test results and CFD analyses results are in the objectives of this study. The effects of the design parameters on the hydraulic characteristics of the pump are aimed to be investigated by the applying CFD analyses to the pump.

The general information of the vertical turbine pumps is given in Chapter 1. The design of the pump is presented in Chapter 2 by means of impeller layout profile, impeller, bowl and suction bell designs. The numerical experimentation is performed with using the CFD code and the steps of the CFD analysis is given in Chapter 3. In Chapter 4, the information about the test facility and the test setup for the pump tests are explained and methodology which is followed during the tests is given. The discussions on the design procedure, CFD analyses methodology and the comparison between the actual test results and CFD analyses results are given in Chapter 5.

1.2 General Information on Vertical Turbine and Mixed Flow Pumps

“ The pumps are divided into two basic groups, depending on the way in which the liquid is transferred from suction side to the delivery side of the casing as positive displacement pumps and impeller or rotodynamic pumps”, [1]. The rotodynamic pump and impeller pump terms are firstly introduced by H. Addison, [1]. Based on the direction of the flow, the rotodynamic pumps are in the category of cased pumps,

[2]. The moving element in rotodynamic pumps is the impeller which is the rotor mounted on the rotating shaft and increases the moment of momentum of the flowing liquid in the impeller, [1].

"According to David Gordon Wilson, the first known vaned diffuser pump was patented by Osborne Reynolds in 1875 and was called a turbine pump", [3]. The pump that is patented by Osborne Reynolds is named as "turbine pump" because of the similarity on the appearance of the pump to the steam turbine, [3]. The turbine pumps are first used as lifting water from the small diameter water supplies and irrigation wells, [3]. However they are used in wide range of applications other then lifting water from irrigation wells such as used in circulation systems in the steel industry for cooling, water extraction from boreholes and rivers, sea water services, deep sea mining, extraction water from geothermal wells, city water district systems and etc, [3] and [4]. Moreover, the main advantage of using the vertical turbine pumps is the ability to assemble the stages in series connection thus increasing the pressure rise across the pump easily.

The pumps are classified by their specific speed. Non-dimensional specific speed or type number, N, of the pump is defined as, [2].

$$N = \frac{\omega . Q^{1/2}}{(g.H)^{3/4}} \tag{1.1}$$

Where, ω is in rad/s, Q is in m^3/s, g is in m/s^2 and H is in m. The mixed flow pumps by means of specific speed range are located between the centrifugal pumps and axial flow pumps, [1]. The overlapping region between the centrifugal and mixed flow pumps are named as Francis type, [5]. The specific speed range of the mixed flow pumps are given differently in the literature because of the overlapping regions of the mixed flow range with axial flow pumps and centrifugal pumps. The range for the mixed flow pumps by means of specific speed is given between 1.5 and 3 in References [1] and [3]. The mixed flow pumps discharges relatively low heads however the usage of mixed flow pumps as vertical turbine type assembly allows series connection, [1]. Thus the head of the pump assembly may be increased by series connection of the stages for the desired flow rate. The pump efficiency concerns are playing a major role in the usage of mixed flow type vertical turbine pumps. The Francis type and mixed flow type pumps have better efficiency characteristics among the other types. This is also illustrated in Figure 1.1 and Figure 1.2, [5] and [6] respectively. In Figure 1.1 the specific speed is in English units, [5] where ω is in rpm, Q is in gallons per minute (gpm), and H is in feet.

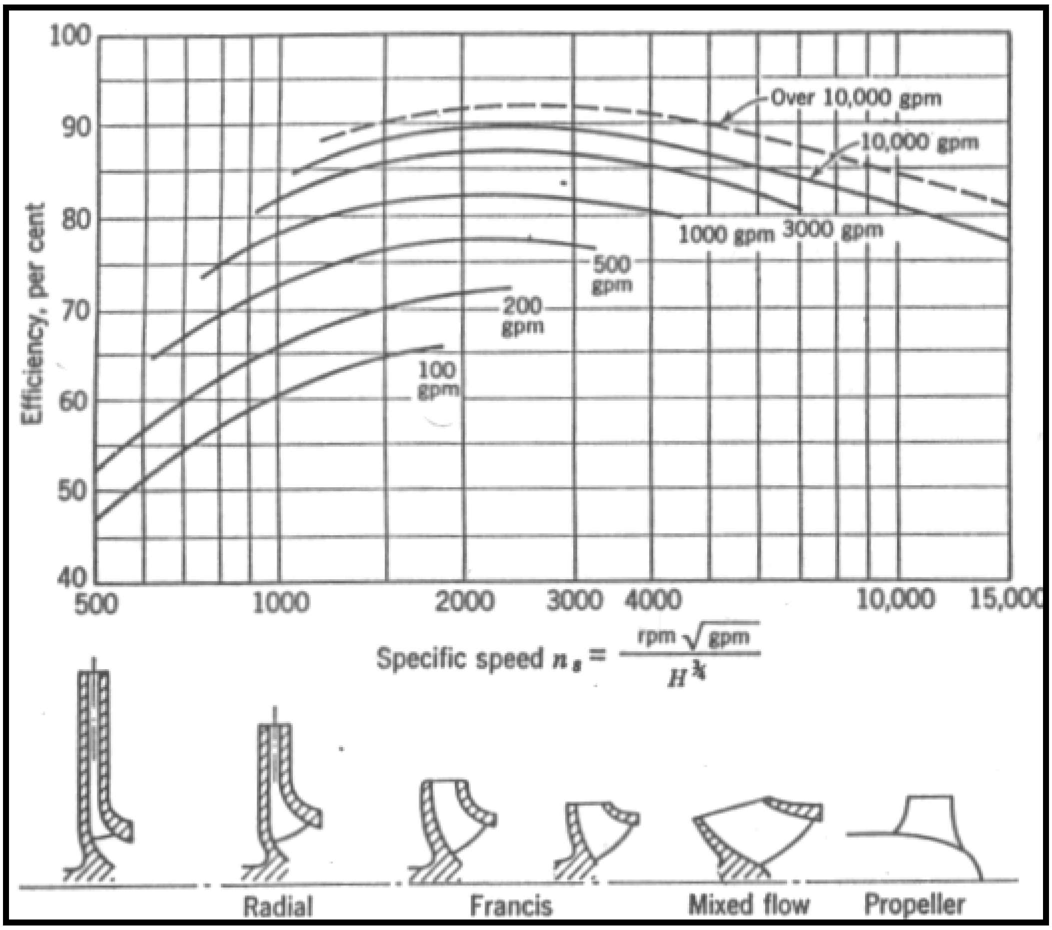

Figure 1.1 – Pump efficiency versus specific speed and impeller types (Worthington), [5]

However in Figure 1.2 the specific speed is given in non-dimensional form as defined in Equation (1.1). The range of the mixed flow pump impellers in English units is given as between 4,500 and 10,000 in Reference [3] and [5]. On the other hand the mixed flow pump impellers are given in the range between 0.7 and 3 in non-dimensional form, [6]. The overlapping region between mixed flow definition and radial flow definition is shown in Figure 1.2.

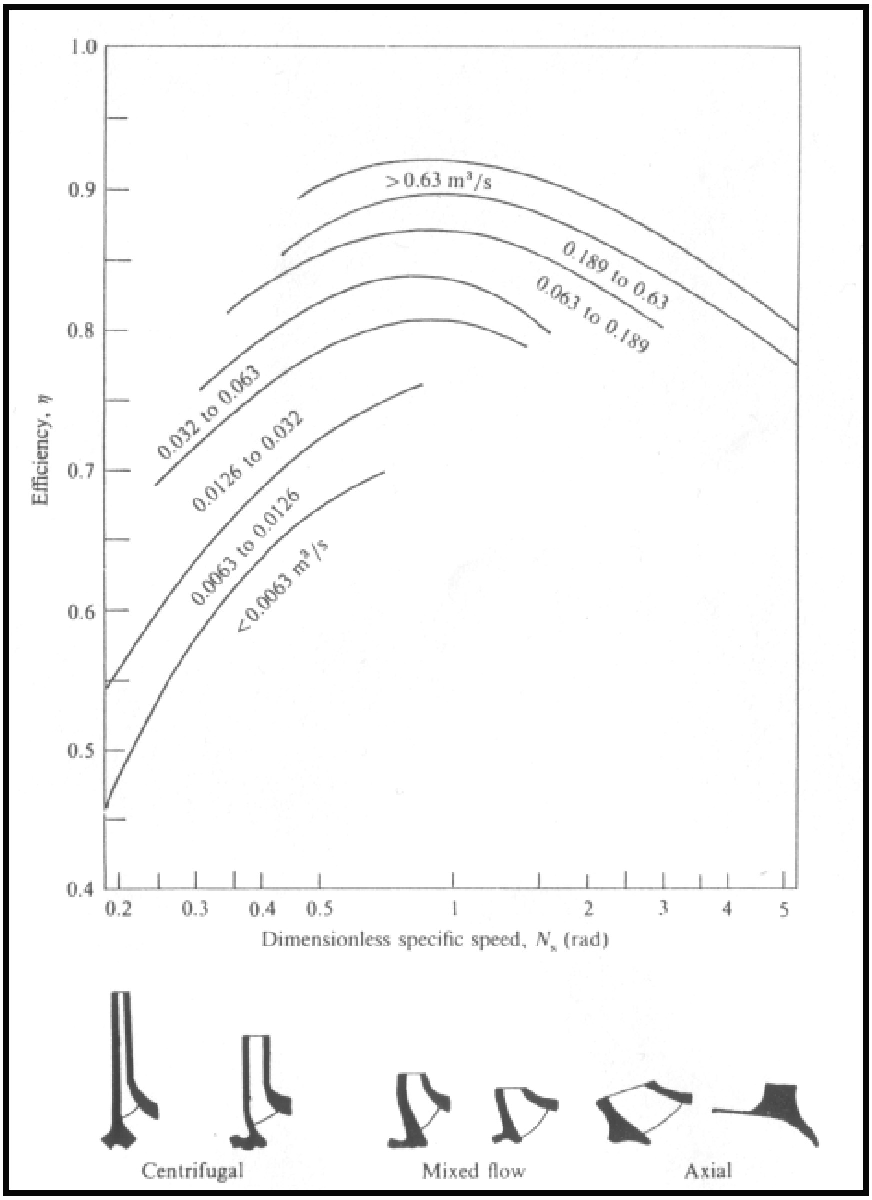

Figure 1.2 – Pump efficiency versus specific speed and impeller types, [6]

The development of the mixed flow type turbine type pumps are highly related to the demands of the market. The different application types developed during the years. However the concerns about energy consumption are the most important factor in the development of all type of pumps. The improvements in manufacturing techniques such as casting, surface finish on the impellers, rapid prototyping and precise measuring devices lead the industry to produce pumps with better efficiencies.

1.3 Parts of the Vertical Turbine Pump and Working Principle

The vertical turbine type mixed flow pumps are mainly composed of four subassemblies, [5]. These subassemblies are the driver, discharge head, column assembly and the pump assembly. The pump assembly is also composed of several parts which are shown in Figure 1.3.

The power is transmitted from the electric motor or any other type of driver such as diesel engine to the pump. There are different types of electric motors used in different applications. If the pump is driven from the top, the discharge head is used and Vertical Hollow Shaft (VHS) or Vertical Solid Shaft electric motors may be applicable for this kind of applications, [3]. Moreover, if the pump is driven from the bottom, submersible motors are used where the motor is also submerged with the pump inside to the working environment. The line shaft type installation of vertical turbine pumps is illustrated in Figure 1.3. The length of the column pipe and the intermediate shaft is adjusted for the different installations. If the length of the installation is increased the number of the bearings which are used to hold the intermediate shaft is also increased.

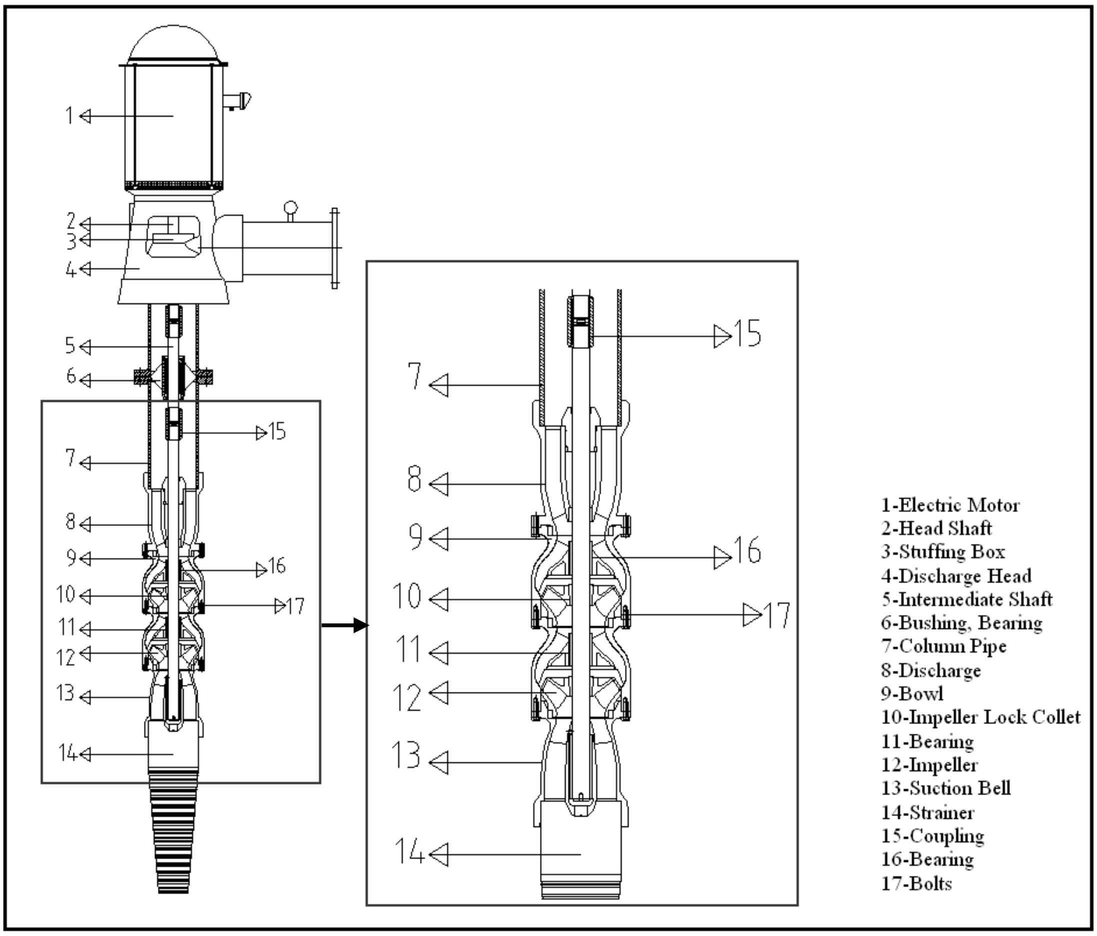

Figure 1.3 – The parts of the Pump Assembly

In the applications where the driver is located on the top of the discharge head, the power is transmitted to the pump by means of several shaft connections. The reason of using several shafts to transmit the power is due to flexibility of the installation. The head shaft which goes through the discharge head is placed between the intermediate shaft and motor. The stuffing box is placed into the discharge head which is preventing the water coming from the column assembly leak into the motor side. The column assembly is composed of pipes which are connected to each other and the bottom end of the column assembly in the vertical direction is connected to the discharge part of the pump. The intermediate shaft is located in the column assembly and connected to the head shaft and pump shaft by means of coupling connections. However the intermediate shaft is centred in the column assembly by means of journal bearings. The distance between the bearings are adjusted by concerning the rotational speed of the pump. The pump shaft which is holding the impeller is connected to the intermediate shaft. The impellers are locked on the shafts by means of impeller lock collets or key connections, [3]. The bowls are connected to each other by means of bolt and nut. The impeller is located inside the bowl in vertical turbine pumps and is shown in Figure 1.2. The bearing inside the bowl is used to align the shafts inside the pump assembly. The manufacturing tolerances are important while producing the bearing inside the bowls due to mechanical efficiency point of view. Nevertheless the balance occurring due to manufacturing of the impeller is also checked before the impeller is connected to the pump shaft. At the lower end the suction intake is located where the journal bearing inside it, allows the shaft to be aligned from the bottom end of the pump assembly.

1.4 General Information on CFD Analyses of the Pumps

"The first major example CFD was the work of Kopal, who in 1947 compiled massive tables of the supersonic flow over sharp cones by numerically solving the governing differential equations", [7]. In deed the work of Kopal is named as the first generation of CFD and the second generation of CFD is formed by the usage of full Navier-Stokes equations for exact solutions and introduction of the time-dependent techniques in mid 1960s, [7]. The turbomachinery design is affected by the development of CFD techniques during these years. However, depending upon on the complexity of the flow structure and dynamics inside the turbomachines, the first applications of CFD to the turbomachines are introduced in late 1980s and at the beginning of 1990s, [8]. The Reynolds averaged Navier-Stokes Equations solver is used by Dawes N-S solver in 1990, [9]. "The 3-D flow fields within the impellers/diffusers are analyzed and evaluated by Dawes N-S solver", [8]. Moreover Akira Goto is used the stage version of Dawes code in a diffuser pump stage to analyze the 3-D flow fields, [10]. The usage of commercially available CFD software such as Fluent, CFX, Star-CD, CFdesign and Numeca in the market fasten the development of different type of applications on the pumps.

The main application of CFD to the pumps is in the computation of the pump characteristics. There are two main methodology found applicable to the pump applications while simulating the motion of the rotor, [11]. The first one is the frozen rotor model which is the steady state solution. “In frozen rotor model, the frame of reference is changed but the relative orientation of the components across the interface is fixed. The two frames of reference connect in such a way that they each have a fixed relative position throughout the calculation, but with the appropriate frame transformation occurring across the interface”, [11]. There are two main disadvantages of frozen rotor model, [11] and [12]. The first disadvantage is caused by not modeling the transient effects at the frame change interface and the second one is the losses occurred in transient case as the flow is mixed between the rotating and stationary components. The second methodology used for simulating the motion of the rotor is the transient rotor-stator model, [11] and [13]. In this model, the transient motion of the rotor is simulated within the rotating reference frame and interface position between the rotor and stator is updated in each time step, [11]. The time step is related to the rotational speed of the rotor, [11], [13], [14] and [15]. The rotor-stator model is the unsteady solution type of turbomachinery CFD solutions. The main advantage of this model is modeling the transient effects and calculation the losses occurring between the rotating and stationary parts, [11]. However the solution periods are longer and more computational power is needed for the solution by means of CPU clock speed and memory of the computer when it is compared to the frozen rotor model. There are studies in the literature, [15] and [16] where these two models are used simultaneously. The steady analysis is performed by frozen rotor model first in order to understand the flow inside the pump and then the outputs of the frozen rotor analyses are used as the initial guess for the transient analyses which are carried by rotor-stator model. Nevertheless, the rotor stator interaction regions are also studied in order to predict the pressure fluctuations in these regions by using CFD, [17].

The second important aim of application of CFD analyses to the pumps is improving the pump characteristics by means of hydraulic efficiency. Nevertheless in order to perform full CFD analyses for improving the hydraulic characteristics of the pumps require, selection of proper boundary conditions, generating high quality sets of elements and choosing proper turbulence model. There are several boundary condition definitions applied to the inlet and outlet of the pump, [16]. For numerical stability reasons, two additional volumes are added to the inlet and outlet of the pump stage and the boundary conditions are defined at the faces of these volumes, [18]. In most of the applications, velocity is specified at the entire inlet face of the inlet domain and pressure rise is specified at the outlet face of the outlet domain, [16]. While modeling the inlet and outlet volumes that are added to the pump in this study, it is tried to simulate the actual test conditions which are given in Chapter 3. The total number of elements that are generated for the solution domain affects the solution in the pump analyses, [14], [15], [16], [17] and [18]. The number of elements that is generated by the commercial CFD software is related to the memory capacity of the computer used for analyses, [13], [14] and [17]. It is possible to find out mesh independency limit of total number of elements in steady state solutions that are applied to the pumps by using frozen rotor model. However in transient analyses that are performed on the pumps do not demonstrate mesh independence solutions due to turbulence models, [14]. It is known that in order to find out the suitable number elements that are required to minimize the errors in the calculations that are performed in CFD analyses, the output of the code should be verified with the real life experiment results, [14]. The different numbers of elements are used in CFD applications on pumps and the results of these analyses are compared with the test results during the recent studies in Layne Bowler. These studies are performed in different specific speed pumps. The output of these studies showed that by using around 1,500,000 fluid elements and k-ε turbulence model in the analyses give reliable results when they are compared with the actual test results.

CHAPTER 2

HYDRAULIC DESIGN AND PRODUCTION OF THE PUMP

2.1 General Information on the Design of the Pump

The pump that is aimed to be designed in this study is a vertical turbine type mixed flow pump. Hydraulic design of the pump is mainly composed of impeller, bowl and suction bell design. The design procedures in the literature together with the experience and know-how coming from the company are used during the design of these parts. Since there is not enough information on the impeller layout design, a trial and error procedure is applied in order to design the impeller layout. Moreover, the preliminary design and impeller layout design are performed together in order to get the best impeller layout profile for the designed pump. The shaping of the blade is performed by using point by point method described in the related section of the impeller design. The bowl design is performed mainly by considering the absolute velocity distribution inside the vane to vane passage of the bowl. The suction intake is also designed in this chapter.

2.2 Hydraulic Design of Impeller

In this study, hydraulic design of the impeller consists of three parts. First part is the design of impeller layout profile. Starting with an existing impeller layout profile, new impeller layout is designed in order to meet the hydraulic characteristics of the pump to be designed. The iterations are performed to adjust the best shape of the impeller layout as discussed in design of impeller layout profile section. The preliminary design, which is the second part, is performed coupled with impeller layout profile design for finding out the necessary parameters for the design. The experience and recent design studies are used while eliminating these parameters.

The last part which is the shaping of the blades is followed by the preliminary design in this section. Point by point method is selected to be used for shaping the impeller blades.

2.2.1 Design of Impeller Layout Profile

The shape of the impeller layout profile is related to the specific speed of the pump. In order start the design of the impeller layout profile, non-dimensional specific speed, N, of the pump to be designed is calculated.

$$N = \frac{\omega . Q^{1/2}}{(g.H)^{3/4}} \tag{2.1}$$

where, ω is in rad/s, Q is in m^3/s, g is in m/s^2 and H is in m. The non-dimensional specific speed of the pump to be designed is found to be 2.32. “Impellers with blades of single curvature are among the simplest. They are used in pumps with low specific speeds (N<0.57) and discharges of up to 140 l/s” [1]. Since the specific speed of the pump to be designed is above this limit, impeller with blades of double curvature is decided to be used.

“If an impeller already exists, it is always a good idea to analyze the existing design.” [19]. In order to design the impeller layout, first the impeller layout of the pump which has the closest specific speed at best efficiency point is chosen from the impeller layout library of Layne Bowler. The selected profile from Layne Bowler impeller layout library is shown in Figure 2.1. The certain parametric changes in the layout are made in order to attain the hydraulic characteristics of the pump to be designed in this study.

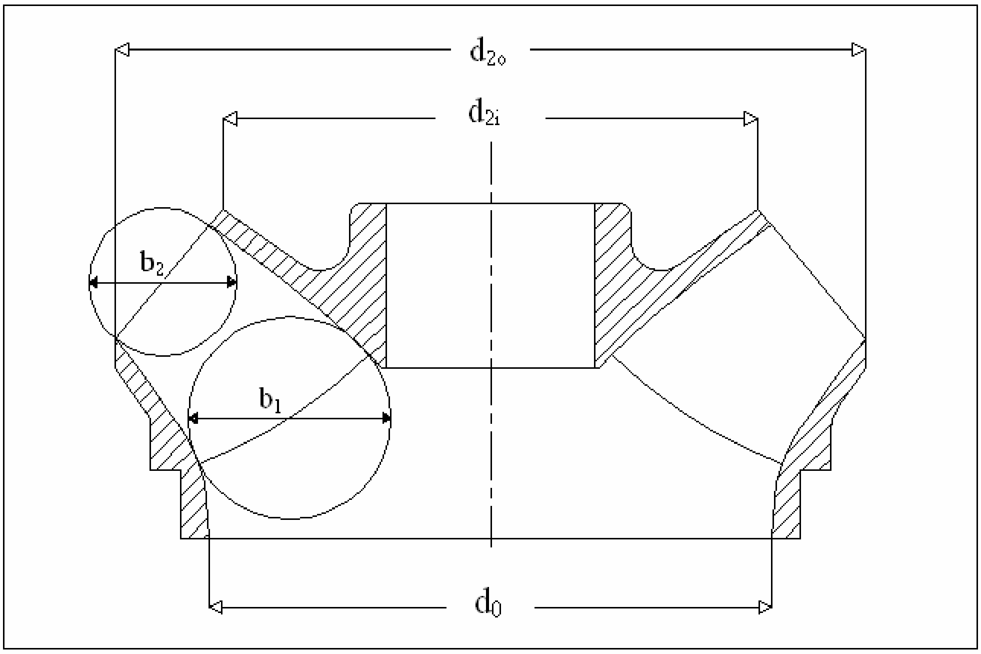

Figure 2.1 –Selected impeller layout profile from Layne Bowler Library

The design point of the pump is stated again in order to define the specific speed and flow properties in other units. “Specific speed in fundamental units is a dimensionless number. However, the more commonly used value is in U.S. Customary (English) units.” [3]. Specific speed in U.S Customary units is given by:

$$N_{(U.S)} = \frac{n.Q^{1/2}}{(H)^{3/4}} \tag{2.2}$$

where n is in rpm, Q is in gal/min and H is in feet. The specific speed of the pump in U.S. Customary units is 6348. The non-dimensional specific diameter, Δ, is selected from Figure 2.2, which is given in Reference 3. Specific speed in English units, $N_{(U.S)}$, is used in Cordier Diagram given in Reference 3.

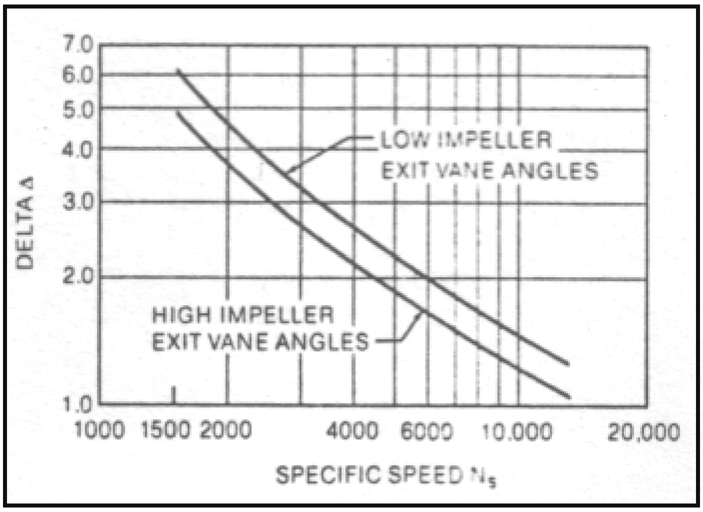

Figure 2.2 – Cordier Diagram for selecting Δ value, [3]

After determining Δ_{high} and Δ_{low} from Figure 2.2, the upper and lower values for the median impeller diameter, d_{2m}, are calculated by putting the Δ_{high} and Δ_{low} values to the formula given by, [3]:

$$\Delta = \frac{(g.H)^{1/4}.d_{2m}}{(Q)^{1/2}} \tag{2.3}$$

The dimensional parameters that are evaluated during the design of the impeller layout profile are illustrated in Figure 2.3. Those parameters are the median diameter, d_{2m}, impeller shroud diameter at the trailing edge, d_{2o}, impeller hub diameter at the trailing edge, d_{2i}, impeller inlet breadth, b_1, impeller outlet breadth, b_2, impeller hub diameter at the inlet, d_h and impeller inlet eye diameter d_0.

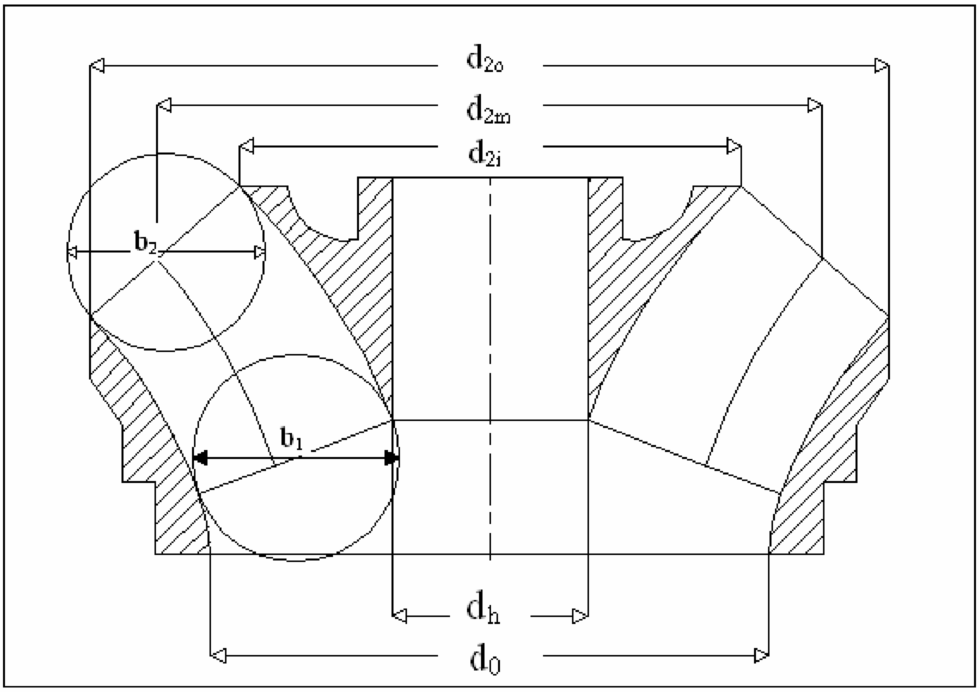

Figure 2.3 – Impeller layout profile of a mixed flow pump impeller showing the main geometrical parameters

After determining the d_{2m} values for high and low impeller exit vane angles the average value of $d_{2m\text{-}high}$ and $d_{2m\text{-}low}$ is taken for the first assumption. d_{2o} value is calculated by using the chart given in Figure 2.4, [3]:

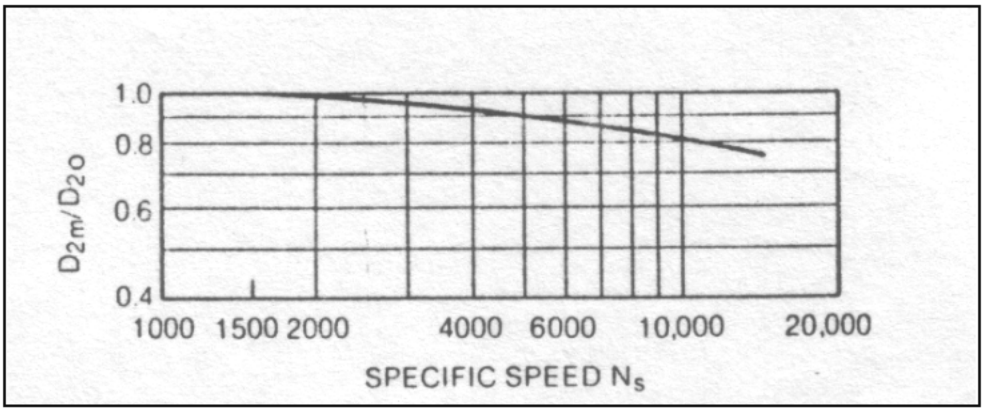

Figure 2.4 – Design chart showing d_{2m}/d_{2o} ratio, [3]

Found d_{2o} and d_{2m} values are drawn on the impeller layout in order to check the dimensions as shown in Figure 2.5.

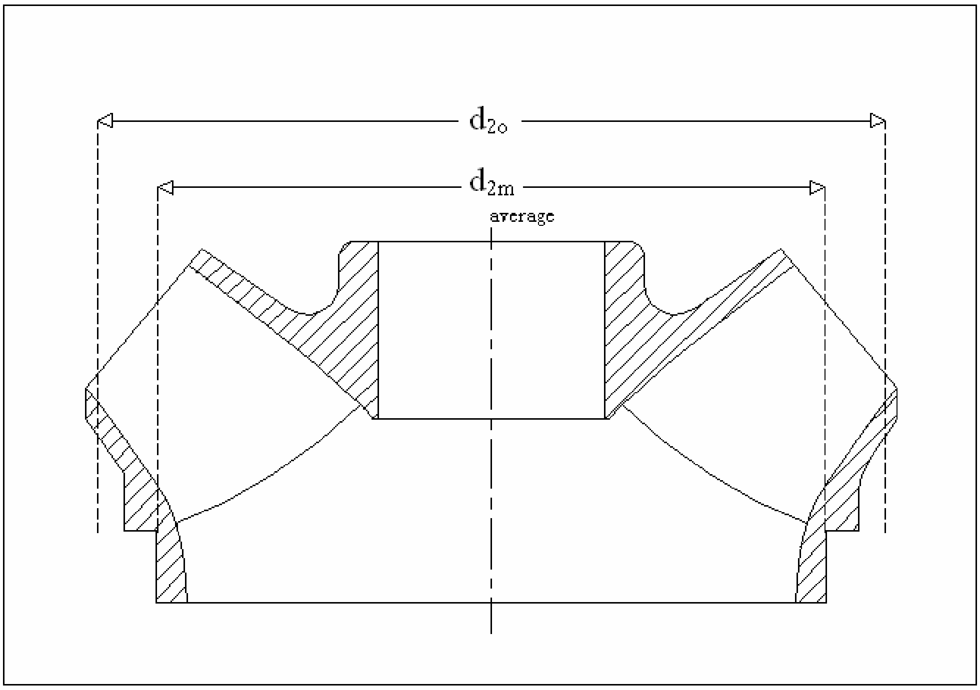

Figure 2.5 –Impeller layout showing found d_{2o} and $d_{2m\text{-average}}$ values

d_{2i} value, which is shown in Figure 2.3, is calculated by using the formula, [3]:

$$d_{2m} = \sqrt{\left(\frac{(d_{2o})^2 + (d_{2i})^2}{2}\right)} \tag{2.4}$$

The outlet breadth, b_2 is determined by using the chart shown in Figure 2.6, [3]. The average value of the b_2 is taken for the first guess. However the value is corrected within the range shown in Figure 2.6 during the iteration procedure as explained in the later steps of the impeller layout design. It is kept in mind that meridional velocity at the exit depends on the value of b_2. The relation of b_2 and exit area is given in the impeller exit calculation part of the preliminary design.

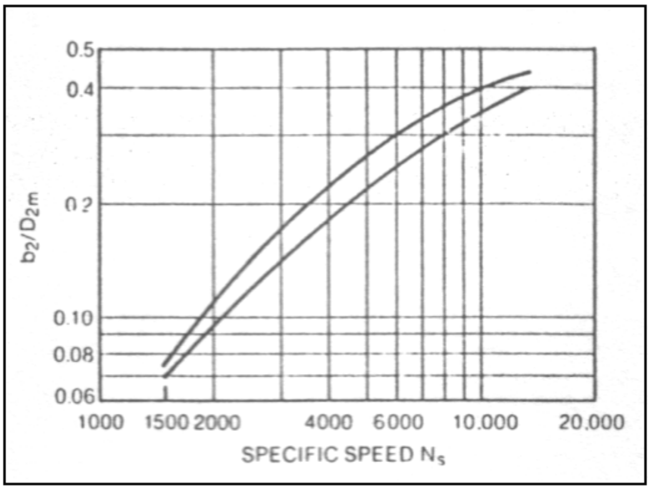

Figure 2.6 – Design chart showing b_2/d_{2m} ratio

After determining the b_2 value, the circle which has the radius of b_2 is drawn. The center of this circle lies at the intersection points of the d_{2o} and existing outlet breadth of selected profile from the library. The circle which is drawn in order to construct the outlet breadth of the pump to be designed is shown in Figure 2.7.

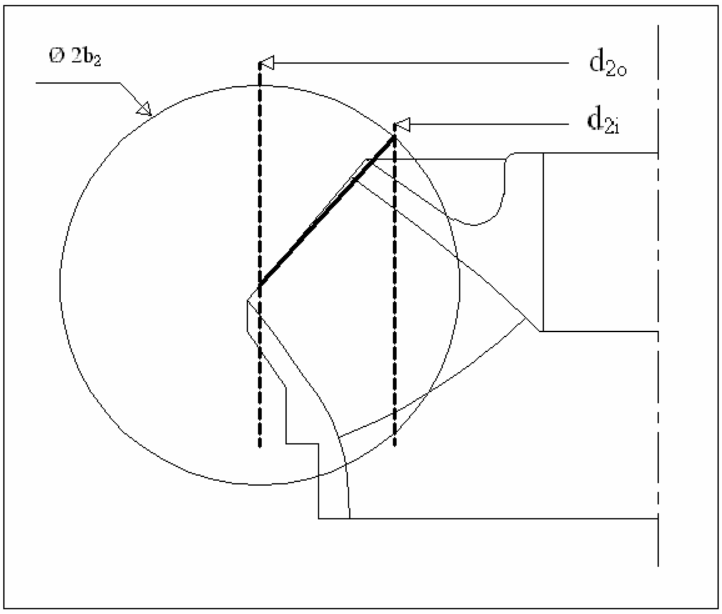

Figure 2.7 – Impeller layout showing found d_{2o} and d_{2i} values

However in order to construct the starting point of the arc for the hub side; the shaft size and the hub diameter should be determined. The shaft size of the impeller is calculated for multiple stages. The selection of the stage number is made by considering the demand for the pump to be designed from the previous sales statistics and adding several stages to this value as safety factor. In deed, the shaft material is also important as seen in Equation (2.5). Available shaft materials in the company and future demands are analyzed and suitable material is selected. The selected material is AISI 316. The diameter of the shaft is calculated, [1];

$$d_s = \sqrt[3]{\frac{360000.P_m}{\tau_{torsion}.n}} \tag{2.5}$$

where d_s is the shaft diameter in cm, τ_s is the permissible torsion stress in kPa/cm^2, P_m is the transmitted power in Metric H.P and n is speed in rpm, [1].

The transmitted power for multiple stages, P_m, is defined as the multistage pump power which is calculated as:

$$P_m = \frac{\rho.g.Q.H}{\eta}.m \tag{2.6}$$

where, m is the number of stages.

"In the U.S.S.R. the inlet diameter is calculated from the empirical formula", [1]. The impeller inlet eye diameter is found by using this formula, [1]:

$$d_o = K_o.(\frac{Q}{n})^{1/3} \tag{2.7}$$

K_0 term in Equation (2.7) varies between 4 and 4.5. " K_0 is selected close to the 4 where better pump efficiency is desired and K_0 is selected close to the 4.5 where better cavitation performance is desired during the design", [20]. The K_0 term is selected close to 4 for the pump to be designed in terms of concerning better efficiency in the design. Impeller inlet eye diameter is also shown in Figure 2.3.

The hub and shroud profiles are constructed by fitting the smooth arcs between the impeller inlet breadth, b_1, and impeller exit breadth, b_2. The blade meridional profile is extended through the impeller inlet eye in order to lower the blade number of the impeller. The blade number of the impeller is selected to be 6 from the recent design experience, know how coming from the company and the literature [1] and [21]. If the blade number is higher then these values, it is hard to produce and assemble the cores in order to obtain the impeller. The design of impeller layout then completed with a trial and error procedure which is shown as a flow chart in Figure 2.8. The main aim of this process is to construct the best impeller layout in order to satisfy the flow characteristics of the pump to be designed. The unknown parameters are eliminated by the iterative procedure coupled with the preliminary design which is explained in the following sections. In deed the impeller layout design is highly dependent on the previous studies and experience. Heuristic and intuitive approaches become mainly the most important bases of the impeller layout design. However these approaches have to be supported by theoretical approaches in fluid dynamics, numerical experimentation and experimental results. Once the desired pump characteristics are achieved by numerical experimentation and validated by the experimental results, the designed impeller layout is added to the impeller layout library. The aim of creating the library is shortening the design periods of the pumps by means of impeller layout profile design. The designer may design the impeller layout which lies between close specific speed layouts easily if a library exists. Nevertheless the blade passage of the impeller layout may be enlarged and used if higher flow rates are expected from an existing pump layout. This process is named as simply building up a pump family which uses the same bowl for different impellers with different flow rates or heads. The extension procedure is mainly done by adjusting the exit breadth and inlet breadth of the impeller layout.

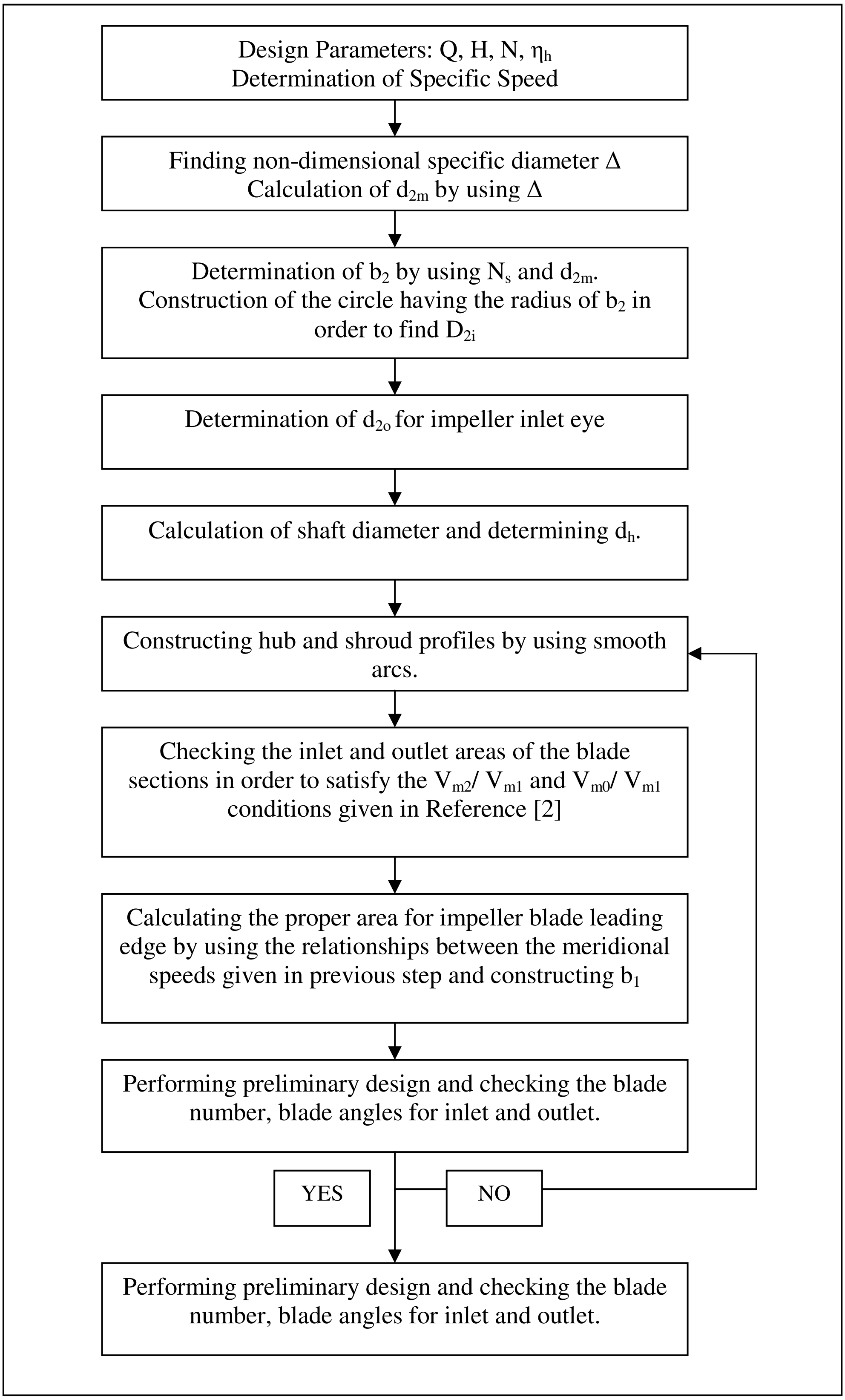

Figure 2.8 – Flow Chart showing impeller layout design

The designed impeller layout which is used to design the impeller is shown in Figure 2.9. The schematic representation of designed and selected impeller layout profile is also shown in Figure 2.10.

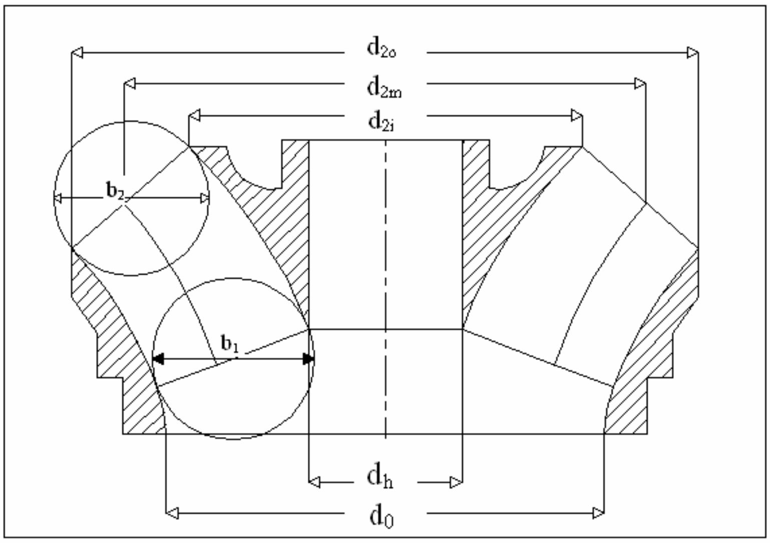

Figure 2.9 – Designed impeller layout profile

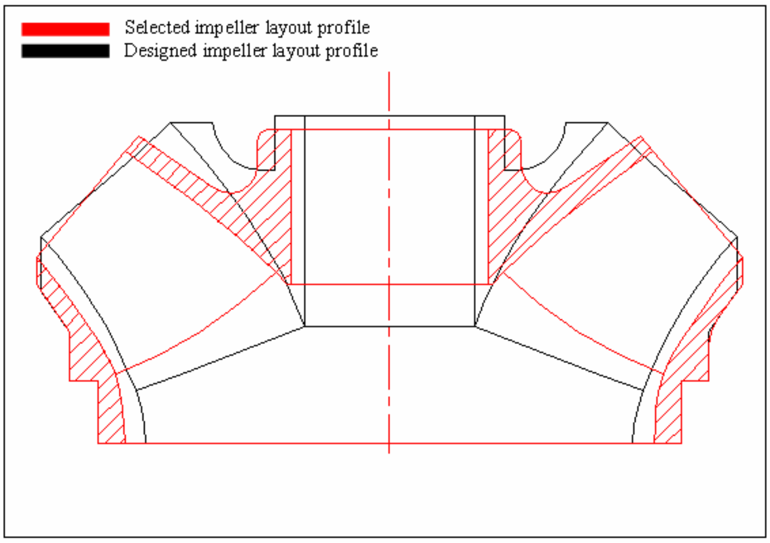

Figure 2.10 – Schematic representation of designed and selected impeller layout profiles

2.2.2 Preliminary Design

The preliminary design is performed for midstreamline which is explained in the following sections. Necessary parameters are evaluated by using the methodology given below.

2.2.2.1 Pump Performance Data

The design input values of the pump to be designed in this study are; volumetric flow rate, Q, head, H and rotational speed ω.

2.2.2.2 Efficiencies

" The overall efficiency η is almost invariably determined experimentally on the basis of the measurements of the discharge Q, head H and input power P, taken during a pump test", [1]. The overall efficiency of the pump is also known as pump efficiency is defined with three efficiency components. These efficiency components are hydraulic efficiency, $\eta_{h,}$ volumetric efficiency, η_v and mechanical efficiency, η_m. The pump efficiency is given as:

$$\eta = \eta_h . \eta_v . \eta_m \tag{2.8}$$

The volumetric and mechanical efficiencies are assumed to be 96% for the pump to be designed. The pump efficiency is taken from the chart given in Reference [1] and [4] as 76%. Using the volumetric efficiency, mechanical efficiency and pump efficiency, the hydraulic efficiency of the pump to be designed is calculated as:

$$\eta_h = \left(\frac{\eta}{\eta_m . \eta_v}\right) \tag{2.9}$$

The general view of the impeller which is designed in the impeller layout design part is shown in Figure 2.11. The necessary parameters are taken from the layout in order to determine the values on the following steps of the design of the pump.

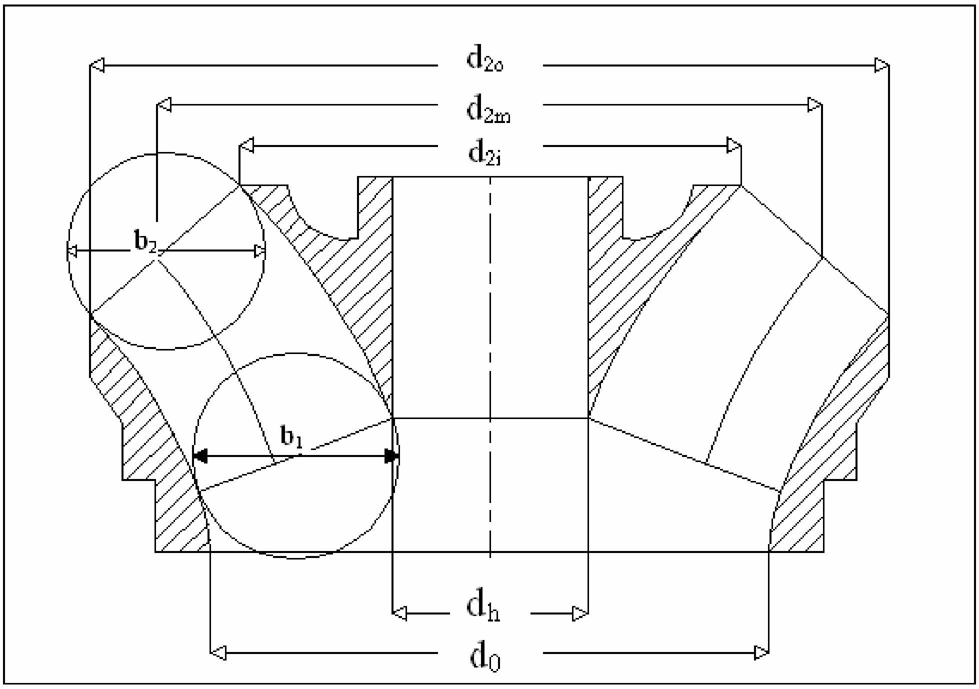

Figure 2.11 – Designed impeller layout profile

2.2.2.3 Impeller Inlet

The flow rate, Q_i which is mainly defined as the volumetric flow rate passing through the impeller blade passage is calculated using the volumetric efficiency, η_v and the design point flow rate Q. The formula is given as, [1]:

$$Q_i = \frac{Q}{\eta_v} \tag{2.10}$$

The net area in the impeller inlet eye, A_0, is calculated with considering the shaft in the impeller inlet eye as:

$$A_o = \frac{\pi.(d_o{}^2 - d_s{}^2)}{4} \tag{2.11}$$

The net impeller inlet eye diameter, d_o, is taken from the designed impeller layout. The axial velocity in the impeller inlet eye which is also named as meridional velocity is given by, [1]:

$$V_{m0} = \frac{Q_i}{A_0} \tag{2.12}$$

The hub diameter is taken from the impeller layout and the blade inlet area without blade thicknesses, $A_{1'}$ is calculated by revolving the blade inlet breadth, b_1, around the rotating axis. The blade thickness is the important parameter in the design. The thickness of the blade is highly dependent on the production techniques used in the company. If the thickness is taken too small and not adjusted with the other wall thicknesses in the impeller, casting of the impeller may not be achieved in the desired manner. The thickness of the blade ,s , is taken as, 3 mm at leading edge, 4 mm in the middle and 3 mm at the trailing edge of the blade.

The inlet constriction coefficient, φ_1, is assumed as the first guess. The net area at the leading edge of the blade is calculated by using, [1]:

$$A_1 = \frac{A_{1'}}{\varphi_1} \tag{2.13}$$

The meridional velocity at leading edge, V_{m1}, of the blade is calculated as follows, [1]:

$$V_{m1} = \frac{Q_i}{A_1} \tag{2.14}$$

"In order to calculate angles β_1 and β_2 and hence to determine the shape of the blade, the impeller is divided into two or four (depending on the size of the impeller) elementary streams of equal rate of flow", [1]. The streamline which is drawn by following the method described in Reference [1] is named as A_1A_2 and shown in Figure 2.12. The design of the impeller is made for five streamlines which constitutes to 3 streams of equal flow rate. Although the other streamlines which are between A_1A_2 and hub profile and also A_1A_2 and shroud profile are drawn with the same methodology.

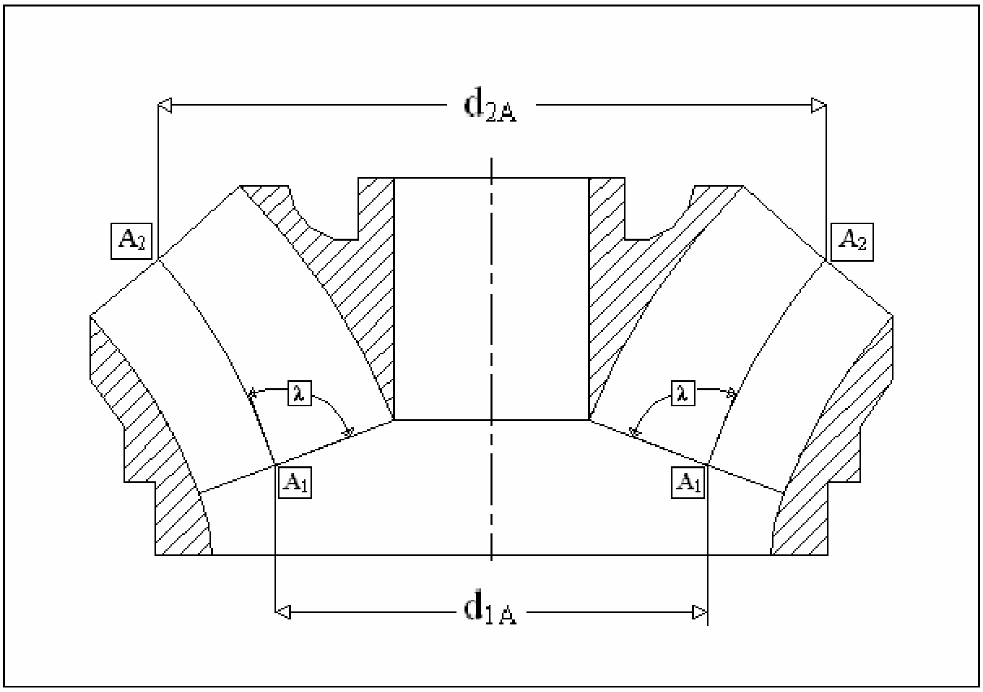

Figure 2.12 – Designed impeller layout showing found midstreamline A_1A_2

The peripheral velocity at the impeller inlet is calculated as:

$$U_1 = \frac{\omega.d_1}{2} \tag{2.15}$$

The blade inlet angle β_1, which is shown in Figure 2.13, is calculated using the formula:

$$\beta_1 = \tan^{-1}\frac{V_{m1}}{U_1} \tag{2.16}$$

The blade inlet angle β_1 is increased by the angle of incidence, δ_1, which is between 2^o-6^o in order to attain the required discharge and improve the suction performance, [1].

$$\beta_{1A} = \beta_1 + \delta_1 \tag{2.17}$$

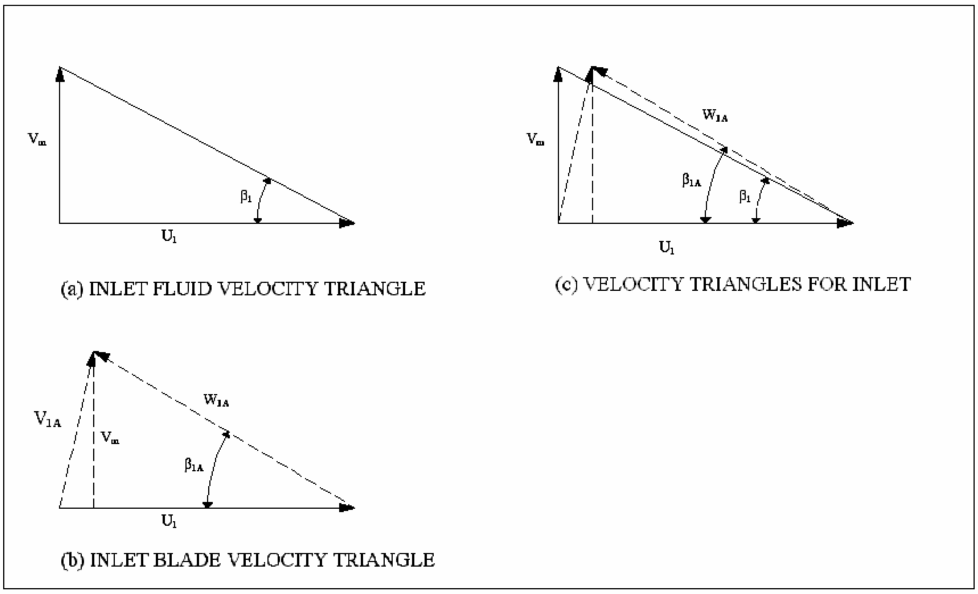

Figure 2.13 – Velocity triangles for inlet of the blade

The blade number of the pump to be designed, z, is assumed in order to correct the φ_1 value with an iterative procedure. The blade number assumption is based on the experience coming from the previous similar pump designs and the References [1] and [21]. The arc length between the adjacent blades, t_1, is calculated by the equation given in Reference 1 by:

$$t_1 = \frac{\pi . d_1}{z} \tag{2.18}$$

The correction of the φ_1 is an iterative procedure. λ is the angle between the tangent line to the hub profile and tangent line to the mid-streamline A_1A_2 and shown in Figure 2.11. The formula used to iterate and correct φ_1 is, [1]:

$$\varphi_1 = \frac{1}{1 - \frac{s_1}{t_1} . \sqrt{1 + \frac{1}{\tan^2(\beta_{1A}) . \sin^2(\lambda)}}} \tag{2.19}$$

Using the β_{1A} found in Equation (2.17), φ_1 is calculated and checked with the assumed value of the φ_1 in Equation (2.19). If the φ_1 value found in Equation (2.19) is different then the value used in Equation (2.13) for finding out the β_{1A} value and this procedure continues until the φ_1 converges with the correct value of β_{1A}.

2.2.2.4 Impeller Exit

The theoretical head, H_{th}, of the pump to be designed is calculated as:

$$H_{th} = \frac{H}{\eta_h} \tag{2.20}$$

The blade outlet breadth, b_2, is taken from the designed impeller layout. The area at the exit of the impeller without blade thickness, $A_{2'}$, is calculated by constructing the surface with revolving b_2 around the rotation axis of the impeller. The net area at the impeller exit with blade thickness, A_2, is calculated assuming the outlet constriction coefficient, φ_2, with the formula, [1]:

$$A_2 = \frac{A_{2'}}{\varphi_2} \tag{2.21}$$

Meridional velocity, V_{m2}, is calculated as, [1]:

$$V_{m2} = \frac{Q_i}{A_2} \tag{2.22}$$

The peripheral velocity, U_2, is calculated by using the D_2 value which is the diameter of the mid-streamline at the blade exit of the impeller by the equation:

$$U_2 = \frac{\omega . d_2}{2} \tag{2.23}$$

"In order to determine the velocity U_2, we use the fundamental equation for the impeller pumps", [1]. The fundamental equation defined in Reference 1 is basically the form of Euler equation. The Euler equation was first introduced by L.Euler in 1754 for water turbines, [1]. Thus the angular momentum increase of the flowing liquid is achieved by the driving motor. The torque is defined by the formula, [1]:

$$T = \frac{\gamma . Q . (r_2 . V_2 \cos\alpha_2 - r_1 . V_1 \cos\alpha_1)}{g} \tag{2.24}$$

The terms in Equation (2.24) $V_2 \cos\alpha_2$ is defined as $V_{\theta 2}$ and $V_1 \cos\alpha_1$ is defined as, $V_{\theta 1}$ which is shown in the velocity triangle for the impeller blade exit in Figure 2.14. "For flow of a perfect liquid through an ideal pump, the power imparted to the liquid by the impeller $T.\omega$ is equal to the power carried out of the pump by the stream of liquid of specific weight γ, the rate of flow Q and pressure head $H_{th\infty}$", [1]. The formula is given for infinite number of blades:

$$T.\omega = \gamma.Q.H_{th\infty} \qquad (2.25)$$

Thus, after using Equations (2.24) and (2.25), the theoretical head $H_{th\infty}$ of the pump which is defined as the head that a pump could generate, if there is no losses due to hydraulic resistance or mechanical friction during the operation of the pump becomes [1]:

$$H_{th\infty} = \frac{(V_{\theta 2}U_2 - V_{\theta 1}U_1)}{g} \qquad (2.26)$$

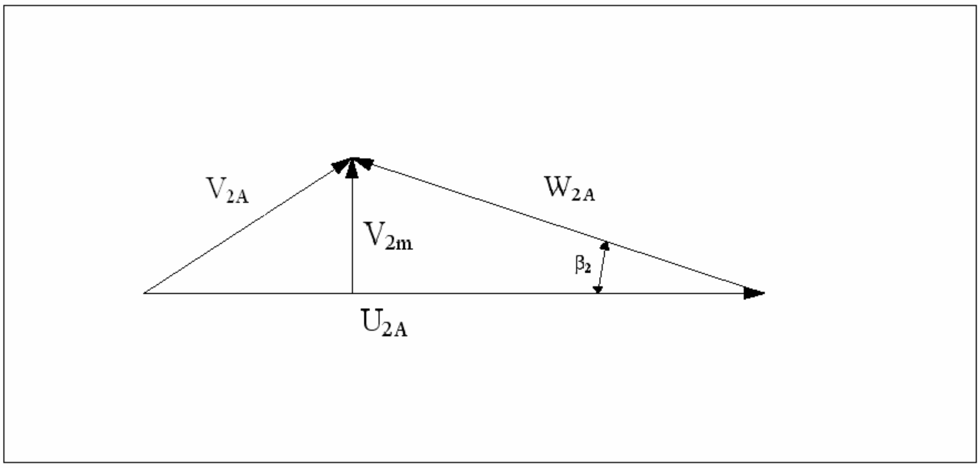

Figure 2.14 – Velocity triangle for exit of the impeller blade

From the velocity triangle as shown in Figure 2.14;

$$V_{\theta 2} = U_2 - \frac{(V_{m2})}{\tan\beta_2} \tag{2.27}$$

When $V_{\theta 2}$ is put into Equation (2.26) the following formula is achieved:

$$g.H_{th\infty} = U_2(U_2 - \frac{V_{m2}}{\tan\beta_2}) - V_{\theta 1}U_1 \tag{2.28}$$

Assuming no-inlet whirl condition for the inlet of the blade of the impeller, then $V_{\theta 1}.U_1$ term becomes zero. The Equation (2.28) reduces to:

$$g.H_{th\infty} = U_2(U_2 - \frac{V_{m2}}{\tan\beta_2}) \tag{2.29}$$

The positive root of this equation is taken in order to determine the U_2 value as:

$$U_2 = \frac{V_{m2}}{2\tan\beta_2} + \sqrt{(\frac{V_{m2}}{2\tan\beta_2})^2 + gH_{th\infty}} \tag{2.30}$$

Since the theoretical head for infinite number of blades is, [1]:

$$H_{th\infty} = H_{th}.\left(1 + C_p\right) \tag{2.31}$$

where, C_p is the Pfleiderer’s correction factor. C_p is used as a value which lies between 0.25 and 0.35 in preliminary calculations, [1]. Then Equation (2.30) becomes:

$$U_2 = \frac{V_{m2}}{2\tan\beta_2} + \sqrt{(\frac{V_{m2}}{2\tan\beta_2})^2 + gH_{th}.\left(1 + C_p\right)} \tag{2.32}$$

Determining β_2 is an iterative procedure. Firstly the β_2 and C_p is assumed. The meridional velocity at the blade exit, $V_{m2,}$ is used which is calculated before with Equation (2.22). Second step is calculating the C_p value with the formula given as, [1]:

$$C_p = \frac{d_2^{\,2}.\psi}{4.z.M} \tag{2.33}$$

M is the static moment of the midstreamline. In order to calculate the static moment of the midstreamline, it is divided into m segments. The moments of each segment with respect to the rotation axis of the impeller are calculated by simply multiplying of the length of each segment with the perpendicular distance to the rotation axis of the impeller. Figure 2.15 shows the static moment calculation in schematic form as explained above.

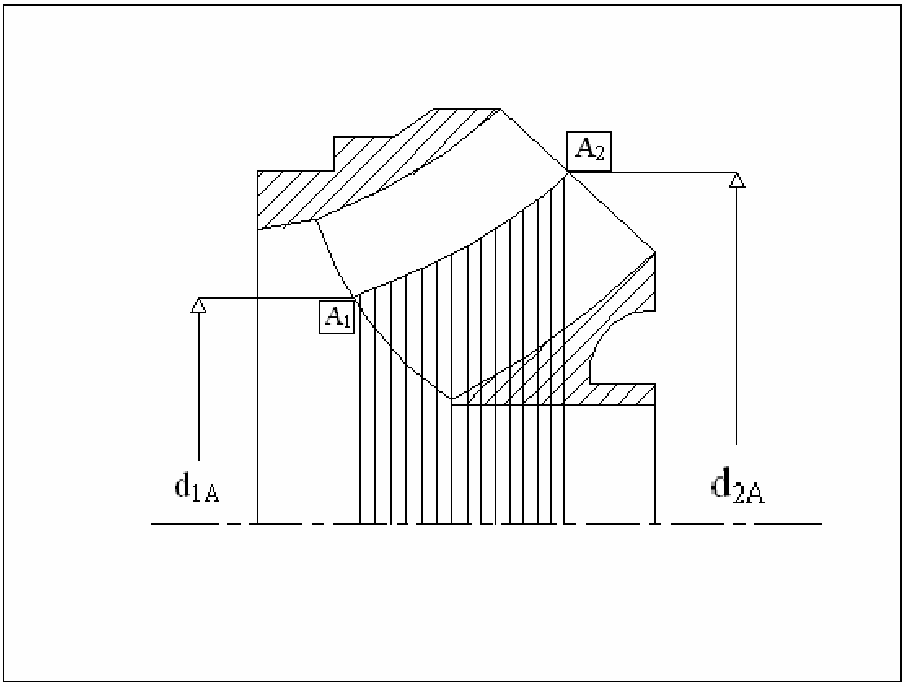

Figure 2.15 – Schematic representation of static moment calculation for midstreamline A_1A_2

The coefficient, ψ, is given in Reference [1] for blades of double curvature:

$$\psi = (1-1.2).(1+\sin\beta_2).(\frac{d_{1A}}{d_{2A}}) \tag{2.34}$$

When Equation (2.34) is substituted into Equation (2.33), then Equation (2.33) becomes:

$$C_p = \frac{d_2^{\,2}.(1-1.2).(1+\sin\beta_2).(\frac{d_{1A}}{d_{2A}})}{4.z.M} \tag{2.35}$$

Two equations which are Equations (2.32) and (2.35) with two unknown parameters which are C_p and β_2 are solved iteratively because of the complexity of the equations. After determining the β_2 value, φ_2 is checked in order to validate the assumption made to calculation of the blade exit area with blade thickness, A_2, calculated in Equation (2.21). The correction of φ_2 is made by using β_2 and calculating the thickness along the outer radius of the impeller, s_{u2}. The formula is given by, [1]:

$$s_{u2} = \frac{s_2}{\sin\beta_2} \tag{2.36}$$

Then φ_2 is calculated using the value of arc length between adjacent blades on the outlet of the impeller, t_2 as, [1]:

$$t_2 = \frac{\pi.d_2}{z} \tag{2.37}$$

φ_2 is calculated with the formula, [1]:

$$\varphi_2 = \frac{t_2}{(t_2 - s_{u2})} \tag{2.38}$$

If the assumption for φ_2 is not correct, the procedure started with Equation (2.21) down to Equation (2.38) is repeated again in order to correct the φ_2 value.

The blade number, z, check is made with the equation, [1]:

$$z = 13.\frac{r}{e}.\sin(\frac{\beta_1 + \beta_2}{2}) \tag{2.39}$$

The r value in Equation (2.39) is the mean radius of the mid-streamline and e value is the arc length of the mid-streamline. The value of e is taken from the designed impeller layout and r value is calculated as:

$$r = \frac{M}{e} \tag{2.40}$$

If the blade number calculated with Equation (2.39) is close to the value assumed before, the preliminary design is completed. However if the value of z is different then the assumed value, the resultant value of the Equation (2.39) is used in order to correct the design. In case of the resultant value of the blade number being not an integer, the decision of the blade number is made by depending on the experience of the designer. The blade number is adjusted by concerning the blade shape and swirl of the blade which is the angle between the start point of the streamline and the end point of it. The production point of view should be considered while making the decision of blade number. The later steps described in point by point method is followed and velocity distributions should be examined while making the decision of the blade number.

2.2.3 Shaping the Blades of Impeller

There are several methods in the literature for shaping the blades of the impeller. In this study, point by point method which is introduced by C. Pfleiderer is used. The blade of the impeller is shaped by adjusting the distributions of the velocity components from leading edge to the trailing edge of the blade. Nevertheless, the blade angle distribution should be checked from leading edge to trailing edge of the blade. The distributions are adjusted in order to find out better blade angle distribution or stacking condition on the blade exit. The stacking condition is the position of the blade at trailing edge from hub to shroud. The impellers that are produced in the company have different configuration of stacking conditions. However, in this study the stacking is adjusted by means of following the linear distribution of relative velocity from leading edge to trailing edge for each streamline that are used in the design. The distributions by means of relative velocity, meridional velocity and blade angle for mid-streamline A_1A_2 is shown in the following Figure 2.16.

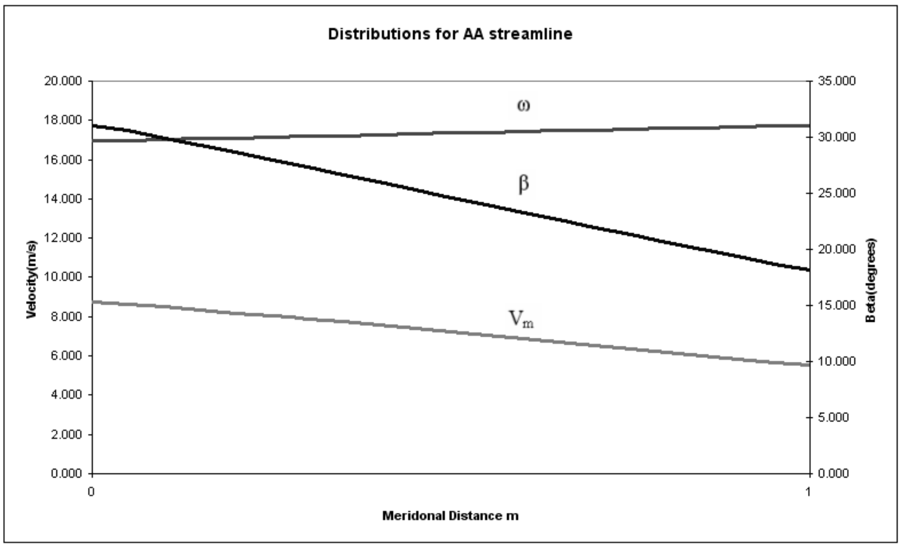

Figure 2.16 – The distributions of relative velocity, meridional velocity and blade angle for mid-streamline A_1A_2

The designed impeller blade represented with midstreamline A_1A_2 from top view is shown in Figure 2.17. The swirl angle which is between the starting point and end point of the midstreamline is seen also in Figure 2.16.

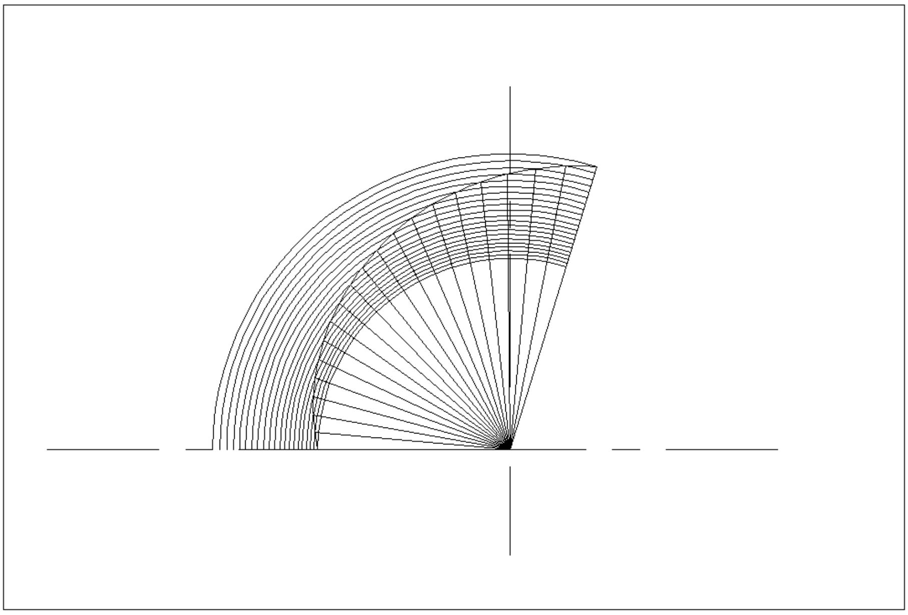

Figure 2.17 – Designed impeller blade showing found midstreamline A_1A_2 from top view

2.3 Design of the Bowl

The main function of the bowl used in vertical turbine pump that is designed in this study is, changing the direction of flow of the liquid leaving the impeller and directing the flow along the axis of rotation. However while changing the direction of flow; the design should minimize the losses inside the bowl. In order to satisfy this need, the bowl should be designed not too long that may increase the friction losses and not too short that may cause the flow not to be directed properly to the second stage.

The length of the bowl is also important from the manufacturing point of view because of the raw material used in the casting. The bowl layout used in the design is shown in Figure 2.18.

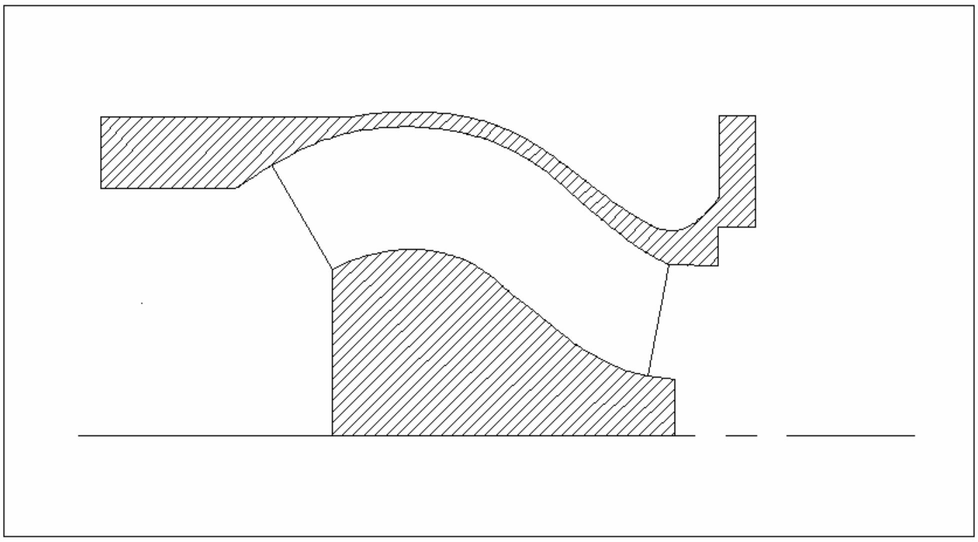

Figure 2.18 – The bowl layout used in the bowl design

Firstly the bowl inlet and outlet breadth dimensions are checked. "The breadth of the diffuser at the inlet is about 10% larger than the breadth of the impeller.", [1]. The purpose of this adjustment is placing different impellers of a pump family into the same bowl. However in this study the length of the inlet breadth of the bowl vane, b_3, is selected close to the exit breadth, b_2 of the impeller because of not concerning a pump family. The exit breadth of the bowl vane, b_4, is adjusted to the inlet breadth of the impeller, b_1. The schematic representation of two stage pump assembly is shown in Figure 2.19.

While designing the outlet part of the bowl especially the exit flange of the bowl, the clearance is also adjusted. The clearance is important from the assembling point of view of the pump. However the gap between the exit of the bowl vane and leading edge of the impeller blade should be taken as small as possible in order to get close to no inlet whirl assumption in the impeller blade design.

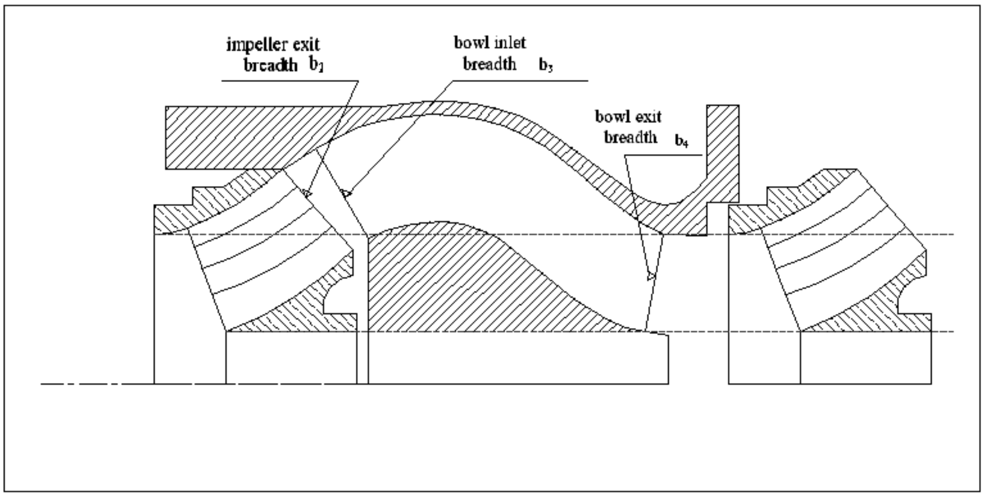

Figure 2.19 – Schematic representation of two stage pump assembly

The mid-streamline is drawn with the same method which is also followed while designing the impeller that is given in Reference [1]. The midstreamline A_3A_4 is shown in Figure 2.20.

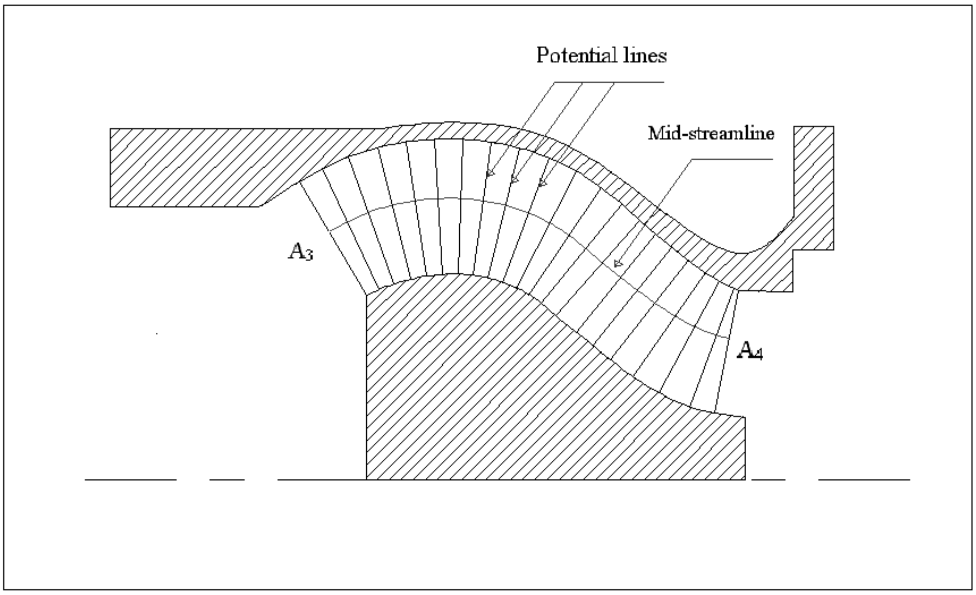

Figure 2.20 – Midstreamline A_3A_4 and potential lines for the design of the bowl vane

The mid-streamline is divided into segments of equal length Δs and potential lines are drawn. The potential lines are the arc segments where the axial component of the absolute velocity, V_y, is along the normal of the surfaces obtained by revolving these potential lines around the axis of the bowl. The potential lines are also shown in Figure 2.20.

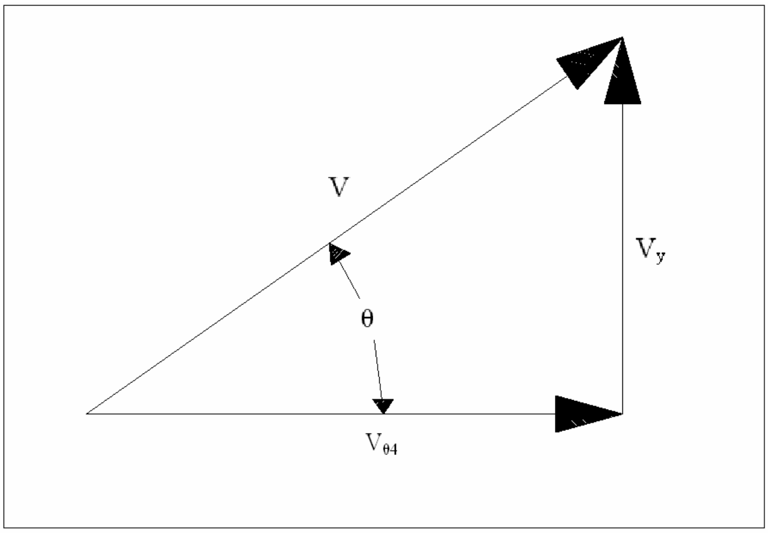

Figure 2.21 – Velocity vectors for the vane inlet of the bowl

The tangential component of the velocity at the blade exit for the flowing fluid, $V_{\theta 3}$, as shown in Figure 2.21 is calculated as:

$$V_{\theta 3} = \frac{V_{\theta 2}}{(1 + C_p)} \tag{2.41}$$

The fluid angle leaving the impeller, θ_3, is calculated by:

$$\tan \theta_3 = \frac{V_{m2}}{V_{\theta 3}} \tag{2.42}$$

The arc length between adjacent vanes of the bowl for inlet, t_4 is calculated as, [1]:

$$t_4 = \frac{\pi . D_s}{z_b} \tag{2.43}$$

where D_s is the diameter of the streamline and z_b is the vane number of the bowl.

The vane inlet angle, θ_4, is calculated using the formula, [1]:

$$\tan \theta_4 = \tan \theta_3 . \frac{t_4}{(t_4 - \frac{s_v}{\sin \theta_3})} \tag{2.44}$$

where, s_v is the vane thickness of the bowl. Constant vane thickness of 4 mm is taken for the bowl vane in the bowl design. The thickness along the direction of the flow for the inlet of the bowl, s_{u3}, is calculated as:

$$s_{u4} = \frac{s_4}{\sin \theta_4} \tag{2.45}$$

The inlet constriction coefficient of the bowl, φ_4, is calculated with the formula, [1]:

$$\varphi_4 = \frac{t_4}{(t_4 - s_{u4})} \tag{2.46}$$

The axial component of the absolute velocity, V_y, is calculated using the formula:

$$V_y = \frac{Q}{A_4}.\varphi_4 \tag{2.47}$$

A_4 is the net area obtained by revolving the bowl inlet vane breadth around bowl center axis. The tangential component of the absolute velocity, $V_{\theta 5}$ is calculated by the formula given as:

$$V_{\theta 4} = \frac{V_y}{\tan\theta_4} \tag{2.48}$$

The point by point method is followed for shaping the vane of the bowl. Since the flowing liquid enters the impeller in the second stage with no inlet whirl condition, the flow is in the direction of axis of rotation which means the tangential component of the absolute velocity, $V_{\theta 5,}$ should be zero at the exit of the bowl vane. The vane of the bowl is shaped by considering the distribution of V_θ through out the equal distanced segments from inlet to outlet. The distribution of V_θ is adjusted by the designer by looking at the previous designs by considering the specific speed and the flow rate of the design point of view. On the other hand, the distribution of V_θ between the inlet and exit of the bowl vane is adjusted by considering the swept angle. Swept angle is the angle between the inlet and outlet of each streamline between the inlet and outlet from the top view. The main reason of considering the swept angle is due to manufacturing. If the swept angle is relatively high, the placement of the patterns may not be possible while preparing the core of the bowl.

The comparison of high and low swept angle phenomena is related to the size and specific speed of the pump to be designed. The swept angle is kept constant for the remaining streamlines through out the design and tangential component of the velocity distributions for these streamlines are adjusted in order to fulfill this requirement. The same procedure starting from Equation (2.41) to (2.48) is followed for the remaining streamlines in order to shape the vane of the bowl.

2.4 Design of the Suction Intake

The suction intake for a multistage pump has two main functions, [3]. The first one is the mechanical purpose which is supporting the bearing housing for the shaft at the lower end of the pump. The strainer or suction pipe is attached to the suction intake in different applications. In this study, the standard strainer is attached to the suction intake in order to prevent big size particles to get into the pump. The second function of the suction intake is building up a hydraulic passage before the impeller inlet eye in order to increase the fluid velocity gradually with the proper area change. In this study, the suction bell is designed for the intake element of the pump. “A conservatively designed high specific speed pump has a suction bell diameter large enough so that the inlet velocity is from 1.4 to 1.5 m/s”, [3]. The velocity at the inlet of the suction bell is taken as 1.4 m/s and the area distribution is adjusted from suction bell to the impeller inlet eye. The designed suction bell is shown below in Figure 2.22. In order to visualize the area distribution, the height of the suction bell from inlet to the outlet is divided into 10 equal segments and area distribution is shown in Figure 2.23.

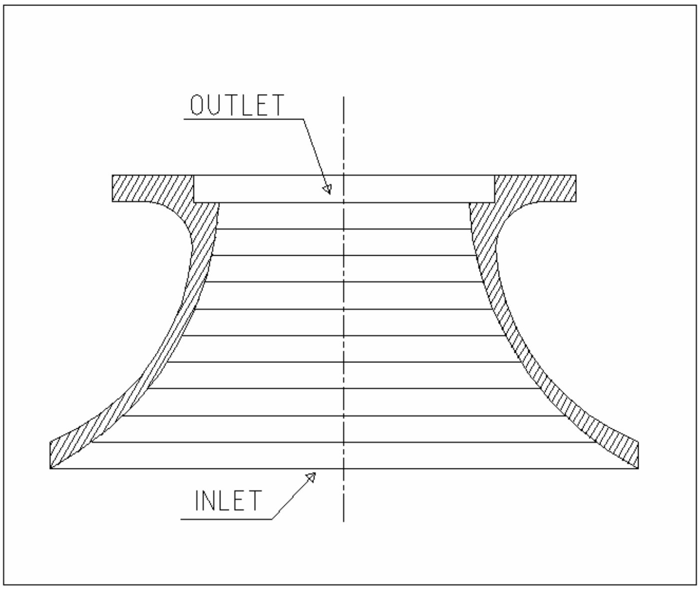

Figure 2.22 – Suction bell

The area distribution of suction bell is adjusted in order not to disturb the flow from inlet to the exit of suction bell as seen in Figure 2.23.

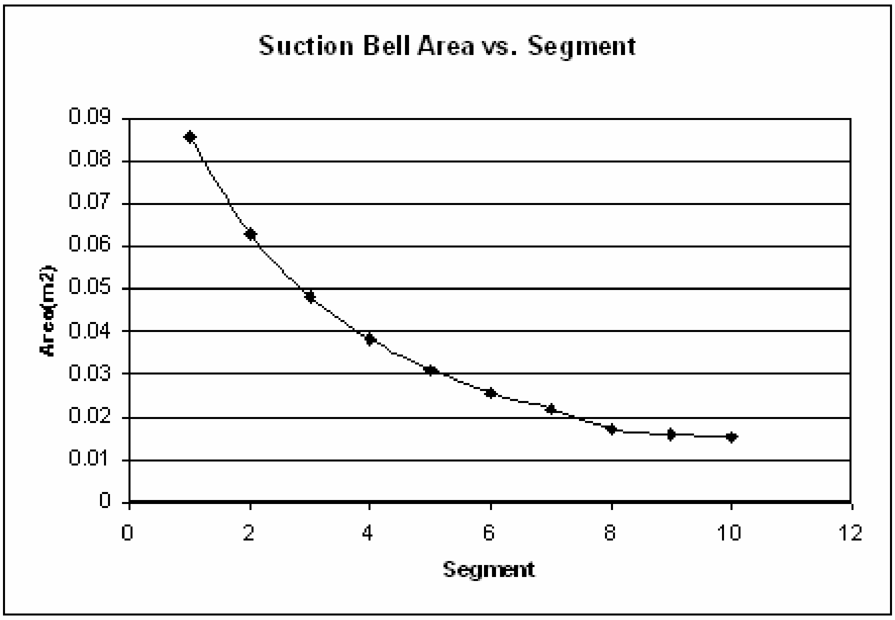

Figure 2.23 – Area distribution of the suction bell

2.5 Production of the Pump

The design of the pump is completed by the preparation of the patterns, core boxes, cores and machining drawings. All parts of the pump that are designed in this study except the pump shaft are manufactured from cast parts. Therefore the cores and the core boxes for the parts are prepared. The CAD models which are prepared for CFD analyses are used to prepare the core boxes of the parts that are designed. In order to prepare the core boxes of the impeller and bowl, the cores of the single flow passage for each part are modeled. In order to properly produce the core boxes, the surfaces of the parts that will be machined are determined. The machining thicknesses are added to these surfaces. Moreover, the models are scaled up in the amount that casting material requires due to shrinkage. The taper angles are given to the necessary surfaces depending upon on the direction which the core would be taken out. The single core that represents the single flow pattern of the impeller and the core assembly which forms the impeller are seen in Figure 2.24.

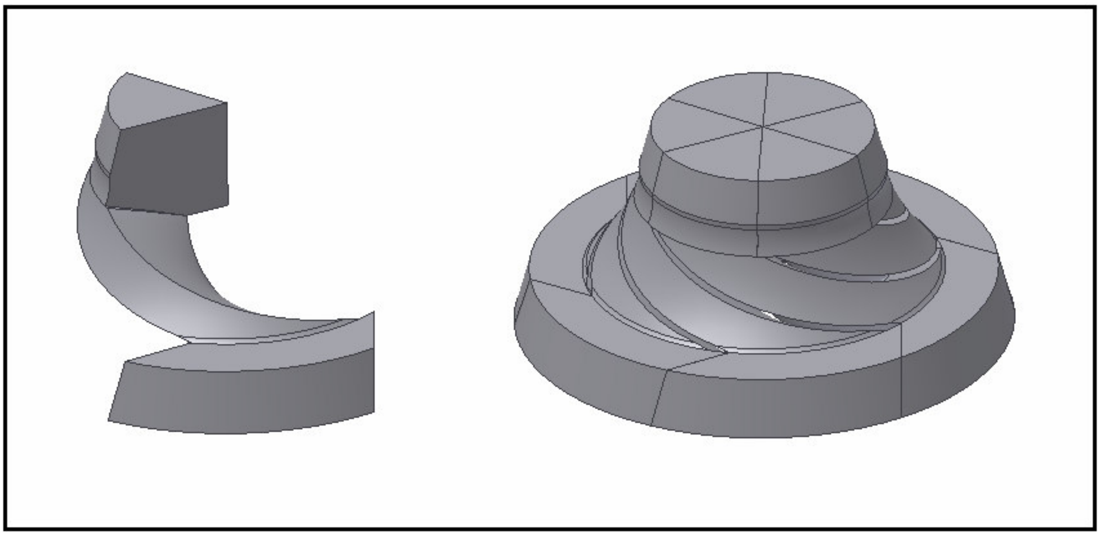

Figure 2.24 – Single core and core assembly of the impeller

The same configuration for the bowl is shown in Figure 2.25.

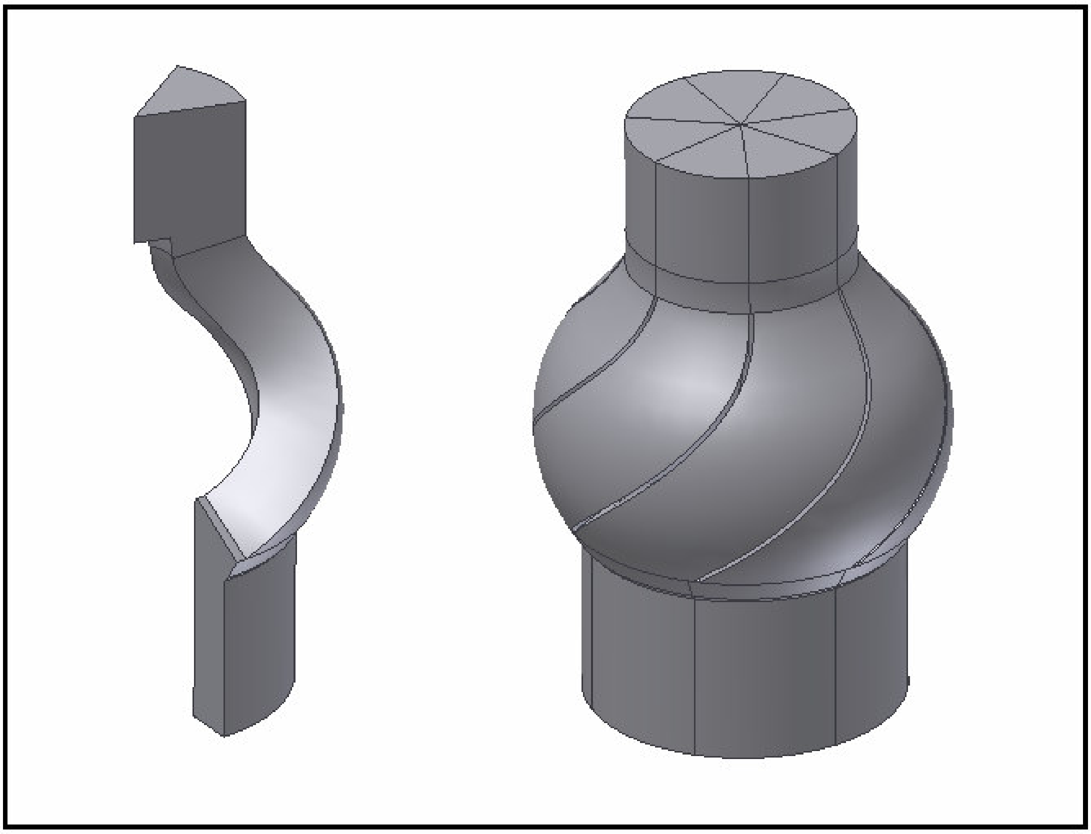

Figure 2.25 – Single core and core assembly of the bowl

After both cores for the impeller and bowl are modeled the core boxes are modeled by using these components. The core boxes are machined using the CAM process and numerical codes are prepared by the manufacturing department of the company. The core boxes of the impeller and bowl are shown in Figures 2.26 and 2.27, respectively. The photographs of cores and core boxes for impeller and bowl are given in Appendix A.

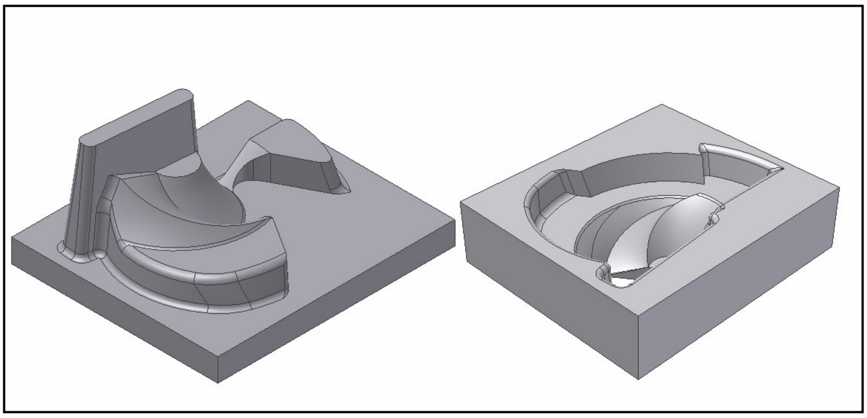

Figure 2.26 – Core box of the impeller

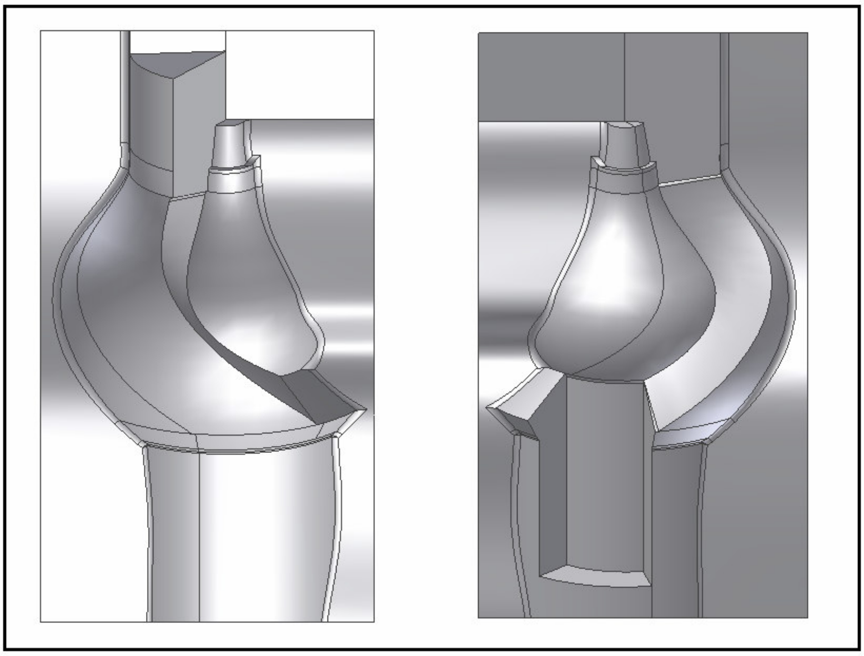

Figure 2.27 – Core box of the bowl

The cores are produced by using the core machine where the core boxes are used. The produced cores are assembled together and the casting is made.

CHAPTER 3

CFD ANALYSES OF THE PUMP

3.1 General Information on CFD Analyses and Software

In order to shorten the design periods and lowering the manufacturing, prototyping and test costs of the pump, a commercial Computational Fluid Dynamics (CFD) software is used in the design procedure. The main aim of this study by means of applying numerical experimentation to the designed pump is CFD code integration into the design procedure and verification of the design before the pump is produced. The CFD code is used to obtain pump characteristics curves such as head vs. flow rate and efficiency vs. flow rate. In deed, investigations of the internal flow structure are also performed in order to correct the design and obtain better performance characteristics from the designed pump. The flow inside the impeller and bowl is studied by using the capabilities of CFD code used in the company such as pathline traces, velocity vector representations, and physical quantities such as pressure and velocity distributions inside the pump which are explained in the following parts of Chapter 3. However, before the CFD software is integrated into the design procedure, the verification of the code is done by applying CFD analyses to the previously designed pumps. The comparison of the CFD results is made with the calibrated and certified test stand of the company.

The conventional design and CFD integrated design procedures are shown in Figure 3.1. The CFD code is used as a tool in the design and verification of the physical quantities are cross checked with the design parameters.

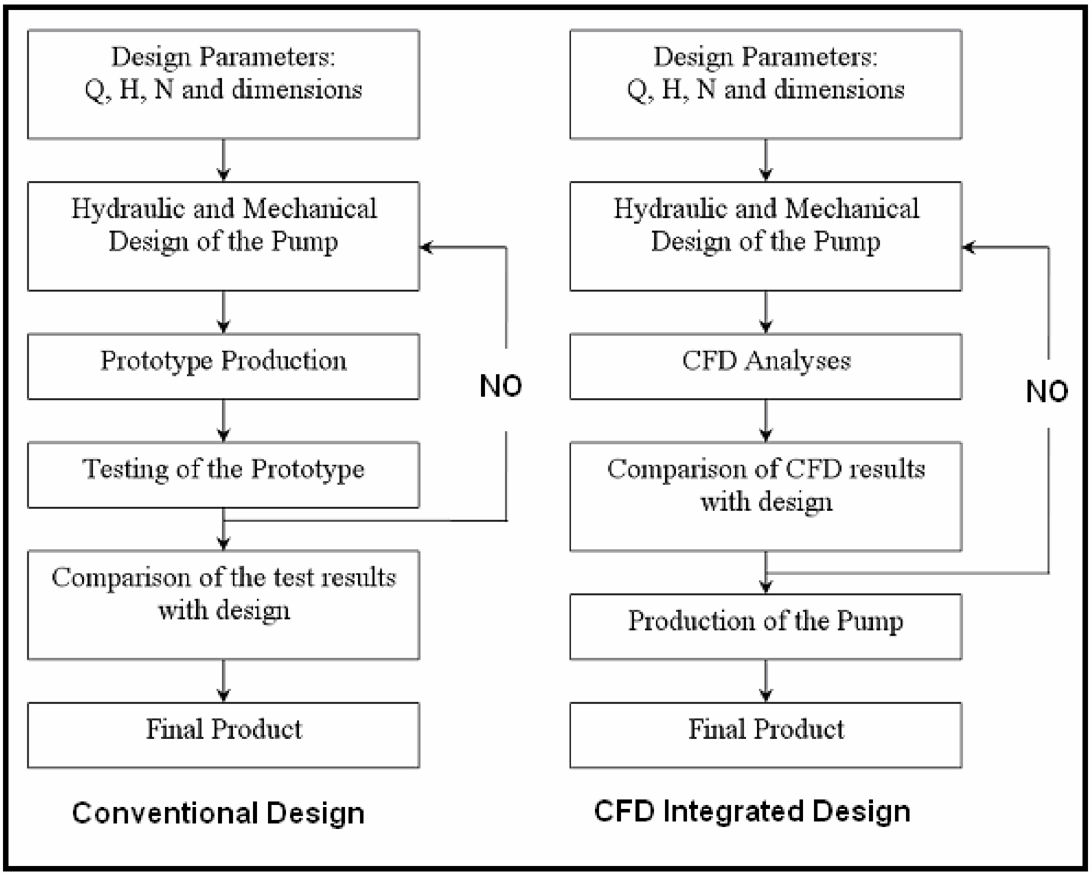

Figure 3.1 – Conventional and CFD integrated design procedures

In the conventional design procedure, the pump is designed for the design parameters which meet the customer needs. During the design procedure, the designer evaluates the necessary parameters within the experience coming from the previous studies. After the design is completed, the prototype is produced in order to validate the design. Simply, if the pump characteristics that are found in the experiments are different then the desired characteristics in the design, the design is renewed and best performance characteristics of the pump is tried to be achieved. If the flow rate or head of the pump is close to the desired operating point, it is possible to adjust the pump characteristics in the manufacturing step by means of impeller diameter reduction, underfiling or better surface finish operations. Nevertheless, if the best efficiency is not met by the designed pump, it is a must to renew the design in order to get the desired efficiency. However those operations may increase the design periods and overall costs of the pump.

When the CFD software is integrated into the design procedure, the designer may use the code as a tool in the design. After designing the pump, CFD analyses are performed and the best performance characteristics may be achieved without producing the prototype if the code is validated by the experimental results. Since CFD code is a tool in the design step, the verification should be done in each case study and the behavior of the code should be investigated for different types of the pumps by means of specific speed, flow rate and geometry.

The pump that is designed in this study is analyzed by using two different CAD models of the impeller. The first one is the impeller with designed blade and the second one is the impeller with underfiled blades. "For best results with pump design it is very important that the vane trailing edge be made as thin as possible", [19]. The underfiling operation frequently increases the efficiency and head at the best efficiency point of the pumps that are previously designed and tested in the company.

Commercial CFD software solves 6 equations which are mainly conservation of mass, conservation of momentum in three principle directions, energy equations apply to the laminar as well as turbulent flow and turbulence equations. The solution of these equations involves an iterative procedure and requires great deal of elements in order to properly model the flow. Nevertheless, the computing power is an important fact in CFD analyses both for modeling the flow geometry and solving the equations. A desktop PC which has a Pentium 4 3.2 GHz processor with 2 GB RAM in 32 bit environment is used for the analyses. The memory of the computer involves in modeling of the flow geometry which is related to grid size and solution speed is proportional to the clock speed of the processor. Computers with faster processors and high capacity of memories may shorten the analyses solution periods. However the analysis strategy is playing a major role in shorten the solution periods. The instabilities occurring during the analyses are directly affected by the improper grid size and flow geometry. The turbomachinery CFD solutions are one of the difficult solutions in CFD because of the nature of the flow and complexity of the geometries.

CFdesign V7 and V8 are used in CFD analyses. CFdesign solves time averaged governing equations which are stated above. “In CFdesign, the finite element method is used to reduce the governing partial differential equations to set of algebraic equations”, [13]. “CFdesign uses the finite element method primarily because of its flexibility in modeling any geometrical shape”, [13]. Since the geometry of the pump is very complex, the code is chosen for the analysis tool in the company.

The solution algorithm of CFdesign is based on Semi Implicit Method for Pressure Linked Equations Revised (SIMPLE-R).

The automatic mesh generator and diagnostics in mesh generation is used in CFdesign. Diagnostics module shows the solid model parts where problems may occur during the mesh generation. The quadrilateral, triangular, tetrahedral, hexahedral, wedge and pyramid elements are available in CFdesign mesh generator module for the analyses of fluid flow, [13]. The boundary layer is controlled by the boundary layer thickness factor located in the mesh enhancement module of CFdesign. The thickness of the layer near the wall and the number of layers within this layer may be adjusted. “Mesh Enhancement is a great feature that considerably simplifies the mesh definition process. Mesh Enhancement automatically constructs layers of prismatic elements (extruded triangles) along all walls and all fluid-solid interfaces in the model, based on the tetrahedral mesh that is defined. These additional elements serve two primary purposes; elements are concentrated in the boundary layer region, where high velocity, pressure, and turbulence gradients most often occur and enough nodes are automatically placed in all gaps (area between walls) in the model.”, [13].

The RNG model, low Reynolds k-epsilon model, k-epsilon model and Eddy Viscosity models are available in CFdesign. The k-epsilon model is used in this study. The reason of using k-epsilon model is; it is typically more accurate than the constant eddy viscosity and constant eddy viscosity is recommended for lower speed turbulent models, [13].

In deed, the RNG model works best for predicting the reattachment point for separated flows, particularly for flow over a backward-facing step, [13]. The recent studies are showed that k-epsilon model works fine in CFD pump applications.

3.2 Steps of the CFD Analysis

3.2.1 Solid Modeling

The design parts are modeled by using Mechanical Desktop 2007. The important point while modeling the parts is working clearly in order not to face with any problems during the CFD analyses. The problems may occur during the grid generation if any unwanted surfaces or solid parts left during the solid modeling.

CFdesign has a CAD modeler module which makes cut and boolean operations. The inner fluid structure of the pump is automatically obtained by closing the exit flange of the bowl and lower part of the suction of the pump with proper extensions. These extensions simulate the part of suction reservoir on the lower part of the pump and discharge pipe on the upper part of the bowl. In the analyses of turbomachines, the impeller flow field calculations are performed within the relative reference frame in CFdesign, [13]. The relative reference frame rotates with the rotating device. The rotating region is formed around the rotating device which is the impeller in this study. The gap between the impeller and bowl where the volumetric losses are occurred is closed during the analyses. For this reason the volumetric efficiency is not calculated in this study. The rotating region (a), upper (b) and lower (c) extensions are shown schematically in Figure 3.2.

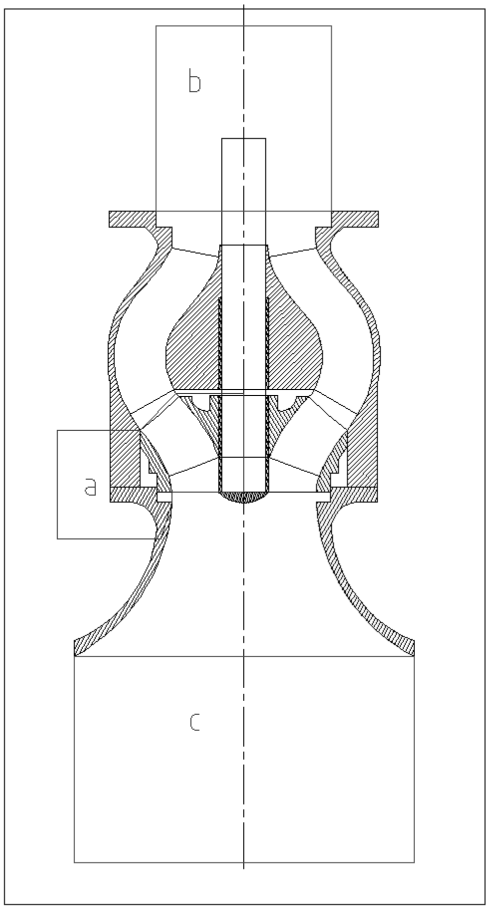

Figure 3.2 – Figure showing the extensions and rotating region for CFD analysis in the section view representation of the pump

The solid models are kept as simple as possible in order to simplify the analyses. Nevertheless the parts which are suction bell, impeller and bowl are modeled in their original forms in order not to disturb the hydraulic performance of the pump to be simulated in CFD. The solid models are shown in Figure 3.3.

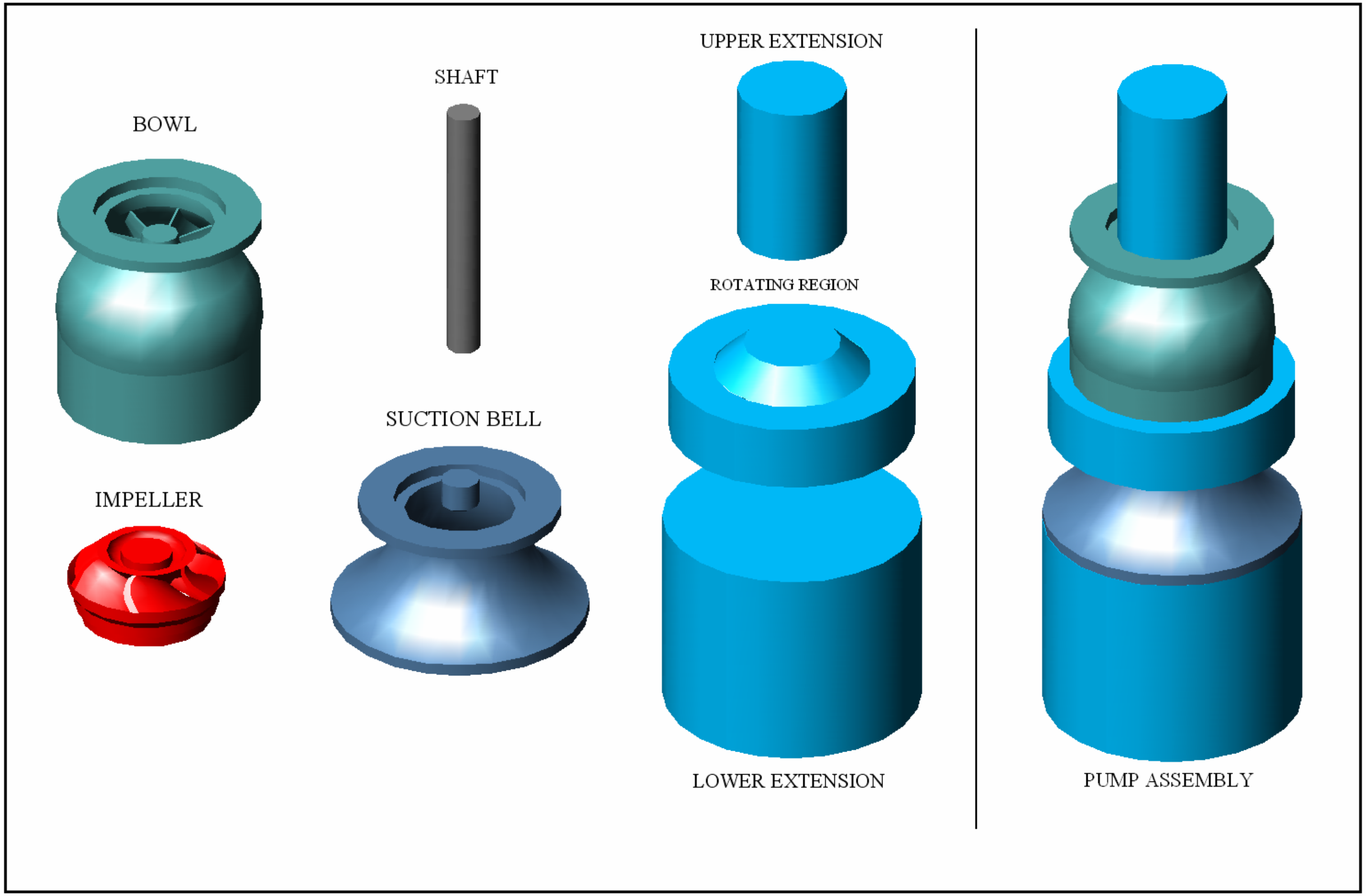

Figure 3.3 – Solid models prepared for the pump and pump assembly

The solid parts are assembled together for the analysis as shown in Figure 3.3. The CAD data is then translated as ACIS file format for the CFD analysis. The ACIS format is a universal CAD file format. The prepared file is launched with CFdesign. The converted CAD data is seen in CFdesign screen as shown in Figure 3.4. The control of cleanness of the data is made by investigating the volumes and surfaces by the user in CFdesign. If any unwanted surfaces or volumes are investigated, the CAD data should be overviewed and corrected in order to obtain successful analyses.

The solid model of the impeller is prepared also with underfile blade. The scope of this operation is observing the affect of underfile operation. There are different underfiling operations employed to the impeller blades. "Underfiling operation is a must in impeller blades", [19]. The CFD analyses are performed for both cases in order to compare with test results.

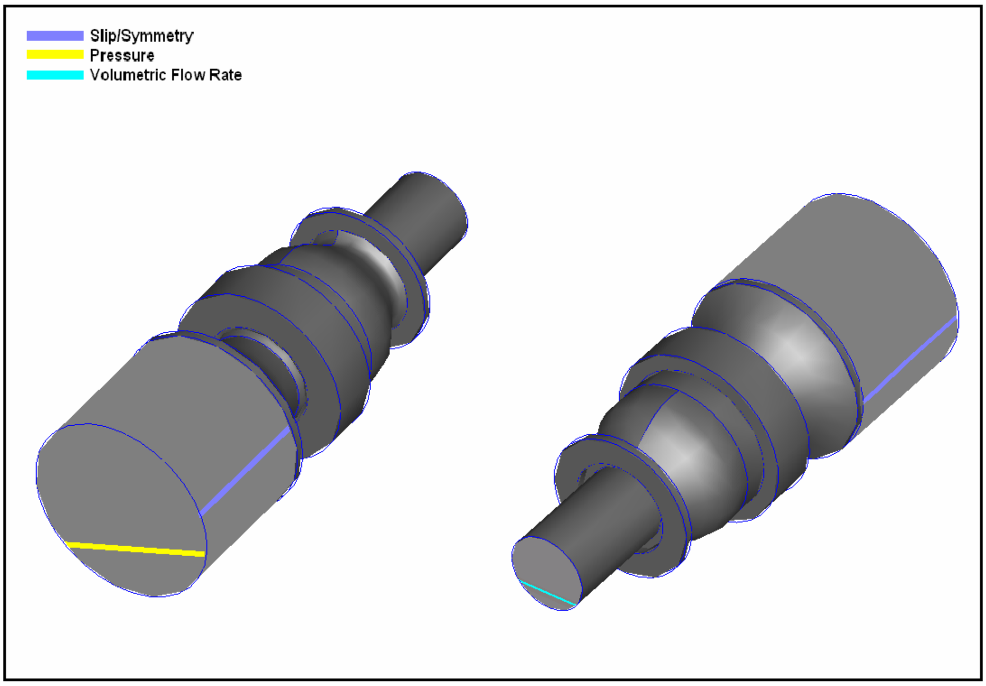

Figure 3.4 – Definition of boundary conditions

3.2.2 Definition of Boundary Conditions

The pressure rise across the inlet and outlet of the pump is aimed to be found through out the analyses. In order to find the pressure rise, the volumetric flow rate is defined at the outlet of the pump and 0 gage pressure is defined at the inlet of the pump. In real life experiments the pump is submerged into the large reservoir. Defining the slip/symmetry boundary condition to the lateral surface of the lower extension simulates this condition in CFD analyses. The pipe is connected to the outlet flange of the bowl at the upper part of the pump assembly in experiments. Thus no boundary condition definitions are applied to the lateral surface of the upper extension. The boundary condition definitions are shown in Figure 3.4.

3.2.3 Mesh Generation

The fluid structure which is formed by placing the extensions to the inlet and outlet of the pump is divided into finite elements. "Prior to running a CFdesign analysis, the geometry has to be broken up into small, manageable pieces called elements. The corner of each element is called a node, and it is at each node that a calculation is performed. All together these elements and nodes comprise the mesh (also known as the finite element mesh)", [13]. In order to achieve reliable solutions in CFD analyses the number of elements should be increased as much as possible. However when the total number of elements increased, the solution periods become longer. On the other hand, 32 bit environment does not allow using more then 2 GB of memory in the computer hardware. The mesh independency can not be investigated in the turbomachinery CFD analyses, [14]. The grid size used in this study is the result of the recent studies and completed projects with CFdesign.

The meshing strategy is simply, using smaller elements for the impeller and surrounding rotating region and increasing the element size for the other parts. The starting point of the impeller meshing is defining the element size which is closer to the impeller blade minimum thickness. The same element size is applied to the impeller and rotating region. The bowl is also meshed with an element size of the minimum bowl vane thickness. For the boundary layer simulation and meshing, default values of the software "number of layers" and "thickness factor", being 3 and 0.45 respectively, are used, [13]. The software generates 3 layers of elements in the vicinity of walls into a gap having a height of 0.45 times the original element size assigned to that region, [13].

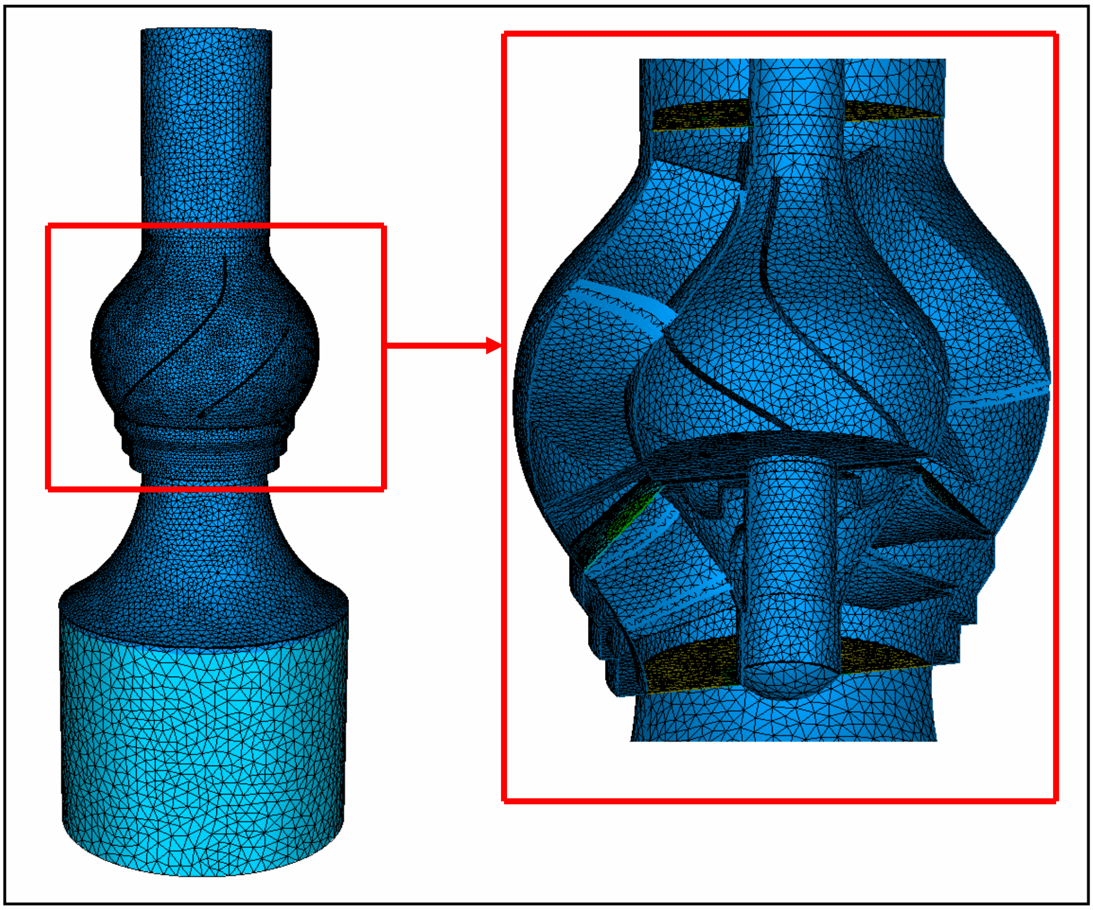

Figure 3.5 – Generated mesh for the designed pump.

3.2.4 Material Assignment

The materials are assigned to the parts where the CFD calculations are performed. The water is assigned to the volume inside the bowl and suction intake, the lower and upper extensions. Impeller is selected as a solid material in which the torque calculations are performed. Nevertheless the volume surrounds the impeller is selected as rotating region. While defining the rotating region, the known rotational speed and axis of rotation are defined. The assigned materials are shown in Figure 3.6.

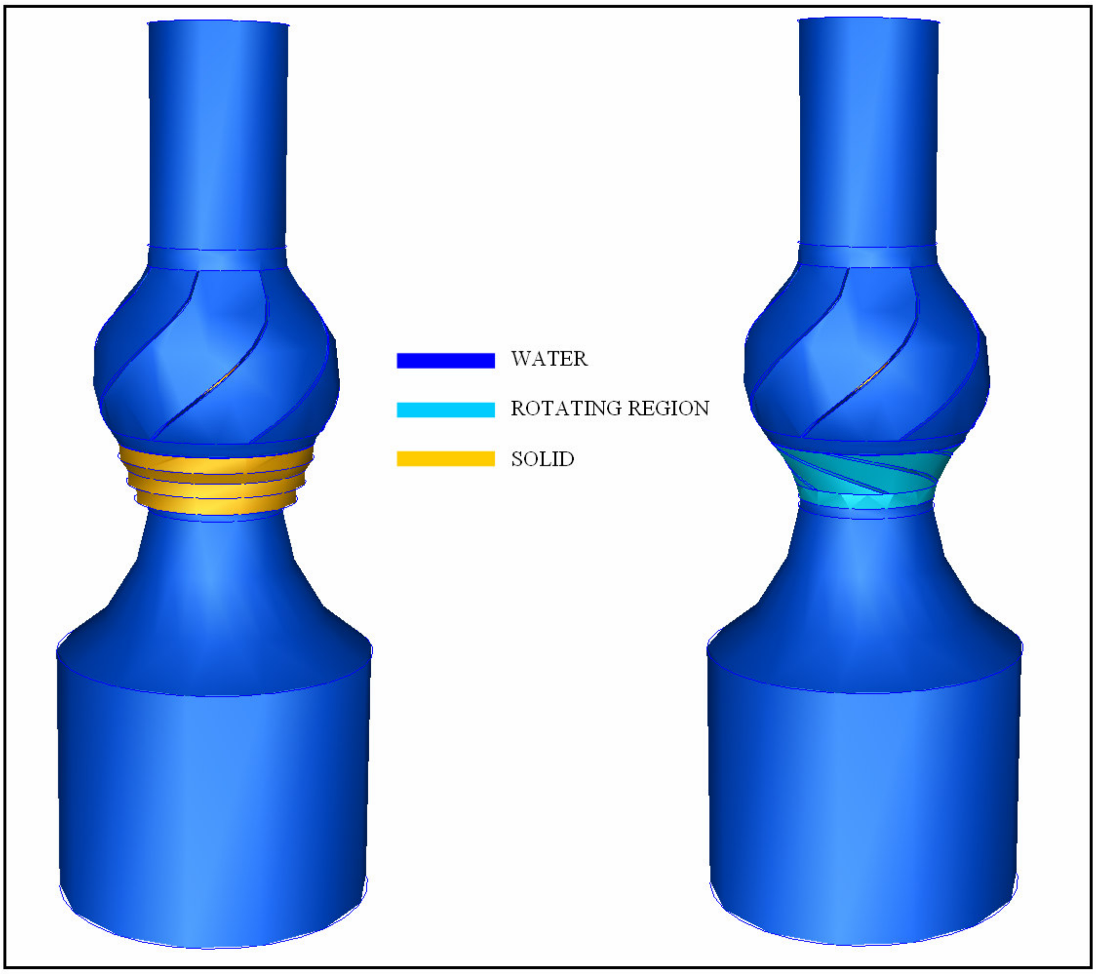

Figure 3.6 – Material assignment for the designed pump.

3.2.5 Analysis Setup

The incompressible flow is automatically selected by the software when the water material is assigned to the volumes. Since the analysis is using relative reference frame by rotating region, transient analysis is also switched on. Single iteration for the analysis is performed for the 3 degrees of rotation of the impeller, [13]. Each analysis is run for 680 iterations. The convergence monitor allows following the analysis interactively and if any problems occur during the analysis, the analysis may be stopped and solution may be investigated.

3.3 CFD Analyses of the Designed Pump

The CFD analyses are performed in order to determine the hydraulic characteristics of the pump. The pump impeller is modeled for two different cases. The impeller with the designed blade is used in the Case 1 and the impeller which the underfiling operation is performed at the trailing edge of the blade is used in the Case 2. The flow inside the impeller and bowl is observed by using the post processing tools of CFdesign.

3.3.1 CFD Analyses of CASE 1

The pump is solved with 1,504,748 elements in which, 139,442 of them are fluid elements and remaining 110,306 elements are solid elements. The recent studies are showed that the total number of elements around 1.5 million used in these kinds of pumps give reliable results when they are compared with the experiment results. The pump model is solved for 6 different operating points defined by the boundary conditions. The slip symmetry on the lateral surface and 0 gage pressure on the inlet surface of the lower extension is kept same for each analysis. The analyses are performed for 2900 rpm. The volumetric flow rate boundary condition definition is changed for each analysis in order to simulate different operating points. Those volumetric flow rate values are 60 l/s, 70 l/s, 90 l/s, 100 l/s, 120 l/s and 135 l/s. The pump in Case 1 is also solved for 1450 rpm rotational speed of the impeller. The volumetric flow rate of 30 l/s, 35 l/s, 45 l/s, 50 l/s, 55 l/s and 60 l/s are defined in order to simulate different operating points at 1450 rpm. Each analysis is run for 680 iterations and each analysis takes 39 hours for single operating point.

The convergence of the analysis is followed from the convergence monitor of the CFdesign as shown in Figure 3.7. The convergence monitor shows the summary and the average value of each degree of freedom in the analysis, [13]. The pressure and velocity component in the direction of the flow at the outlet flange plane of the bowl are expected to become straight lines in order to have convergence in the analysis. The software records the results for defined intervals. The convergence is also investigated manually by taking the pressure, velocity and hydraulic torque values from cut-planes close to the outlet and inlet of the pump for these intervals. These values are taken for the saved intervals from the beginning to the end of the analysis and convergence is checked by tabulating these values. When the taken values converge the convergence assessment is done.

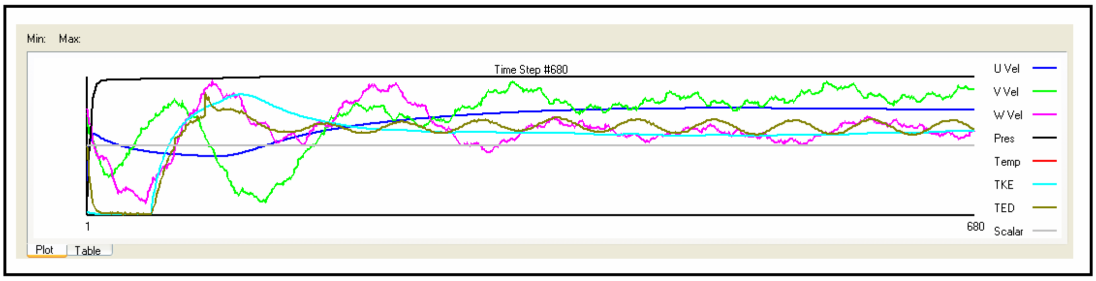

Figure 3.7 – Sample Convergence Monitor for the CFD Analysis

In order to find out the total head of the pump the Bernoulli equation is written between the cut-plane 1 and cut-plane 2 as seen in the figure.

$$\frac{p_1}{\rho.g} + \frac{V_1^{\ 2}}{2.g} + H \ = \frac{p_2}{\rho.g} + \frac{V_2^{\ 2}}{2.g} + h_e \qquad (3.1)$$

where p_1 is the pressure value and V_1 is the mean velocity in the cut-plane 1, p_2 is the pressure value and V_2 is the mean velocity in the cut-plane, h is the head of the pump and h_e is the elevation difference between cut-plane 1 and cut-plane 2 as shown in Figure 3.8.

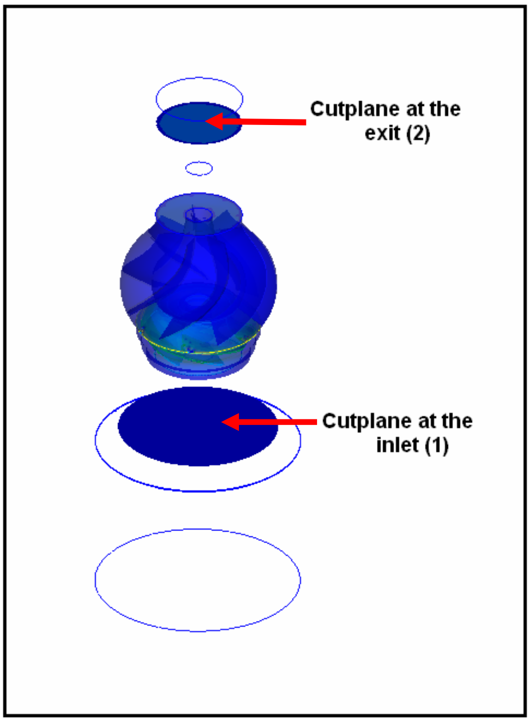

Figure 3.8 – Cut-planes used to calculated the head of the pump

The torque value is read from the CFdesign torque output file. The hydraulic efficiency of the pump is found in the analysis. The gap between the impeller and casing is closed in order not to increase the number of elements used in the analysis. Since the gap between the impeller and casing is between 0.4 to 1 mm in these kinds of pumps, it is not necessary to mesh this volume for the sake of number of elements to be used. If the gap is meshed the number of elements is exceeded to the level where 32 bit environment can handle. However the volumetric efficiency and the mechanical efficiency are used as the same values assumed in the early steps of design of the impeller in order to calculate the pump efficiency. The hydraulic efficiency is calculated by the formula given by:

$$\eta_h = \frac{\rho_{water}.g.Q.H}{T.\omega} \tag{3.2}$$

The flow in the impeller is investigated by using the velocity vector representation of CFdesign for 120 l/s at 2900 rpm. The single blade to blade passage of the impeller is investigated visually for flow separation. Since CFdesign does not have the meridional view representation, if the pump performance is lower then what is expected in the design, the flow inside the impeller and bowl is investigated by the help of post processor functions of CFdesign. If any backflows or separations occur in the impeller blade passage or bowl vane passage, the unexpected flow motion is captured by using these functions of CFdesign after the analysis is converged. The pressure side of the impeller blade is projected to the suction side of the blade. The relative velocity vectors are shown in different positions of the projected surface in Figure 3.9. In this figure the relative velocity vectors which are colored with absolute velocity values are represented.

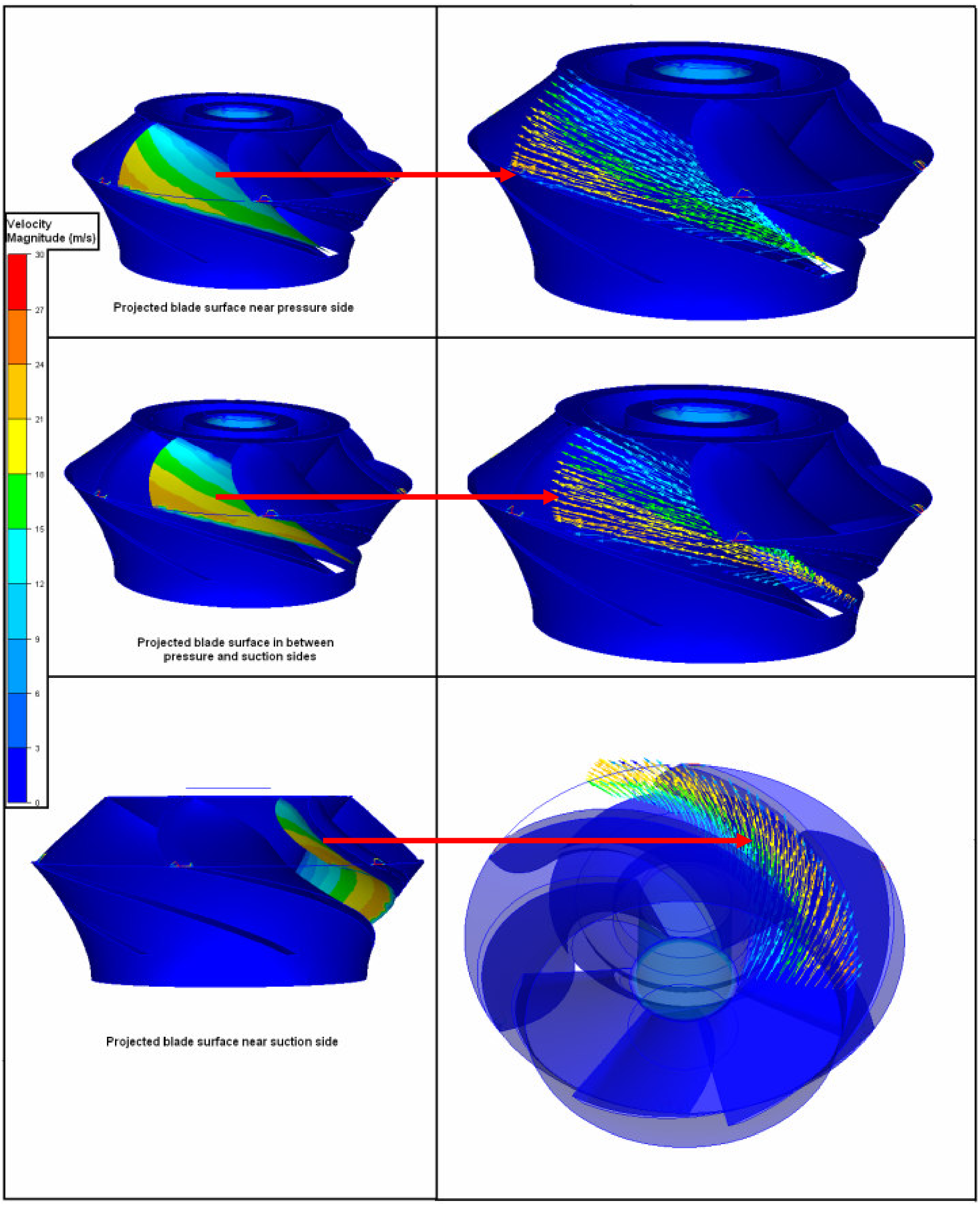

Figure 3.9 – Velocity vectors inside the impeller blade to blade section

The vectors near the hub, shroud and blade surfaces are disturbed due to wall effect however the flow is not separated within these boundaries. The pathlines are also drawn by using the trace menu of CFdesign for the same blade to blade passage of the impeller. The blade to blade passage of the impeller is shown in different views in order to visualize the flow inside it. The pathlines near the pressure side of the blade, suction side of the blade, hub and shroud side are presented. The flow is not separated inside the impeller as seen in Figure 3.10.

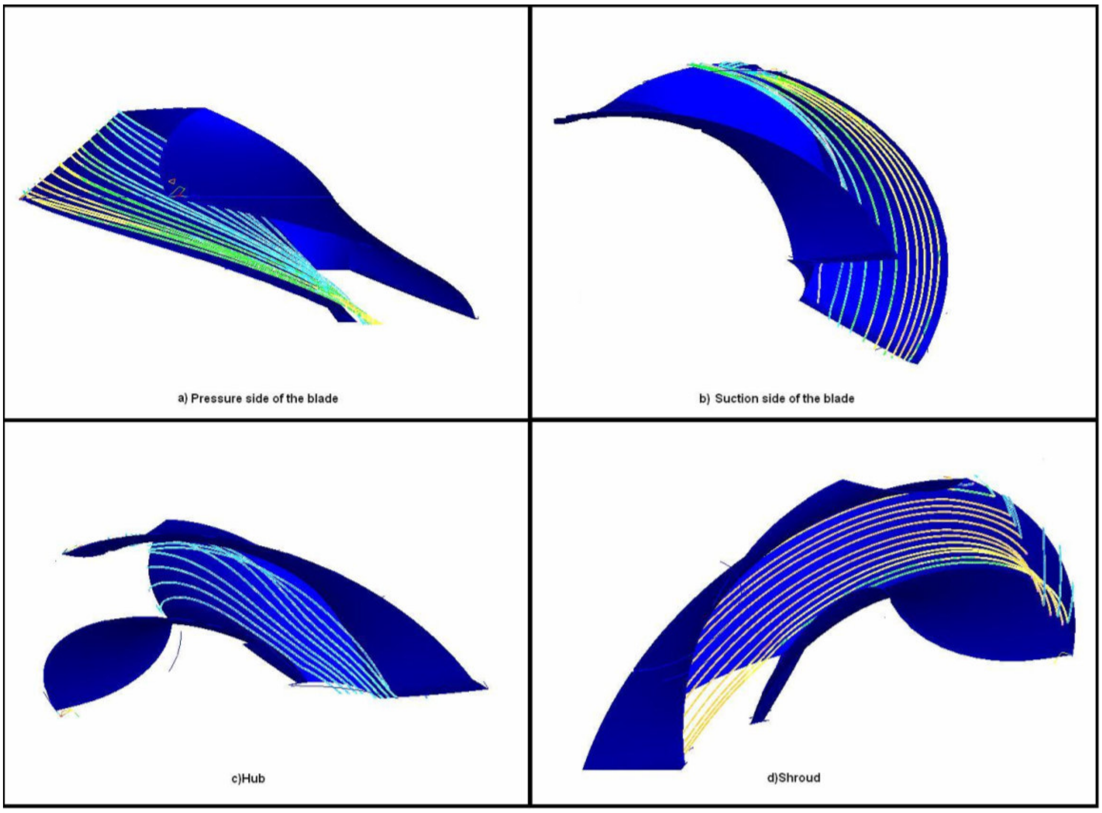

Figure 3.10 – Pathlines inside the impeller blade to blade section

The same investigation is also performed for the bowl of the pump. The absolute velocity vectors colored with pressure value is used for better visualization inside the single flow passage of the bowl. The cut-planes which are perpendicular to the rotation axis are used to perform this study and are shown in Figure 3.11.

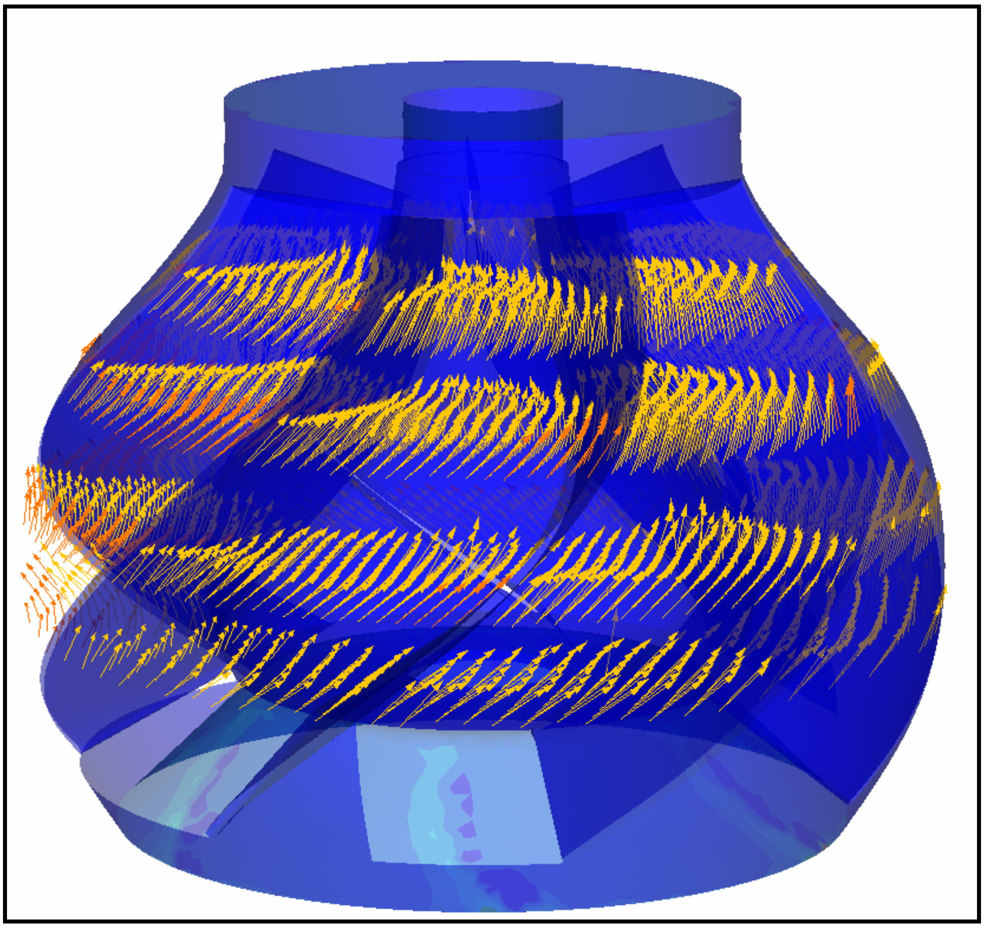

Figure 3.11 – Velocity vectors inside the bowl vane to vane sections.

The one surface of the bowl vane is projected to the other surface in order to visualize the flow inside the bowl. Figure 3.12 shows different positions of the projected surface inside the single flow passage of the bowl. One of the early experiences with a different pump shows the backflow at the leading edge of the bowl vane. It is found out that the backflow is caused by improper selection of the bowl inlet fluid angle. When the fluid angle at the leading edge of the bowl vane is corrected, the backflow is disappeared and the hydraulic efficiency of the pump is increased.

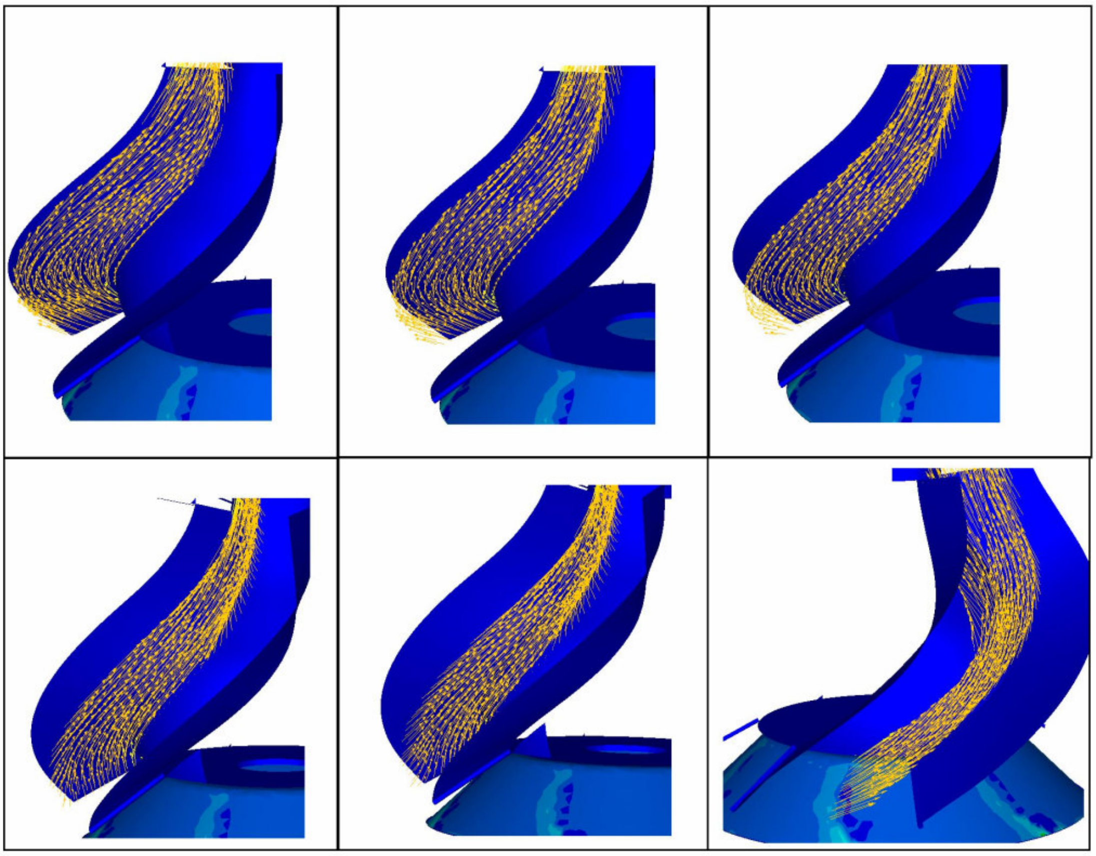

Figure 3.12 – Velocity vectors inside the bowl vane to vane section

The absolute velocity vectors colored by static pressure values are shown in Figure 3.12. From Figure 3.12 the flow separation is not seen inside the bowl. In deed the bowl is working properly and fulfills the requirement of directing the flow to the second stage with the direction along the rotation axis of the impeller. Recent studies showed that if the area distribution is not adjusted properly inside the bowl, the flow is not directed properly to the second stage. However if the area distribution is not adjusted properly, the backflow is occurred inside the bowl.

The pathlines are also traced in order to understand the flow physics better inside the bowl as shown in Figure 3.13. The investigation is made in hub, casing surfaces and the two vane surfaces of the diffuser. If any flow separation is seen, the design may be checked by simply looking at the velocity component distribution and the shape of the bowl vane layout. The continuity of the profile by means of bowl and impeller should be checked by the designer.

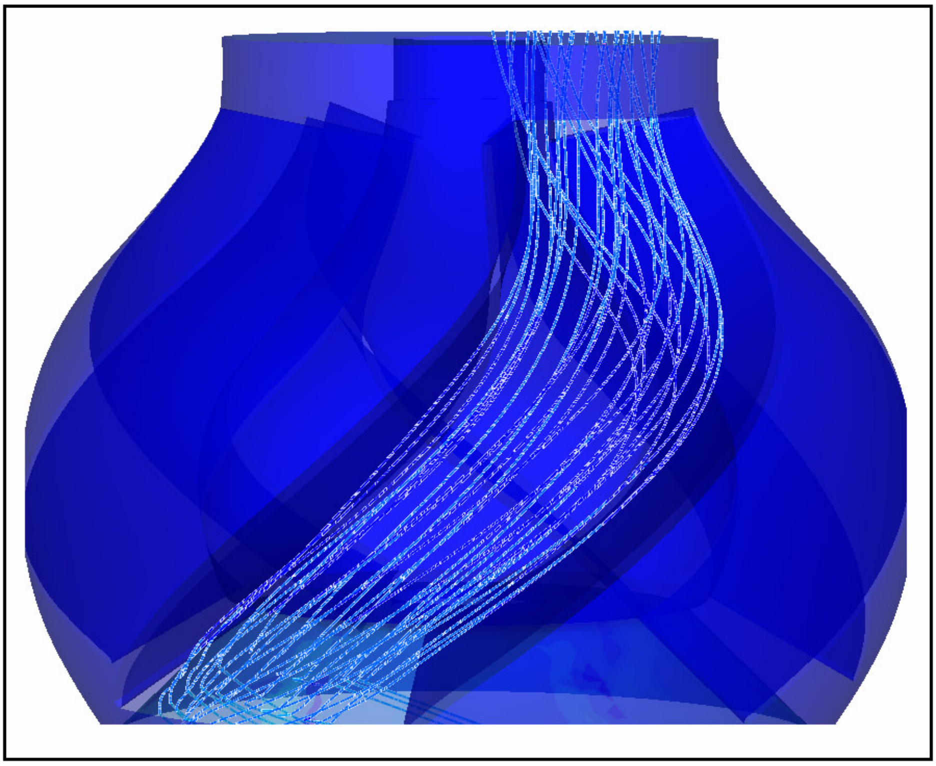

Figure 3.13 – Pathlines inside the bowl vane to vane section

From the previous studies, there are several regions where the flow can be disturbed and showed recirculation in the bowl. The first region is the vane inlet. If the flow angle is not adjusted properly at the leading edge of the vane, separation on may occur. The other region is close to the bowl outlet. If the length of the bowl and the swept angle are not adjusted properly, the flow may show recirculation. On the other hand due to formation of secondary flows in the bowl close to the bowl exit, the flow can not be directed properly to the second stage and this affects the hydraulic characteristics of the pump.

The pathlines are also seen inside the whole pump assembly from inlet to exit of the pump in Figure 3.14.

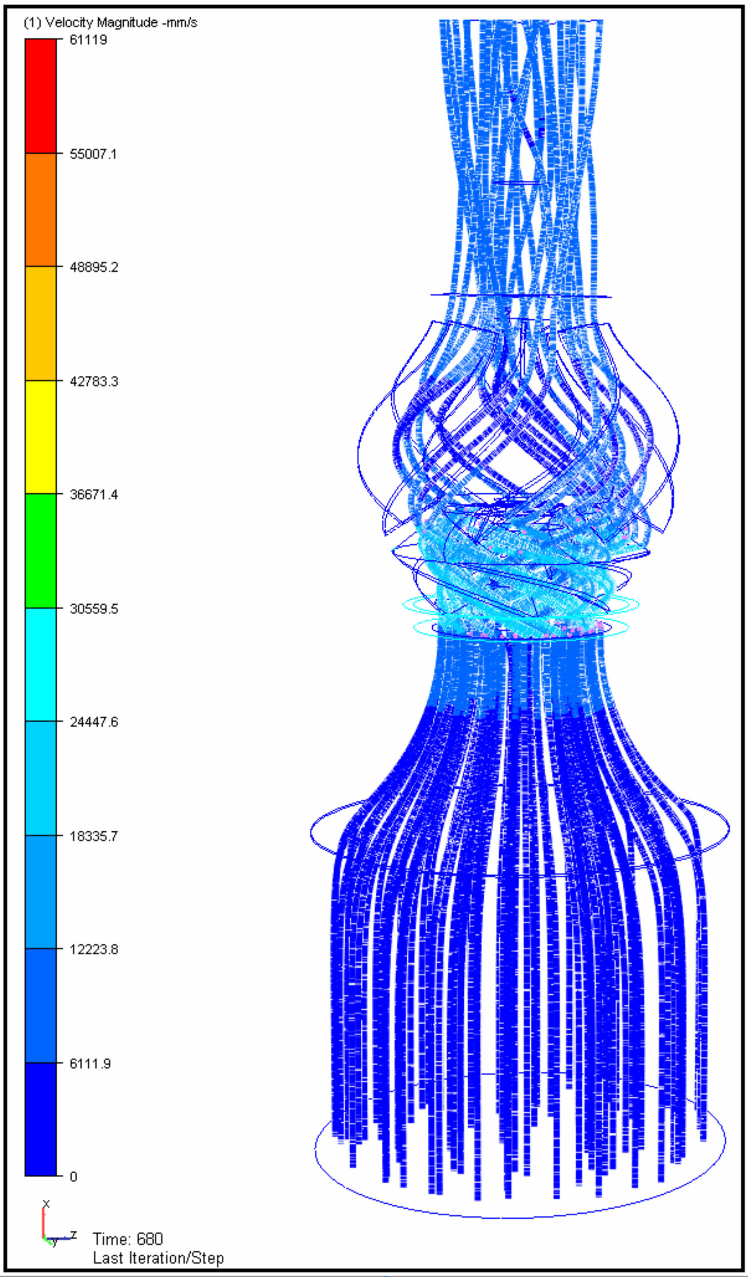

Figure 3.14 – Pathlines inside the pump

3.3.2 CFD Analyses of CASE 2

The impeller is also modeled with blades that are underfiled. The same bowl, suction and extensions with rotating region are used for the underfile impeller case. The control volume is divided into 1,673,016 finite elements. Precisely 1,491,042 fluid elements and 181,974 solid elements are generated by the software which corresponds to 353,407 fluid nodes and 28,036 solid nodes respectively. Generated mesh is seen in Figure 3.15. The analyses are performed for 2900 rpm.

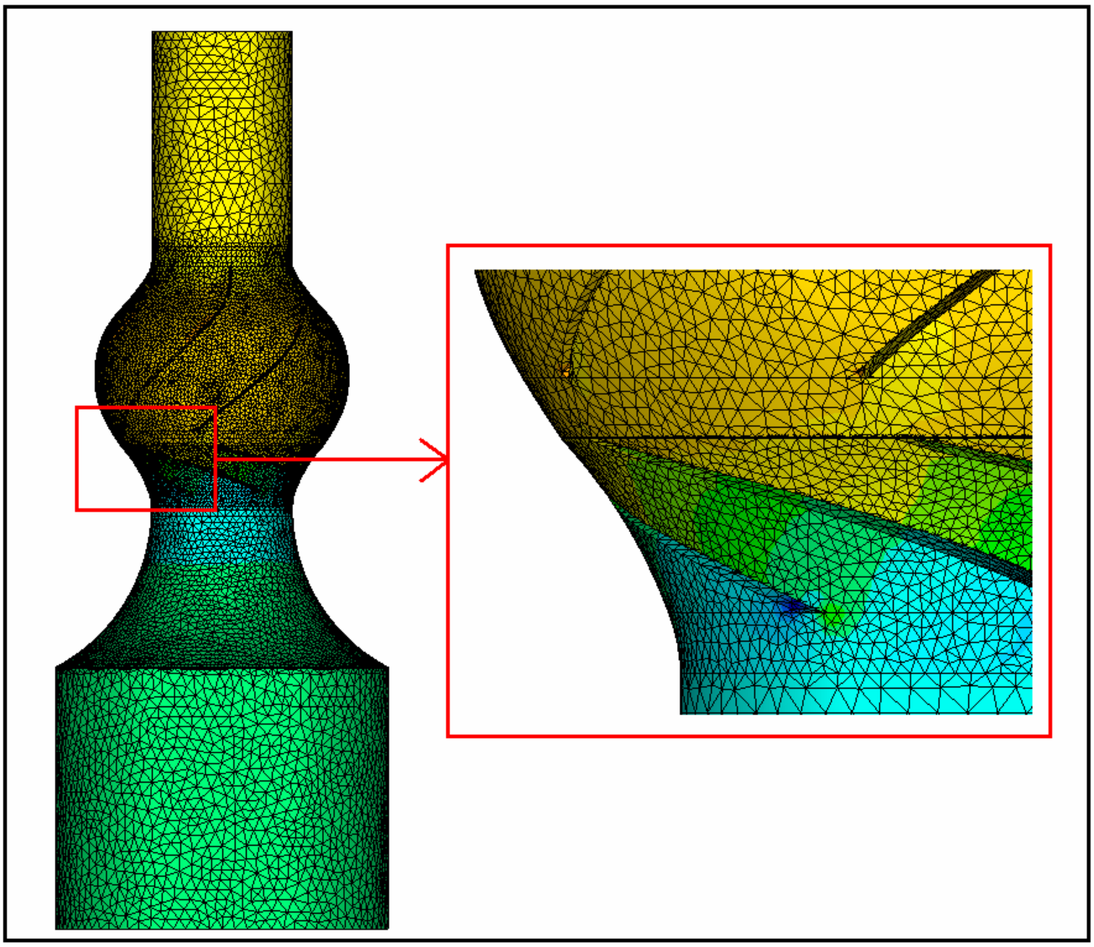

Figure 3.15 – Mesh generated for underfiled impeller

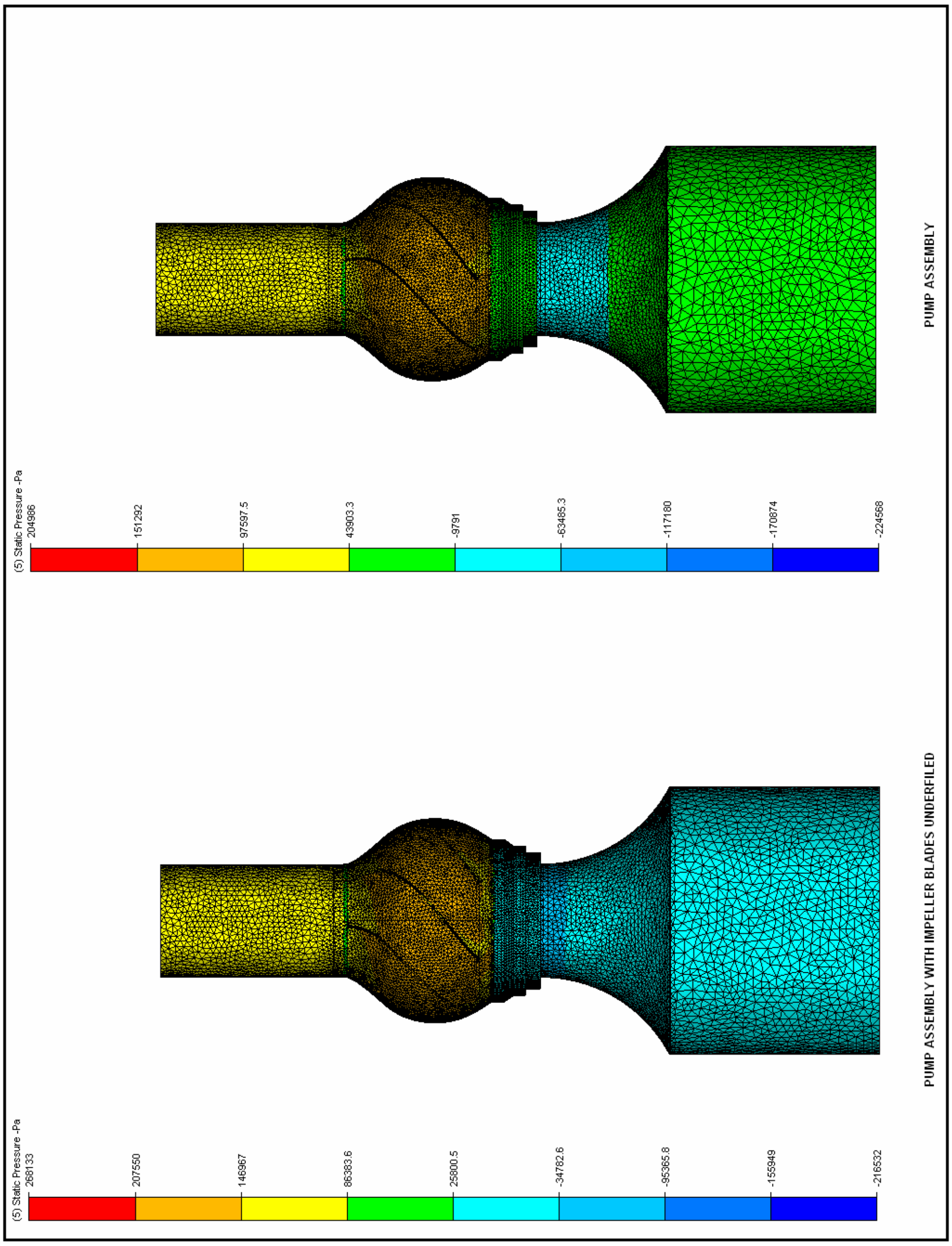

Figure 3.16 – Mesh generated for underfiled impeller and normal impeller

The comparison of mesh generated for Case 1 and 2 are shown in Figure 3.16. The same mesh sizes are used during both analyses.

The pump model with underfile impeller is solved for 7 different operating points defined by the boundary conditions. The slip symmetry on the lateral surface and 0 gage pressure on the inlet surface of the lower extension is kept same for each analysis. The volumetric flow rate definition is changed for each analysis in order to simulate different operating points. Those volumetric flow rate values are 60l/s, 70 l/s, 100 l/s, 110 l/s, 115 l/s, 120 l/s and 130 l/s. The pressure distributions are shown on the cutplane for Case 1 and Case 2 in order to make comparison in Figure 3.17. The pressure difference between the inlet and outlet of the pump in Case 2 is higher then Case 1

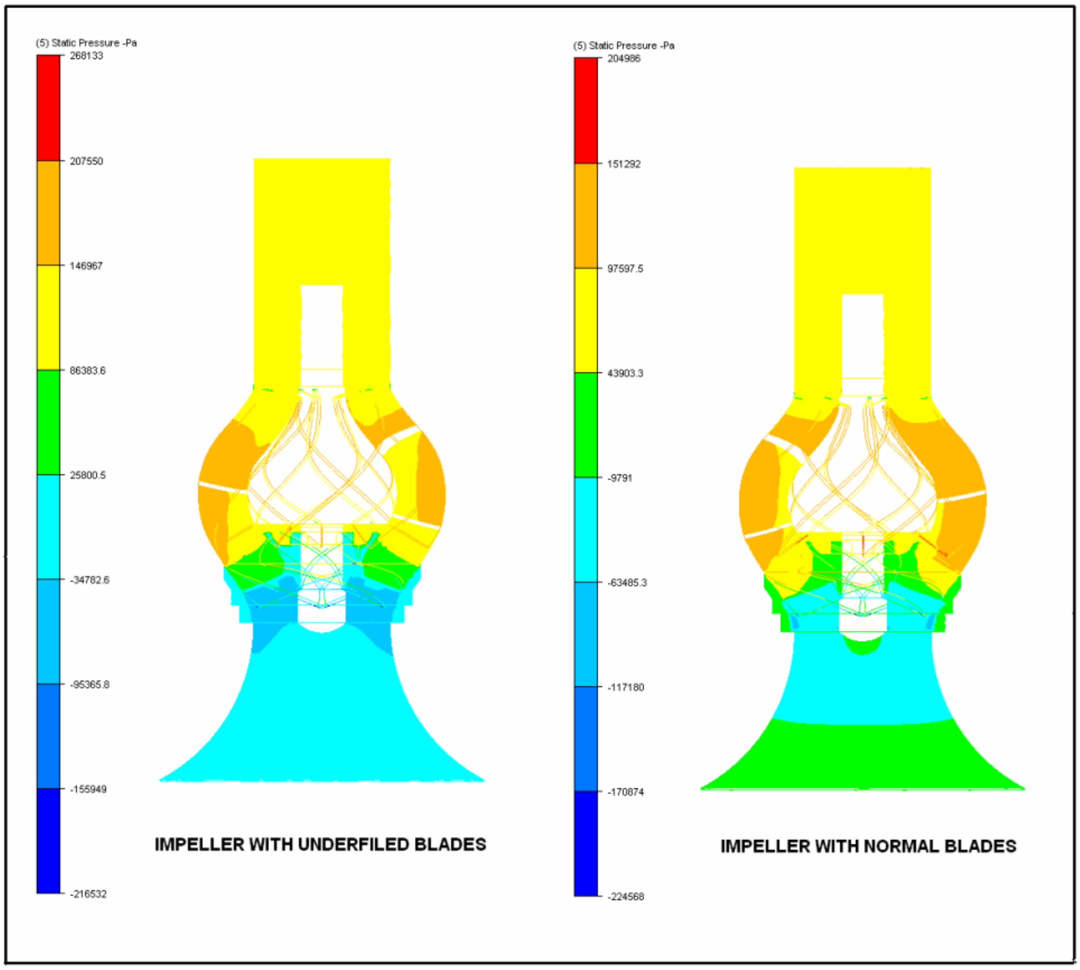

Figure 3.17 – Pressure distributions on the cut-plane which is in the middle of the pump for underfiled and normal blades of the impeller

The pump in Case 2 is also solved for 1450 rpm rotational speed of the impeller. The volumetric flow rate of 30 l/s, 35 l/s, 50 l/s, 55 l/s and 60 l/s are defined in order to simulate different operating points at 1450 rpm. Each analysis is run for 680 iterations and each analysis takes 42 hours for single operating point. The pressure distributions on the impeller for both cases are shown in Figure 3.18. The pressure on the underfiled blades is more uniformly distributed then the normal blade case.

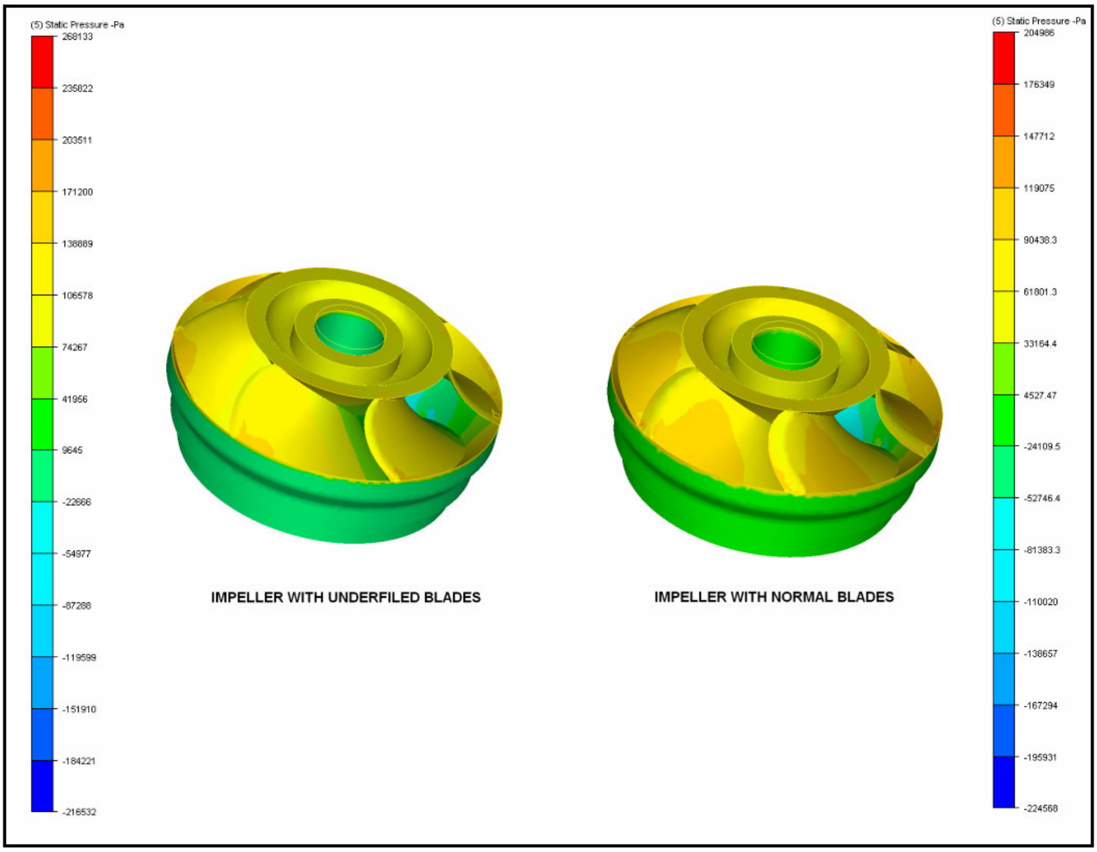

Figure 3.18 – Pressure distributions on the impellers for normal and underfiled cases.

CHAPTER 4

TEST SETUP AND PROCEDURE

4.1 Test Stand

The pump that is designed in this study is tested in the test stand of Layne Bowler Pump Company Inc. The test stand is accredited by Turkish Standards Institute in February 2006. The national standards are applicable in the test stand and it has measurement traceability.

There are three wells in the test stand. Those wells are opened to a pool which has a depth of 9.6 m and diameter of 3 m. The butterfly types of valves are used to discharge and control the flow for pumps to be tested in each well. The flexibility of pump testing by means of discharge flange connection to the butterfly valves is performed by short intermediate pipes between discharge flange and the butterfly valve with different reduction ratios. The reduction in the intermediate pipes is adjusted by taking the flow rate limitations for each pipe into consideration. The crane is used to carry the pumps inside the test stand and position them to the suitable well. The capacity of the crane is 5 tons.

The butterfly valves are connected to the control panel which is located in the control room of the test stand. Outlet pressure of the pumps is adjusted by these valves by the help of joysticks installed on the control panel. The control panel is also connected to the main electric panel in order to start and stop the electric motor that drives the pump. The technical person is responsible from the whole testing procedure and uses the control panel to test the pumps. The test stand has a maximum capacity of 250 kW as electrical input power to the motor. There are four electrical panels which have power ranges of 0-11 kW, 0-37 kW, 11-110 kW and 37-250 kW. There is also a frequency control drive in the test stand.

The pumps up to 90 kW of motor input power is tested at any alternative current frequency lower than 50 Hz. However in cases where the limitation on the torque required to run the pump is exceeded can not be tested by using frequency control drive. This problem may occur when high capacity pumps with large impellers are tried to be tested in the test stand.

The electrical variables on the line driving the motor are measured by the energy analyzer. Energy analyzer has a maximum capacity of 1000 A. There is also a portable energy analyzer with a maximum capacity of 600 A which is used in the test stand. There are 11 manometers and 2 pressure transducers which are capable of measuring pressures up to 40 bars. The flow rate of the pump to be tested is measured by electromagnetic flow meters that are installed on different discharge pipes. The diameters of the discharge pipes are DN80, DN125, DN200, DN300 and DN450. The gate type vane and collector system is used to connect four pipes to each other except DN450. This system is capable of measuring flow rates up to 900 l/s. The periodic calibration of the devices used in the test stand for tests are calibrated by the certified calibration agencies.

The pumps are tested by using "cold clean water" as working fluid. The cold clean water is described in standard as water having a maximum temperature of 40°C , 1.75×10^{-6} m^2/s in kinematic viscosity, 1050 kg/m^3 in density, 2.5 kg/m^3 in non-absorbing solid particles and 50 kg/m^3 in dissolved solid particles, [22]. The limitations of the described clean cold water are satisfied by the test stand working fluid.

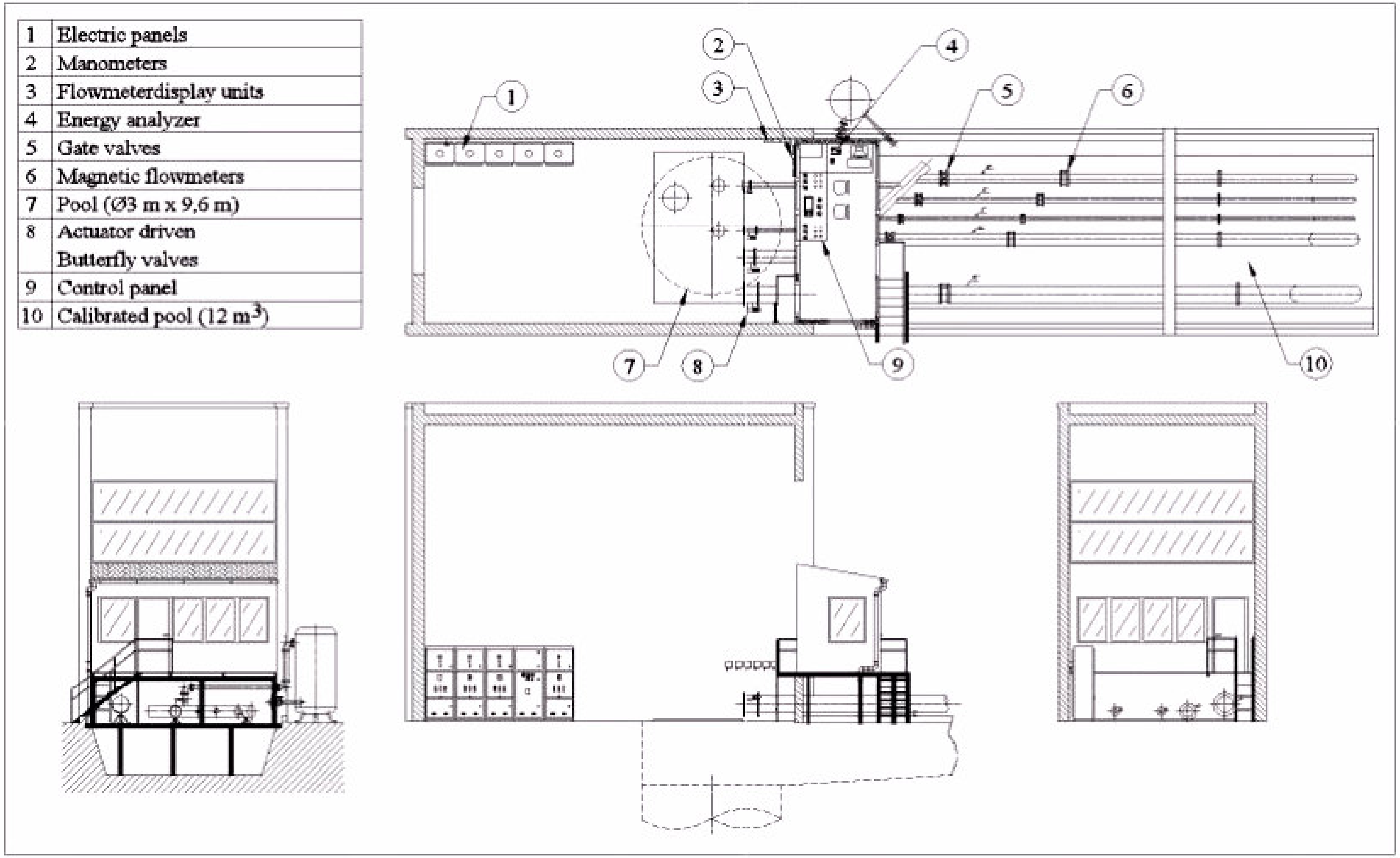

Figure 4.1 – Test Stand

4.2 Test Setup

The pump that is designed in this study is tested as line shaft pump. In this test setup which is shown in Figure 4.2, Vertical Hollow Shaft (VHS) motor is used to drive the pump. Before the pump is carried into the test stand, the parts are assembled in the assembly line of the company. The clearances are controlled in order to check whether the pump is assembled correctly or not. When the pump is carried into the test stand, first of all the strainer is mounted to the bowl assembly which consists of impeller, bowl, suction bell and discharge case. The standard discharge case which is suitable for the upper flange of the bowl is used during tests of the pump. The power is transmitted to the pump from the motor by the shaft connections which go through the water lubricated column assembly. The shaft connection consists of several separate shafts in order to make the setup procedure flexible. The intermediate shaft is placed between the pump shaft and head shaft which is connected to the pump shaft by a coupling on one end and to the head shaft on the other end. The head shaft passes through the stuffing box which is placed in the discharge head and goes into the VHS motor. The stuffing box is used to prevent water to pass through to the motor side by the rotation of the shaft. Moreover, the discharge head is connected to the other end of the column assembly. All connections are performed with flange connections which are fastened with bolts and nuts to the each other. This arrangement which consists of strainer, pump, column assembly and discharge head is placed to the suitable testing line and well position. Positioning the impeller and bowl is performed by fastening the nut which is placed on the upper part of the motor. When the pump assembly is placed in the pump setup, the impeller is in the lower position. The movement of the shaft on the upper direction designates the clearance between the impeller and bowl. However, before the clearance is adjusted the impeller which is connected to the pump shaft is lifted all the way up by the help of the nut in order to control the total clearance between the impeller and bowl.

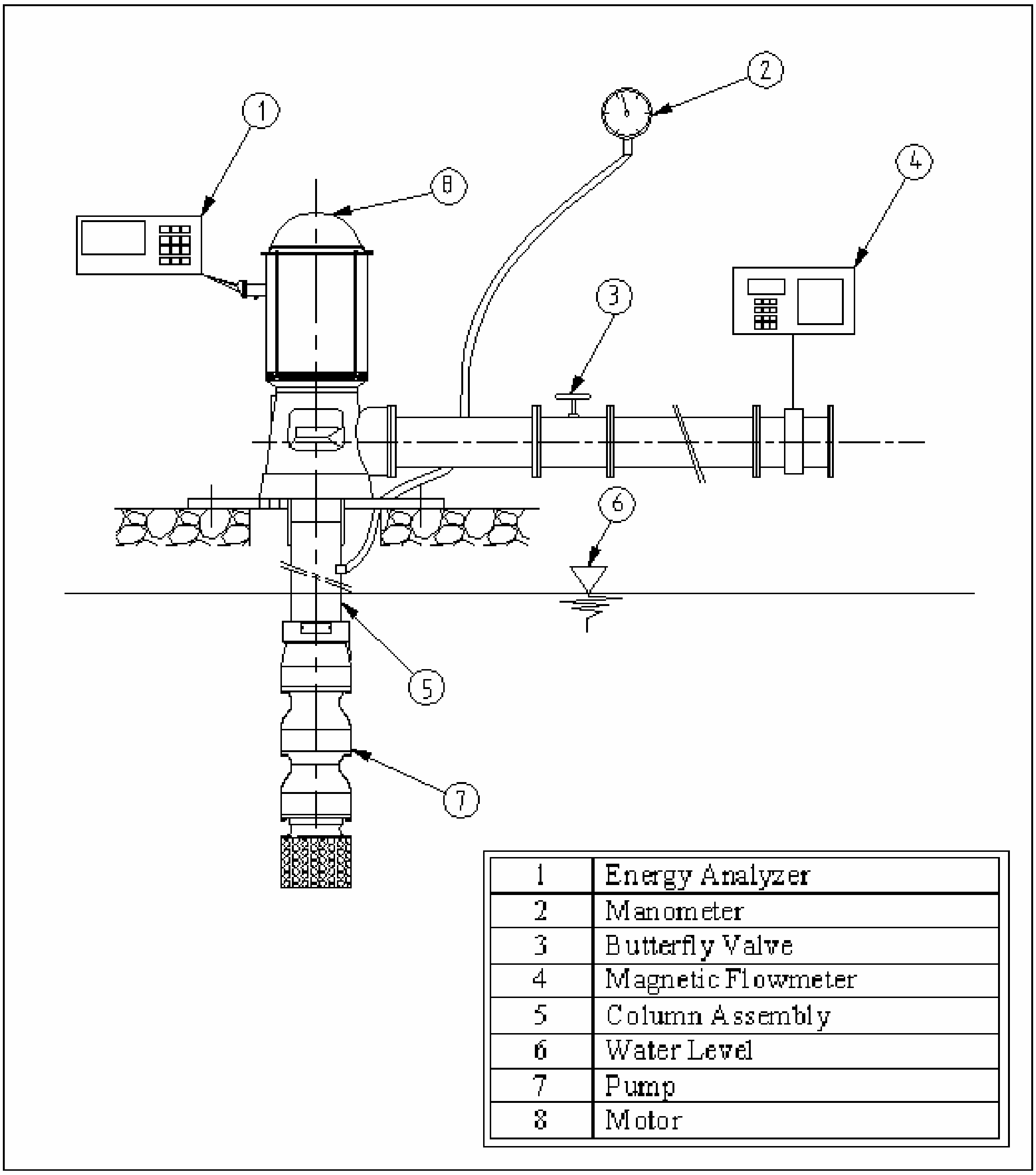

Figure 4.2 – In-line shaft Test Setup

4.3 Test Procedure and Data Processing

The test procedure given below is followed carefully in the pump performance tests. Moreover the processing the data which is collected during the tests are also explained after the test procedure is given.

4.3.1 Test Procedure

The procedure which is given below is followed during the pump tests performed in this study.

1. The pump is assembled and prepared for the test.

2. Test setup is prepared and column assembly is filled with water.

3. The motor is connected to the suitable electrical panel by looking at the motor electrical properties and the protection relay in the panel is set to the required value by technician.

4. The protection relay is adjusted to the required value.

5. The rotation direction of the pump is checked and corrected by simply starting the pump for a short period of time.

6. The connections to the butterfly valve from the intermediate pipe is controlled and fastened in order to prevent the water leakage from the connections.

7. The manometer and flowmeter are selected by looking at the maximum expected head and flowrate of the pump to be tested respectively. The chosen manometer is connected to the discharge pipe in the column assembly. Required valve configuration is set to direct the flow from collector pipe to the chosen flowmeter.

8. Pump is started. If the frequency converter is used in order to operate the pump at different speeds than the motor speed, the frequency is adjusted to the desired working speed.

9. After the pump is started the exit pressure of the pump is adjusted by using butterfly valve. When the pressure is in the desired level, no readings are taken for a while before the pump reaches steady state operation at this point. The decision of reaching the equilibrium is made by looking at the oscillations on both flowmeter and manometer. When the oscillations damp out, the recording is performed by means of flowrate and pressure readings from the displays of flowmeter and manometer, respectively. The procedure described above is repeated for a number of data points that are sufficient to inspect the hydraulic and power consumption characteristics of the pump.

10. The pump is then stopped. The electrical connections are unplugged and the safety regulations are followed to reassemble the pump from the test stand.

4.3.2 Processing the Test Data

The collected data from the pump test is processed by the following the procedure given below to obtain the characteristics of the pump.

The instruments used during tests are periodically calibrated and calibration formulas coming from the calibrations are used while processing the data. The calibration results which are stated in the calibration reports are used to obtain these formulas which have the data read as an input and the corresponding real value as an output. Each recorded data are processed with the regarding formula of the instrument. Then the calculations are performed as stated in the regarding standard, [22].

In order to find the total head of the pump, the velocity head is found as stated in the regarding Reference 22. The velocity head is found simply dividing the flow rate to the cross sectional area of the discharge pipe where the pressure is recorded at. The nominal diameter is taken while calculating the cross sectional area of the discharge pipe. The distance between the water level and the manometer location is added to this value. The sum of these two is added to the pressure reading on the manometer in order to get the pump head. These calculations are coming from the Bernoulli equation written between points 1, 2 and 3 shown in the Figure 4.3.

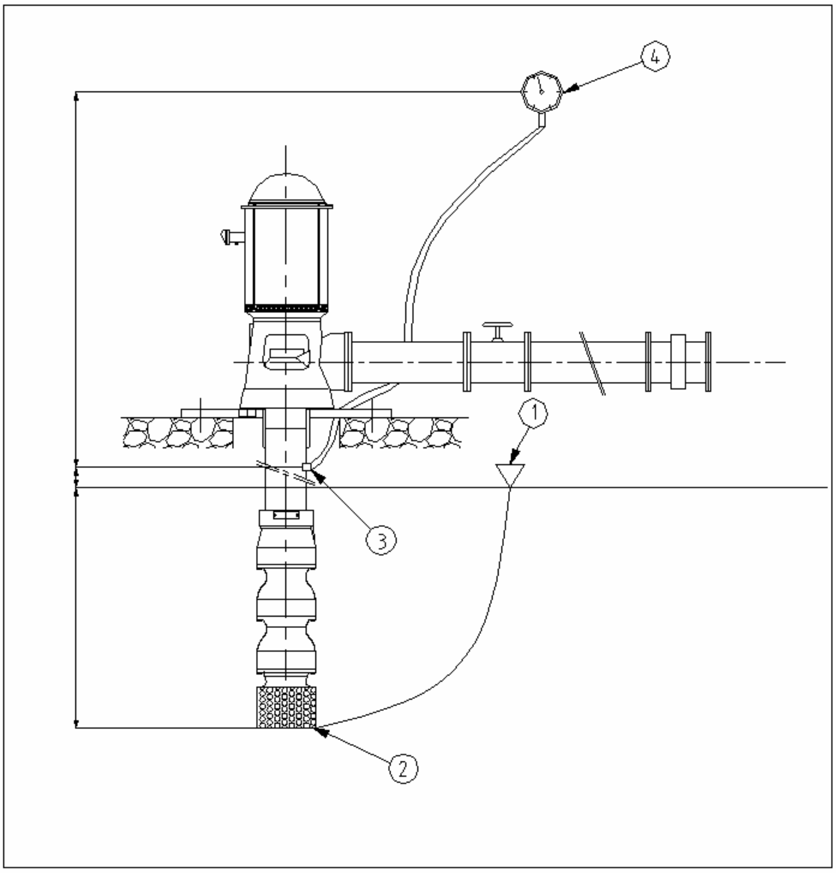

Figure 4.3 – The points where the Bernoulli equation is written in order to find the total head of the pump

4.4 Test Results

The tests are performed in 1450 rpm and four stage series connection of the pump that is designed in this study. The design point of the pump in Chapter 2 is given as:

Q = 115 l/s

H= 16 m

ω = 303.69 rad/s (n = 2900 rpm)

Since the pump is tested in 1450 rpm, the similitude analysis is performed in order to find out the design point in 1450 rpm by using the regarding formulae given in Reference [2]:

$$\pi_Q = \frac{Q}{\omega . d^3} \tag{4.1}$$

$$\pi_h = \frac{g.h}{\omega^2 . d^2} \tag{4.2}$$

From Equation (4.1) and (4.2), the design point of the pump for 1450 rpm is found to be:

Q = 57.5 l/s

H = 4 m

ω = 151.84 rad/s (n = 1450 rpm)

Since the pump is assembled as 4 stages in series connections the head rise is expected to be 16 meters during the tests.

The tests are performed with VHS type motor which has a nominal power of 22 kW. The test results of impellers with normal and underfiled blades are given in Figure 4.4.

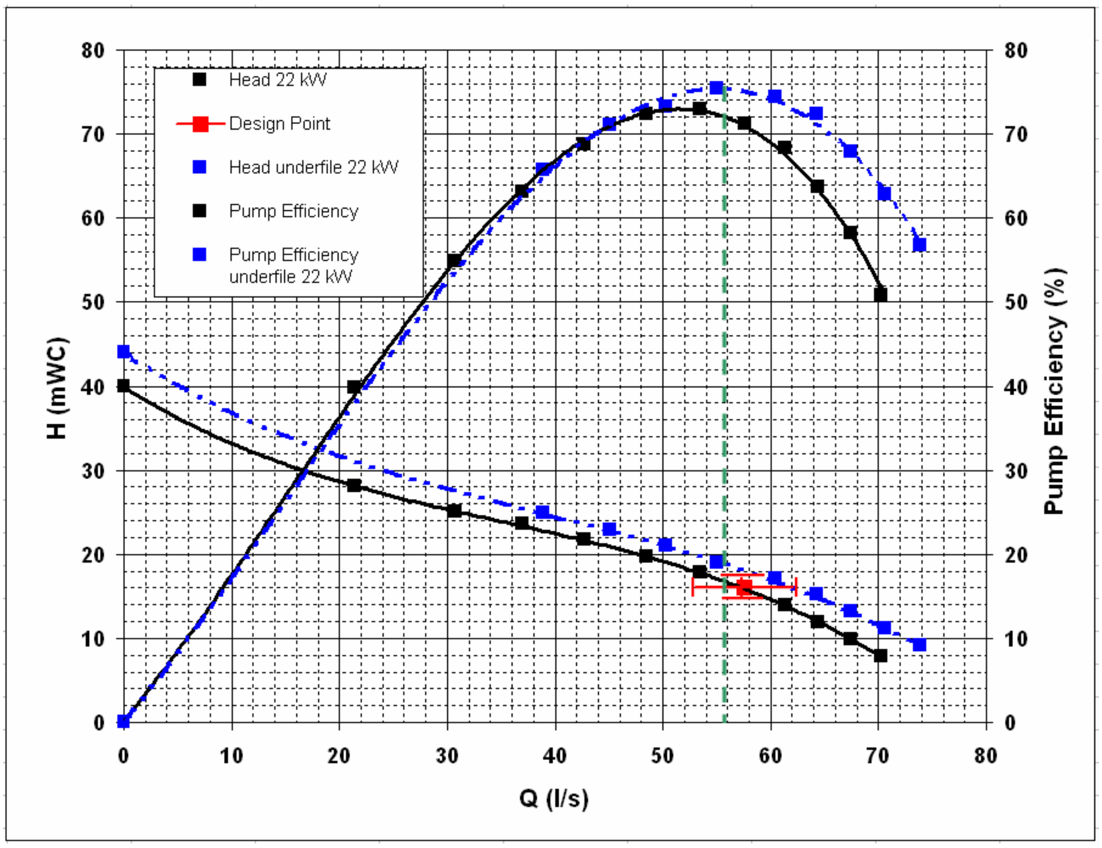

Figure 4.4 – Test Results with 22 kW motor for impellers with normal and underfiled blades

The designed pump satisfies the tolerances given in the regarding standard [22], from the design point of view for impeller with normal blades. The tolerances given in the regarding standard, [22] are; ±8 % for the flow rate and ±5 % for the head of the pump. In deed when the blades are underfiled, the best efficiency point moves towards to the design point.

CHAPTER 5

RESULTS AND CONCLUSION

5.1 Discussion and Results

The discussions on the design, numerical experiments and tests are performed in this chapter. The first part in this chapter is the discussion of the effects of the design parameters on the hydraulic performance of the pump. The discussions on the CFD analyses methodology are taken place after the discussions on the design. The last part is presenting comparisons of actual test results with CFD analyses results of the designed pump.

In this thesis, a vertical turbine type mixed flow pump is designed, manufactured and tested in Layne Bowler Pumps Company Inc. The CFD analyses are performed on the designed pump and CFD results are compared with actual test results. The tests of the pump are performed with an electric motor having the nominal speed of 1450 rpm since suitable motor having 2900 rpm of rotational speed and required power capacity is not found in the company during the testing period.

Since the design of the impeller is started with existing impeller layout, necessary changes are made on this profile in order to meet the design point of the pump. The methodology that is given in Chapter 2 regarding to the design of the impeller layout is a trial and error procedure. In deed once the profile is constructed, the preliminary design is performed and several points are checked in order to continue with shaping the blades of the impeller. First check point is the blade number of the impeller. The number of the blades with respect to the specific speed and the experience coming from the company is followed while controlling the blade number. If the number of blades that is found in the preliminary design are different then what is expected, the geometrical change on the impeller layout is made. While making the geometrical change, the static moment of the midstreamline is changed as the first case. Changing the static moment of the midstreamline is made by increasing or reducing the length of the midstreamline where the preliminary design is performed. If the number of blades that are found in the preliminary design is higher then what is expected the static moment of the midstreamline is decreased and if the number of the blades are lower, the static moment is increased in order to satisfy the expectation. The main reason of changing the characteristics of the midstreamline is coming from Equation (2.39) and (2.40). If Equation (2.40) is put into Equation (2.39), the following Equation is obtained.

$$z = 13.\frac{M}{e^2}.\sin(\frac{\beta_1 + \beta_2}{2}) \tag{5.1}$$

However while changing the static moment of midstreamline, the length of the midstreamline is affected from this change. In order to minimize this change, the midstreamline is moved diagonally in the 2D design plane to satisfy the desired change on the blade number. If the blade number that is found in the preliminary design is higher, the point of the midstreamline on the leading edge is extended towards the impeller inlet eye and the point of midstreamline on the trailing edge is moved close to the rotating axis of the impeller. Moving the blade passage of the impeller layout profile is simply positioning the blade passage close to the axis of rotation of the impeller. Nevertheless if the blade number found in the preliminary design is lower then what is expected, the reverse of this process is performed in order to higher the blade number. The value of the blade number is tried to converge to an integer value by applying these changes. It is found that the hydraulic efficiency is highly affected by finding out the correct value of the blade number for the desired characteristics of the pump.

Another important point for checking the conformity of impeller layout to the expected design is the area distribution from leading edge to trailing edge of the blade. The area distribution should be checked with two methods. The first one is fitting the circles from inlet to outlet of the blade passage of the impeller layout. Those circles are tangent to the hub and shroud profiles and the radius of the circles should be changed well arranged from inlet breadth to the exit breadth. The second method of controlling the area distribution is constructing the potential lines and revolving these potential lines around the axis of rotation of the impeller. The ratio of meridional velocities should be checked in order to attain better pump performance. From the design experience, the ratio of V_{m0}/V_{m1} is between 0.85 - 1 and the ratio of V_{m2}/V_{m1} is between 0.6 - 0.75. However while calculating these ratios, the blade thickness should be considered.

The blade thickness of the impeller is directly affecting the hydraulic performance of the pump. However from the production point of view the blade thickness is selected according to the casting capabilities. Although the meat thicknesses of the impeller should be selected close to the thickness of the blade in order to cast the impeller properly.

The degree of reaction is defined as the ratio between the pressure head of the pump, H_p and the theoretical head of the pump, H_{th}. The degree of reaction of the pump that is designed in this study is 0.74 if the midstreamline is taken into account for calculations. On the other hand when the degrees of reaction for the other streamlines are calculated, the values lie between 0.6 and 0.8, from hub to shroud respectively. The degree of reaction represents the characteristics of the pump. It is stated in Reference [1] that, higher the degree of reaction, the greater the specific speed of the pump. Hence the rotodynamic pump that is designed in this study is a reaction machine.

Pfleiderer's correction factor, C_p is stated to be between 0.25 and 0.35 in preliminary design part of Chapter 2. It is found that C_p is 0.29 for midstreamline. The Cp value is between 0.2 and 0.4 for the other streamlines and C_p value is gradually increasing from hub to shroud. The Pfleiderer's correction factor approach is applicable for the pump that is designed in this study.

While applying numerical experimentation on the designed pump several points should be carefully followed. The first point is selecting the boundary conditions. Defining volumetric flow rate boundary condition to the exit and pressure boundary condition to the inlet of the pump is used in the CFD analyses. These boundary condition definitions are found to be useful while using CFdesign in order to have faster convergence than defining pressure-pressure and volumetric flow rate-volumetric flow rate boundary conditions to the inlet and exit respectively.

The CFD solutions are affected by the quality of generated elements that are forming the solution domain inside the pump. While defining the size of the meshes that are generated for the solution, rotating region and impeller should be meshed with smaller elements then the other parts. However the element size is increased gradually for the other parts in order to keep the aspect ratio as low as possible. When convergence is followed by checking the physical quantities such as pressure and velocity components from different cut-planes at the inlet and outlet of the pump, the oscillations may be investigated. If the oscillations are investigated, the aspect ratio should be checked. The regions having higher aspect ratio should be re-meshed and the aspect ratio is tried to be minimized. It is also found that if the extensions at the inlet and outlet of the pump are not long enough the solutions may diverge. Total number of fluid elements that are generated in pump applications around 1.5 million give reliable results when they are compared with actual test results.

The time step size is the parameter which defines the rotation of the machine in degrees per time step, [13]. When the time step size is adjusted for three degrees of rotation of the machine, in this case the impeller, the results converges slower but the reliable results are investigated.

CFdesign calculates the hydraulic torque on the impeller which is surrounded by the rotating region. This torque value is used to calculate the hydraulic efficiency of the pump that is designed in this study. In order to calculate the pump efficiency, the hydraulic efficiency should be multiplied by the volumetric efficiency and the mechanical efficiency. Since the leakage region between the impeller and bowl is very small compare to the other water passages inside the pump, it is difficult to generate meshes in this region. The difficulty of putting meshes is mainly caused by hardware capabilities. CFD software has an automatic mesh generator and when the user tries to put small size meshes in leakage paths, the total amount of mesh generated in the analysis increases more than the 32 bit environment can handle. Nevertheless the analyses are tried to be performed with a workstation which has 2 XEON 64 bit 3.4 GHz processor, 4 GB of RAM and installed 64 bit Windows operating system. However the both the 64 bit Cfdesign V.8 which is a beta version and 32 bit Cfdesign did not work properly in 64 bit environment. On the other hand it is investigated that more elements are generated with meshing the gaps between stator and rotor in 64 bit environment. The volumetric efficiency is taken as the assumption that is made in Chapter 2 as 96% while calculating the pump efficiency. The mechanical efficiency is also taken as the design value which is 96% percent during pump efficiency calculation. However in order to make comparison between the CFD results and test results the motor efficiency should also be estimated. The motor efficiencies are taken from the motor manufacturers catalogues in order to calculate pump efficiency. The values of the efficiencies of the motors are based on the catalogue values of the motor manufacturer, [23]. Since the pump is solved for single stage in CFD, the head rise that is calculated in the analysis is multiplied by 4 in order to compare the results with actual test results.

The comparison of CFD results which are solved for 1450 rpm of rotational speed of the impeller with actual test results performed with 22 kW motor is given in Figure 5.1 and Figure 5.2. The CFD results by means of head and efficiency characteristics are within the tolerance limits given in the regarding standard, [22].

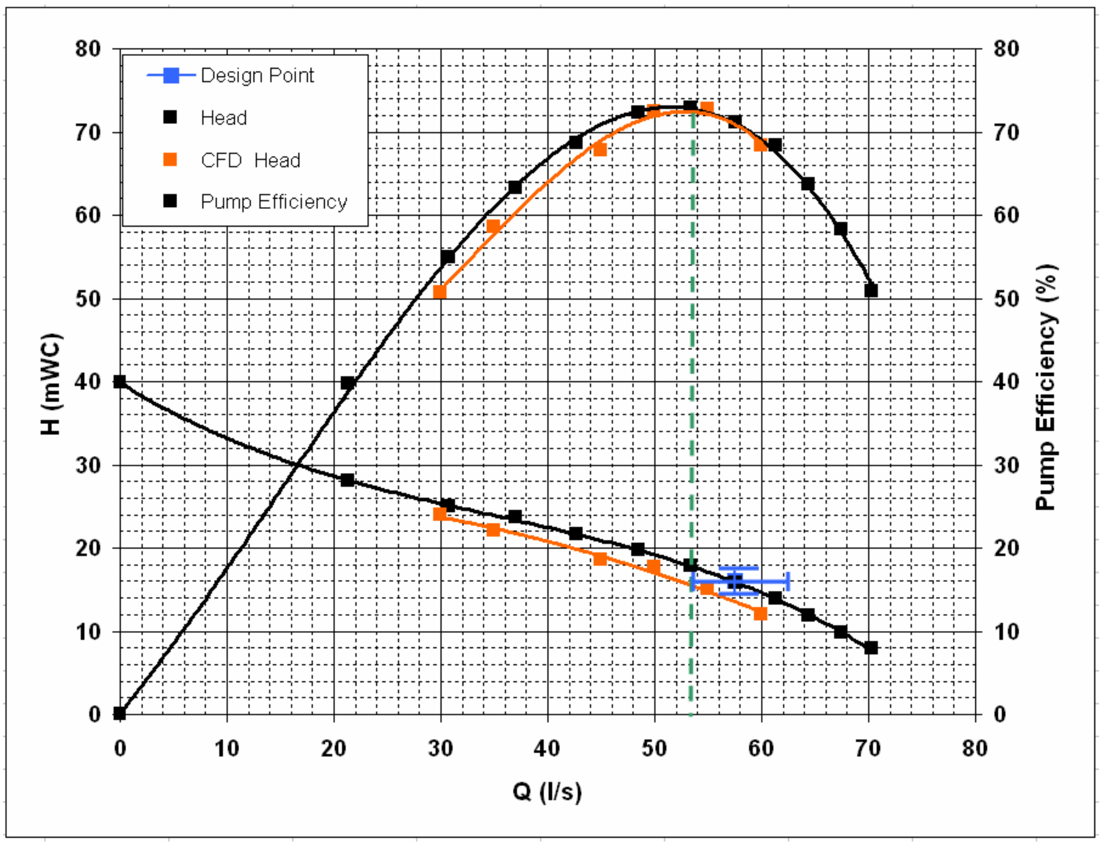

Figure 5.1 – Test results with 22 kW motor and CFD results by means of head versus flow rate and system efficiency versus flow rate

The underfiling is performed in the machine shop with a similar method that is modelled in CAD environment. However it is hard to process the same metal removal that is done in CAD due to manufacturing capabilities.

The assumptions for the volumetric and mechanical efficiencies are also the cause of the errors during the calculations. Improving the hardware of the computers used during the analyses may give the ability to calculate the volumetric efficiency. However from the industrial point of view the CFD results satisfy the needs of the company. In order to control the mechanical efficiency, the pump should be carefully assembled. The manufacturing tolerances should strictly be followed in order not to have wear between the rotating and stationary elements especially in the bearings in the bowl, suction and discharge elements of the pump. If the shafts are contacting to the bearings during the operation, the wear occurs and mechanical efficiency decreases, thus the system efficiency decreases.

The efficiency characteristics shown in Figure 5.6 are overlapping with the actual test results between 50 l/s and 60 l/s. The reason of overlapping may be caused by two main reasons. First one is the miss calculation of the hydraulic torque value of the code and the second one is the problems occurring during the tests.

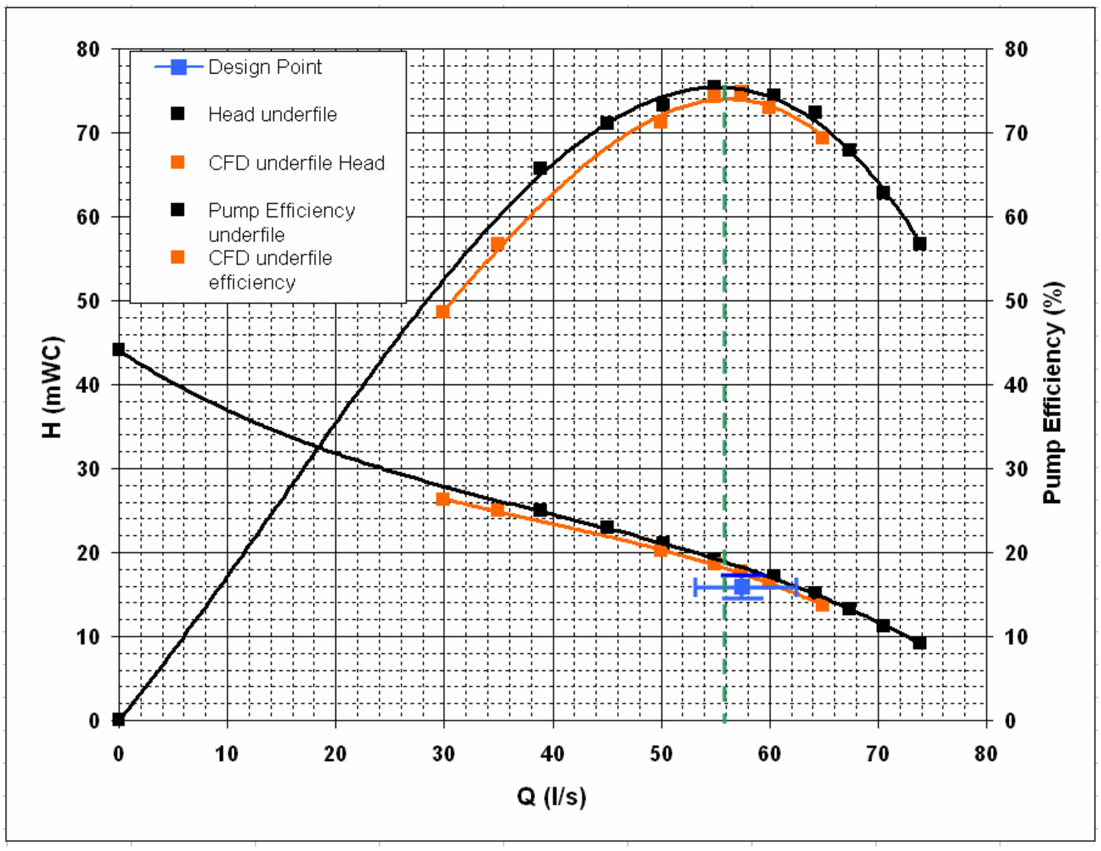

Figure 5.2 – Test results with 22 kW motor and CFD results for impellers with underfiled blades

Since the design of the pump in this study is performed for 2900 rpm in Chapter 2, the test results are converted to 2900 rpm from 1450 rpm. While making the conversion the given relationships in regarding standard, [22] are followed. However in the regarding standard, it is stated that when the actual tests are performed in a range of ±20% of the desired speed, the efficiency may deviate from the actual case, [22]. In order to convert the efficiency of 1450 rpm tests to the 2900 rpm, the efficiency correction formula is used. There are several equations in the literature for efficiency correction but the correction equation that is given in Equation (5.4), [1] is used in this study.

$$\frac{\eta}{\eta_m} = 1-(1-\frac{\eta^{'}}{\eta_m}).(\frac{N^{'}}{N}.\frac{\nu}{\nu^{'}})^{\alpha} \tag{5.4}$$

Where η is the desired test speed efficiency, $\eta^{'}$ is the actual test efficiency which is the performed test efficiency is 1450 rpm for this case, η_m is the mechanical efficiency which is taken as 96 % for both tests, $N^{'}$ is the actual test speed which is 1450 rpm, N is the desired test speed which is 2900 rpm, ν and $\nu^{'}$ are the kinematic viscosities which are same with for both tests.

The conversion of pump tests of normal and underfiled blades are shown in Figure 5.3 and Figure 5.4 respectively.

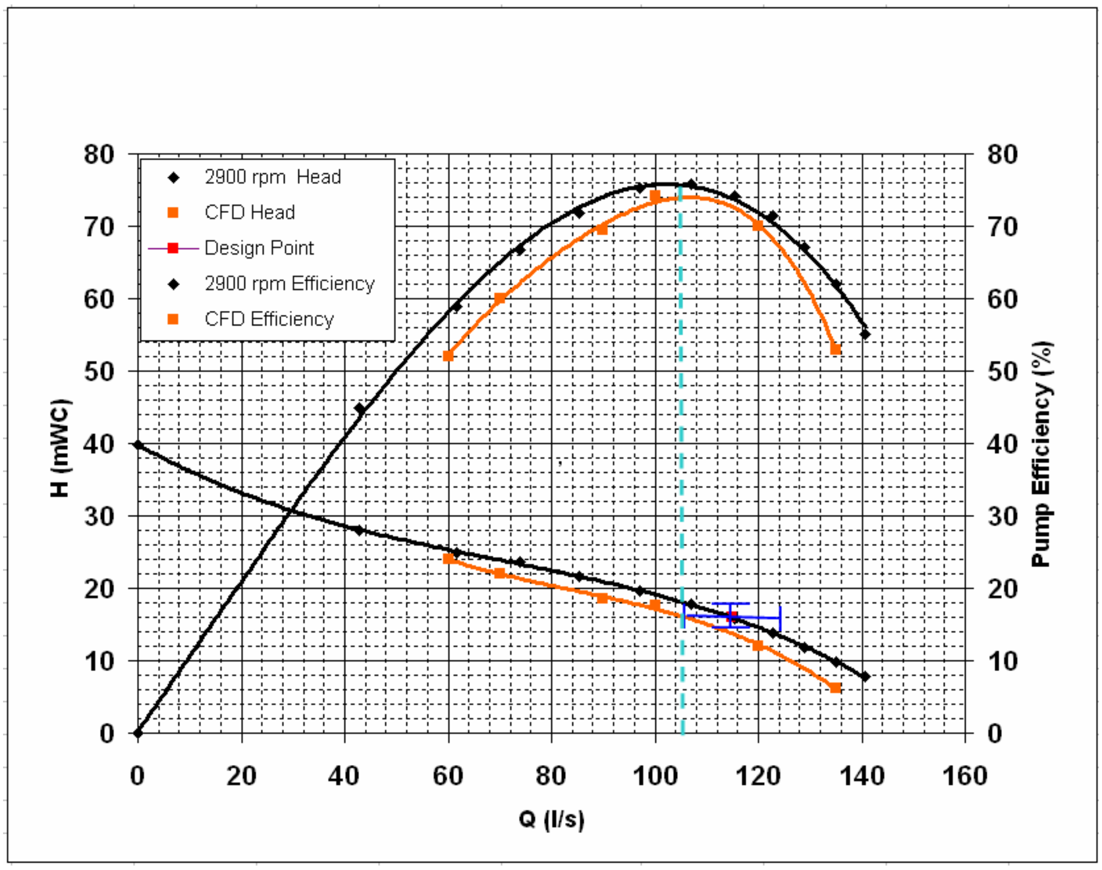

Figure 5.3 – Test results with 22 kW motor converted to 2900 rpm and CFD results

The conversion calculations using Equation (5.4) showed that the design point is satisfied within the given tolerance limits in the regarding reference, [22]. However performing the actual tests with a 2900 rpm electric motor gives more reliable results then converting the 1450 rpm test results to 2900 rpm by using the formula.

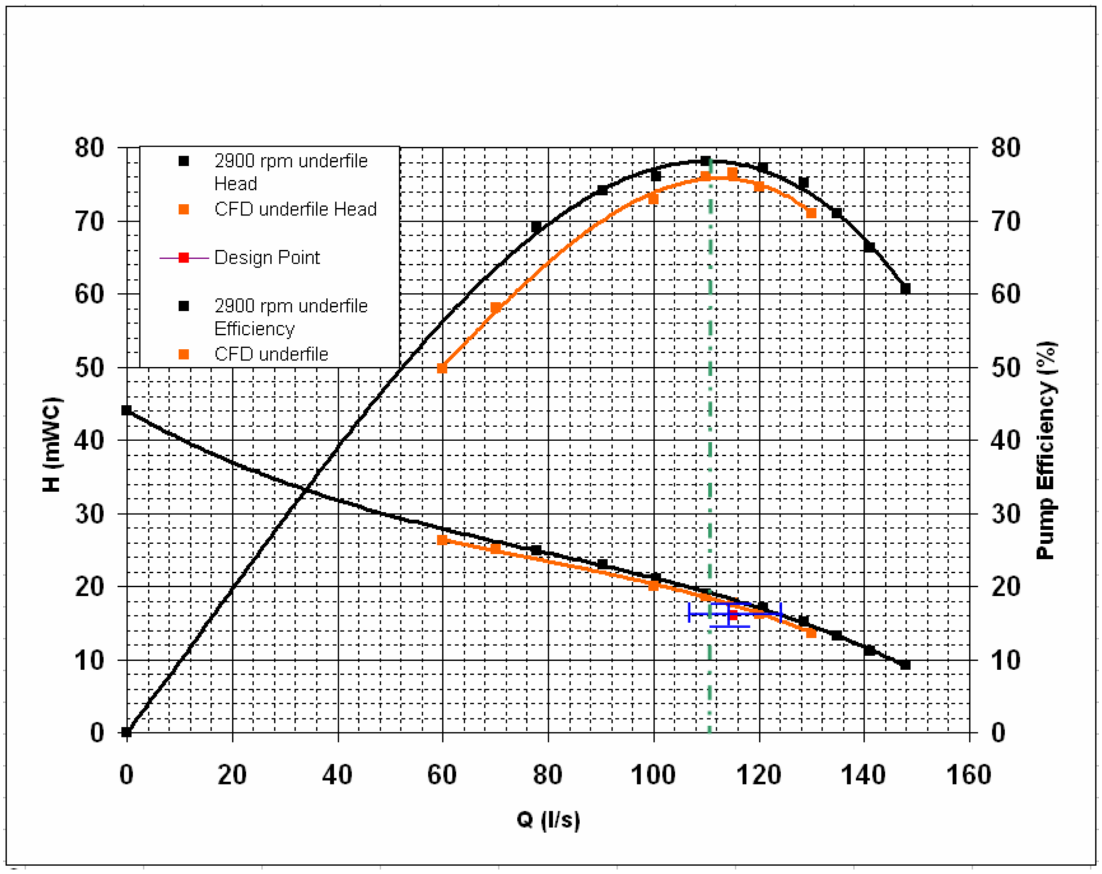

Figure 5.4 – Test results with 22 kW motor converted to 2900 rpm and CFD results for impellers with underfiled blades

When the CFD results are compared to the test results for normal impeller blades, it is investigated from Figure 5.3 that the found best efficiency point in CFD deviates 2% when it is compared by concerning flow rate. The reason of this may be because of the numerical errors while calculating the hydraulic efficiency in CFD and reading errors in experiments. However once again, from the industrial point of view the results satisfy the needs from the pump characteristics point of view.

5.2 Conclusion

Underfiling of impeller blades at the trailing edge improved the performance of the pump that is designed in this study, as stated in References [19]. Best efficiency point of the pump that is designed in this study moves from 53 l/s to 56 l/s and system efficiency increases 2% for the best efficiency point. The best efficiency point of the pump moves towards to the design point when the blades are underfiled. The disturbance on the trailing edge of the blade caused by offsetting the designed surface in order to give thickness the blade is reduced, when underfiling is performed in the impeller blades, [5].

The CFD results and test results are found to be in agreement with each other. The CFD results are in the tolerance limits which are giving in the regarding reference, [22]. However while making the comparison of the CFD results; the convergence of the analyses should be obtained. If the instable analyses are faced by means of convergence, the number of elements should be increased and the analyses should be rerun for the stability.

On the hydraulic design of the impeller, the impeller layout is designed starting with an existing layout. Building an impeller layout library and using this library for the further designs is an important tool from the design point of view. However if the designed impeller layout for a specific design does not satisfy the design parameters, the reverse process may be followed. This process is simply applying the resulting pump characteristics of the CFD results on the best efficiency point to the designed impeller layout. As a result, if the pump performance by means of hydraulic efficiency does not satisfy the designer, the changes which are described in Chapter 5.1 should be followed. On the contrary the impeller layout library usage shortens the design periods if there are different layout in different specific speeds exist.

The design of the pumps still depends on the experience of the designer. However using CFD software which is integrated into the design procedure allows the designers to better understand the flow physics inside the pumps. The integration of the CFD software to the design process is a continuous procedure. The code should be verified in each case study by comparing the CFD results with actual test results.

The manufacturing of the pump is important as the hydraulic design studies and numerical experimentations. While producing the pump, the cores and core boxes should be manufactured by following the original design. However, the designs should be robust in order to manufacture the pumps easily and getting the closest pump characteristics when the test results are compared with the CFD results and hydraulic design of the pump. Selecting the suitable blade and vane thicknesses, blade swirl and vane swept angles are important from the manufacturing point of view.

5.3 Future Work

In order to improve the design procedure that is followed in this thesis, there are several point may be checked. The pressure distribution may be determined on the designed streamlines by using CFD. The plots of the pressure distribution versus meridional distance on the pressure and suction sides of the impeller blade give an idea about the theoretical head of the pump that is aimed to be designed. Moreover, the distribution of the velocity components on the designed streamlines may be drawn by the help of CFD and these distributions can be compared with the velocity distributions on the shaping of the blades part of the design.

The computerized design codes such as CFTurbo, Concepts-NREC's Pumpal, PDC by Hans Spring and TurboDesign^{-1} may be integrated into the design process of the pumps in order to shorten the design periods. However it is kept in mind those codes should be verified with the theoretical calculations on the design procedure and should be used as a tool in the design

The CFD analyses are performed for whole pump in this study. However blade top blade analysis may be performed for the impeller after the design of the impeller is completed. However in order to perform CFD analysis to the single flow passage which is between two adjacent blades, the stacking of the blade at the trailing edge should be uniform. The reason of this uniformity is because of the volumes that are added to the inlet and exit of the impeller. If the impeller leading edge is not uniformly shaped between the hub and shroud, it is hard to assemble the exit volume to the impeller exit for the blade to blade analysis. If the blade to blade analysis is performed the periodic boundary conditions are used and the analyses are run in steady state form. This procedure shortens the analysis run time and allows the designer to investigate the flow structure inside the single flow passage of the impeller. Nevertheless the pressure distribution is investigated and the design may be improved in order to achieve the desired head of the pump.

If the software that is used in this thesis can handle 64 bit environment solutions properly by means of convergence, the pump analysis may be performed by generating elements to the gaps between the stator and rotor where the volumetric leakage occurs.

From the production point of view, the casting technique that is used to cast the products in this study is simple gravity die casting. In this method, the thicknesses that could be cast are limited. However using another casting techniques such as investments casting may allow the designs to be cast with smaller thicknesses. Decreasing the thickness of the blade increases the pump performance. However, decreasing the thicknesses of the blades allows the impellers face with wear when they are operating in environments where the impurities exist in the working fluid such as sand. The thicknesses should be adjusted by considering the overall operating life of the pumps.

REFERENCES

1. Lazarkiewicz, S. and Troskolanski, A. T. (1965) *Impeller Pumps*, Pergamon Press Ltd., Oxford.

2. Aksel, M. H. (1999) *Fluid Mechanics*, Middle East Technical University, Ankara.

3. Dicmas, J. L. (1987) *Vertical Turbine, Mixed Flow, and Propeller Pumps*, McGraw – Hill Inc., U.S.A.

4. Anderson, H. H. (1986) *Submersible Pumps and Their Applications*, *1st Ed*, The Trade and Technical Press Limited, England.

5. Stepanoff, A. J. (1957) *Flow Pumps Design, and Application*, John Wiley & Sons Inc., U.S.A.

6. Sayers, A. T. (1990) *Hydraulic and compressible flow turbomachines*, McGraw-Hill Book Company, England.

7. Wendt J. F. (1992) *Computational Fluid Dynamics: an Introduction, 1st Ed*, Springer-Verlag., New York U.S.A.

8. Goto, A., Nohmi, M., Sakurai, T. and Sogawa, Y., (2002) "*Hydrodynamic Design System for Pumps Based on 3-D CAD, CFD, and Inverse Design Method*", ASME Journal of Fluids Engineering Vol.124 pp. 329-335.

9. Walker, P. J. and Dawes, W. N., (1990) "*The Extension and Application of Three-Dimensional Time-Marching Analysis to Incompressible Turbomachinery Flows*," ASME Journal of Turbomachinery., Vol. 112, pp. 385-390.

10. Goto, A. (1995) "*Numerical and Experimental Study of 3-D Flow Fields within a Diffuser Pump Stage at Off-Design Condition*," ASME Fluids 95, FED-Vol. 227, pp. 1-9.

11. CFX User Manual Version 5.6 (2003) CFX Ltd., United Kingdom.

12. Muggli, F. A., Holbein, P. and Dupont, P., (2002) "*CFD Calculation of a Mixed Flow Pump Characteristics from Shutoff to Maximum Flow*" ASME Journal of Fluids Engineering., Vol. 124, pp. 798-802.

13. CFdesign User's Guide Version 7.0 (2004) Blue Ridge Numerics, Inc., Charlottesville.

14. Hirsch, Ch. (1994) " *CFD Methodology and Validation for Turbomachinery Flows*", Turbomachinery Design Using CFD-AGARD Lecture Series 195, Specialised Printing Services, Essex, pp 4-7.

15. Majidi, K., (2005) " *Numerical Study of Unsteady Flow in a Centrifugal Pump"* ASME Journal of Turbomachinery., Vol. 127, pp. 363-371.

16. Meakhail, T. and Park, O., S., (2005) "*A Study of Impeller-Dıffuser-Volut Interaction in a Centrifugal Fan*," ASME Journal of Turbomachinery., Vol. 127, pp. 84-90.

17. Shi, F. and Tsukamoto, H., (2001) "*Numerical Study of Pressure Fluctuations Caused by Impeller-Diffuser Interaction in a Diffuser Pump Stage*," ASME Journal of Fluids Engineering., Vol. 123, pp. 466-474.

18. Khelladi, S., Kouidri, Bakir, F. and Rey, R., (2005) "*Flow Study in the Impeller-Diffuser Interface of a Vaned Centrifugal Fan*," ASME Journal of Fluids Engineering., Vol. 127, pp. 495-502.

19. Spring, H. (1996) *Pump Design Code Manual*, U.S.A.

20. İTÜ-ME. (2003) *İstanbul Teknik Üniversitesi Hidrolik Makina Ders Notları* İTÜ., İstanbul

21. Lobanoff, V. S. and Ross, R. R. (1992) *Centrifugal Pumps – Design and Application*, Gulf Publishing Co., Houston.

22. *Rotodinamik Pompalar – Hidrolik Performans Kabul Deneyleri – Sınıf 1 ve Sınıf 2*, TS EN ISO 9906 (2002) Türk Standardları Enstitüsü, Ankara.

23. *Norm Elektrik Motorları (Tip NM) Kataloğu* (2005) Elsan Elektrik San. ve Tic. A. Ş., Ankara.

APPENDIX A

Figure A.1 – Photograph of impeller core and core box

Figure A.2 – Photograph of bowl core and core box


Figure A.3 – Photograph of impeller before machining


Figure A.4 – Photograph of impeller after machining

Figure A.5 – Photograph of impeller after and before machining from top view

Figure A.6 – Photograph of bowl

Figure A.7 – Photograph of bowl from bottom view

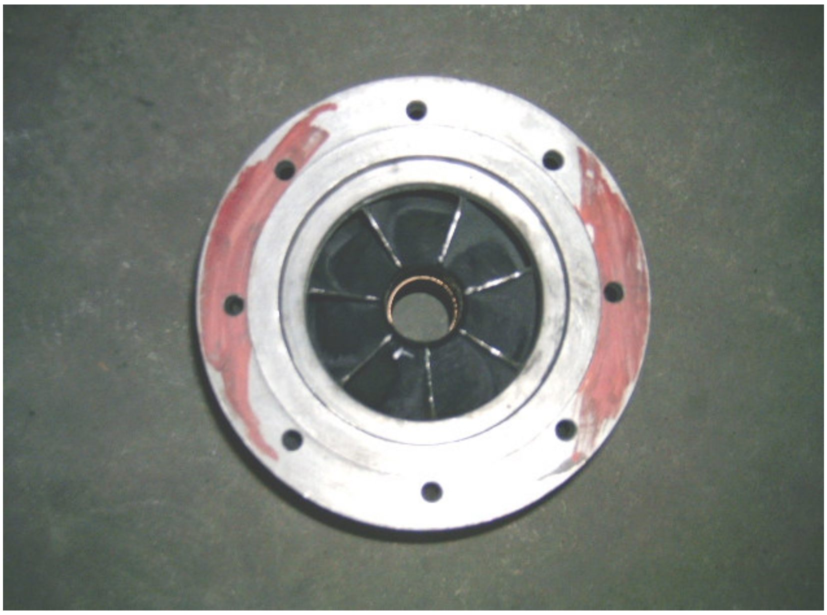

Figure A.8 – Photograph of bowl from top view

APPENDIX B

SAMPLE UNCERTAINTY CALCULATION

The uncertainty calculation of the vertical turbine pump tests are performed regarding to the standard TS EN ISO 9906, [22]. The sample uncertainty calculation that is performed for an operating point is given below.

In order to calculate the uncertainty of the measurements in the tests at least 3 readings should be performed for an operating point. Therefore 10 readings for each measurement quantity and the average value of them for an operating point of 50 l/s are taken and tabulated below.

Table B.1 – Test data for the sample operating point

Reading Number	H_m (m)	Q (l/s)	H_{dyn} (m)	P (kW)
1	14.61	50.05	3.115	13.79
2	14.61	50.04	3.110	13.81
3	14.61	50.05	3.105	13.79
4	14.61	50.01	3.105	13.79
5	14.51	50.04	3.110	13.81
6	14.72	49.94	3.110	13.86
7	14.61	49.95	3.100	13.80
8	14.51	49.97	3.115	13.81
9	14.61	50.01	3.100	13.79
10	14.72	50.04	3.110	13.80
average	14.62	50.01	3.108	13.81

The total uncertainty of a measurement, U_T, is composed of systematic and random uncertainties that are represented by U_S and U_R respectively and the formula is given for U_T is given by:

$$U_T = \sqrt{U_S^{\ 2} + U_R^{\ 2}} \tag{B.1}$$

The random uncertainty of a measurement is defined as two times the standard deviation of it in the regarding standard, [22]. The standard deviation is calculated in order to find out the random uncertainties of each measurement by the formula given as:

$$s = \sqrt{\frac{(x_1 - \overline{x})^2 + (x_2 - \overline{x})^2 + \ldots + (x_n - \overline{x})^2}{n}} \tag{B.2}$$

Where $\overline{x}$ is the average value of the measurement, x_1, x_2, x_3, …, x_n are the measurement values and n is the total number of measurements. The standard deviation, the absolute value and the normalized value of the uncertainties are tabulated below for each measurement quantity.

Table B.2 – Values for standard deviation and random uncertainty for each measured quantity.

	H_m (m)	Q (l/s)	H_{dyn} (m)	P (kW)
Standard deviation	0.065	0.040	0.005	0.020
Absolute random Uncertainty	0.130	0.080	0.010	0.040
Random Uncertainty (%)	0.884	0.160	0.328	0.292

The systematic uncertainty is defined as the sensitivity of the instrument or method used for measuring and constant during the measurements, [22]. The calibration certificates of each instrument that are used during the tests are used to define the systematic uncertainties for each measured quantity.

Table B.3 – Values of systematic uncertainty for each measured quantity

H_m (%)	Q (%)	H_{dyn} (%)	P (%)
2.85	0.70	0.01	1.33

The total uncertainty of each measured quantity is calculated by using the values in Table B.3, B.2 and formula given in Equation (B.1). The results are tabulated below in Table (B.4).

Table B.4 – Values of total uncertainty for each measured quantity

H_m (%)	Q (%)	H_{dyn} (%)	P (%)
2.98	0.72	0.33	1.36

The total head of the pump, H_t, is calculated by the formula given below.

$$H_t = H_m + H_{dyn} + \frac{V_f^{\ 2}}{2.g} \qquad \text{(B.3)}$$

Where H_m is the manometric head, H_{dyn} is the dynamic water level as described in Chapter 4 and V_f is the velocity of the pumping fluid where the pressure reading is performed. In this case V_f is found by dividing the measured flow rate to the cross-section area, A_p, of the pipe where the pressure reading is performed from. The regarding formula is given below.

$$V_f = \frac{Q}{A_p} \tag{B.4}$$

The total uncertainty of V_f, U_{T_f} is calculated using the nominal diameter of the pipe which is 0.018 m^2 and the formula given below:

$$U_{T\_f} = \frac{1}{A_p}.U_{T\_Q} \tag{B.5}$$

Where, U_{T_Q} is the total absolute uncertainty for the flow rate. If the values are substitutes into Equation (B.5):

$$U_{T\_f} = \frac{1}{0.0018} x0.00036$$

$$U_{T\_f} = \pm 0.020 \text{ m/s}$$

The total uncertainty of the total head, U_{T_Ht} is calculated the formula given below:

$$U_{T\_Ht} = \pm\sqrt{U_{T\_Hm}{}^2 + U_{T\_Hdyn}{}^2 + (\frac{V_f}{g}.U_{T\_Vf})^2} \tag{B.6}$$

Substituting the absolute values for each total uncertainty into Equation (B.6), U_{T_Ht} is calculated as:

$$U_{T\_Ht} = \pm\sqrt{0.436^2 + 0.01^2 + (\frac{2.83}{9.81} x0.02)^2}$$

$$U_{T\_Ht} = \pm 0.44 \text{ m}$$

Dividing the absolute total uncertainty value of H_t to the nominal value of it gives the total uncertainty as 2.41%.

The system efficiency, η_s, which is measured during the experiments, is calculated using the formula given below:

$$\eta_s = \frac{\rho g Q H_t}{P} \tag{B.7}$$

However all uncertainties except the uncertainty of the density of the pumping fluid, ρ_f are calculated. In order to calculate the density of the pumping fluid, the graded cylinder is used and the mass of the pumping fluid is divided by the volume of it.

$$\rho_f = \frac{m}{V} \tag{B.8}$$

The volume of 1 litre of pumping fluid is measured with the graded cylinder as 1±0.01 litre. The mass of the regarding amount of the pumping fluid is measured to be 1±0.002 kg. The total uncertainty of the fluid density is calculated using the Equation (B.8) and the formula given below as:

$$U_{T\_\rho} = \pm\sqrt{(mU_{T\_V})^2 + (\frac{1}{V}.U_{T\_m})^2} \tag{B.9}$$

Where the U_{T_V} is the total uncertainty of the graded cylinder, U_{T_m} is the total uncertainty of the measured mass of the pumping fluid.

$$U_{T\_\rho} = \pm\sqrt{(1x10^{-5})^2 + (\frac{1}{10^{-3}}x2x10^{-3})^2}$$

$$U_{T\_\rho} = \pm 2 \text{ kg/m}^3$$

The total uncertainty of the system efficiency, $U_{T\_\eta s}$ which is also defined as wire to water efficiency is derived from Equation (B.7) as given below:

$$U_{T\_\eta s} = \begin{bmatrix} \left(\frac{g.Q.H_t}{P}.U_{T\_\rho}\right) + \left(\frac{\rho.g.H_t}{P}.U_{T\_Q}\right) + \left(\frac{\rho.g.Q}{P}.U_{T\_Ht}\right) \\ + \left(\frac{\rho.g.Q.H_t}{P^2}.U_{T\_P}\right) \end{bmatrix} \qquad \text{(B.10)}$$

If the regarding values are substituted into Equation (B.10):

$$U_{T\_\eta s} = \sqrt{\begin{bmatrix} \left(\frac{9.81x0.050x18.13}{13810}x2\right)^2 + \left(\frac{1000x9.81x18.13}{13810}x0.00036\right)^2 \\ + \left(\frac{1000x9.81x0.050}{13810}x0.44\right)^2 + \left(\frac{1000x9.81x18.13}{13810^2}x0.188\right)^2 \end{bmatrix}}$$

$$U_{T\_\eta s} = \pm 1.64 \ \%$$

The total uncertainty for the wire to water efficiency is normalized by dividing 1.64 % to the wire to water efficiency at the operating point and the value is found to be 2.55 %.

The results are tabulated below for the uncertainty analysis and compared with the given standard limits for TS EN ISO 9906, [22]. While making the calculations for the density of the fluid, the density is taken to be constant through out the experiments.

Table B.5 – Comparison of total uncertainty percentages and their limits in the regarding standard, [22]

Parameters	Class – 1 Limits (%)	Class – 2 Limits (%)	Calculated Uncertainties (%)
Flow Rate, Q	± 2.0	± 3.5	± 0.72
Total Head, H_t	± 1.5	± 5.5	± 2.41
Power P	± 1.5	± 5.5	± 1.36
Efficiency, η_s	± 2.9	± 6.1	± 2.55

The calculated uncertainties are in the range of Class-2 experiments given in the regarding standard, [22].